International Scientific-Technical and Production Journal

The Paton WELDING JOURNAL

November
2006
11

English translation of the monthly «Avtomaticheskaya Svarka» (Automatic Welding) journal published in Russian since 1948

Founders: *E.O. Paton Electric Welding Institute of the NAS of Ukraine*
International Association «Welding»

Publisher: *International Association «Welding»*

Address:
E.O. Paton Electric Welding Institute,
International Association «Welding»,
11, Bozhenko str., 03680, Kyiv, Ukraine
Tel.: (38044) 287 67 57
Fax: (38044) 528 04 86
E-mail: journal@paton.kiev.ua
http://www.nas.gov.ua/pwj

State Registration Certificate
KV 4790 of 09.01.2001

Subscriptions:
$324, 12 issues per year,
postage and packaging included.
Back issues available.

CONTENTS

SCIENTIFIC AND TECHNICAL

INDUSTRIAL

BRIEF INFORMATION

APPLICATION OF NANO-STRUCTURED MATERIALS FOR DIFFUSION BONDING OF HEAT-RESISTANT NICKEL ALLOYS

K.A. YUSHCHENKO, B.A. ZADERY, A.V. ZVYAGINTSEVA, T.N. KUSHNARYOVA, V.S. NESMIKH,
E.P. POLISHCHUK and **V.S. SAVCHENKO**
E.O. Paton Electric Welding Institute, NASU, Kiev, Ukraine

When joining structure-oriented or single-crystal heat-resistant nickel alloys, to maintain their performance it is necessary to retain as much as possible the structural and crystallographic orientation of the initial material in a resulting joint, which can be achieved by solid-state joining, e.g. diffusion bonding. The study considers the possibility of using for diffusion bonding a binding film of nano-structured crystalline monoliths of intermetallics Ni_3Al and $NiAl_3$, produced by the super-rapid solidification method, as well as an intermediate multi-layer film consisting of individual layers of nickel and aluminium, produced by vapour phase deposition. It is established that the presence of an intermediate layer allows intensifying the process of diffusion bonding of nickel alloys.

Keywords: diffusion bonding, nickel alloy, multi-layer films, nano-crystalline films, intermetallics, bond, structural state, diffusion of elements

The need to produce structurally homogeneous joints at the final stages of fabrication of a welded structure hampers the effective use of structure-oriented, textured, single-crystal or composite heat-resistant alloys. This is attributable to violation of the initial structure-oriented state of a material joined during the thermal cycle of the joining process, while the above state determines performance of a product. In the case of joining heat-resistant nickel alloys by fusion welding, the welded joints additionally have a low value of crack resistance both in the weld and HAZ metal.

In this connection, it is appropriate to develop such methods of producing permanent joints, which can provide a minimal change in their structural and crystallographic orientation, and retain as much as possible a phase composition of the initial material. One of such methods is diffusion bonding in solid state using an interlayer. Technologically, diffusion bonding can easily provide a uniform and controlled heating of the mating surfaces, and a negligible level of temporary and residual stresses. In this case the probability of cracking is minimised not only in metal of the transition layer but also in the initial material.

The key problem with diffusion bonding using an interlayer is to choose the interlayer material. To retain the structural state of the initial material, it is necessary that the temperature at which a bond is formed should be lower than the temperature of structural and crystallographic re-arrangement. In addition, it is desirable that the interlayer material should be compatible as much as possible with the base material in physical, structural and strength properties. Such a material in the conventional state could be an initial alloy, but in this case the temperature conditions of formation of a bond are close to the melting point or temperature of a substantial change in phase composition.

With single-crystal heat-resistant nickel alloys, where the γ-phase of the type of $Ni_x(Al, Ti, Ta, Re, Ru)_y$, is the main strengthening phase, alloys of the Ni–Al or Ni–Ti system can be an optimal material of the interlayer. However, intermetallics Ni_x–Al_y or Ni_x–Ti_y in a polycrystalline or single-crystal state are characterised by a high stability within a wide temperature range. Hence, it is extremely difficult to produce a bond using the interlayer of such a material. However, if a special structural state with a high internal energy content is achieved in a material of the Ni–Al or Ni–Ti system, heating will cause activation of the diffusion processes in it [1]. Of high promise in this respect are materials in the amorphous and nano-structured state, as well as microfilms consisting of very thin alternating layers of two or more metals, which are components of the alloy being joined.

It is a known fact [1] that increase in diffusion penetrability along the grain boundaries or interfaces between two phases in a material in the nano-structured state is much higher compared with conventional polycrystalline materials. At the same time, re-crystallisation of materials in the amorphous nano-structured state begins at a lower temperature. For example, according to the data of study [2], crystallisation of the amorphous structure of titanium nickelide begins as early as in heating to 200 °C, and continues inertly up to 300 °C. Holding for 1 h at 350 °C is enough for completion of the crystallisation process and formation of the nano-crystalline structure with a grain size of 20–70 nm in the material.

Metal films used as interlayers in diffusion bonding may have a different structure, depending upon their production conditions. Films of intermetallic Ni_3Al deposited on a cold substrate are characterised by a heavily textured morphology of columnar growth. When heated to 200 °C, texture of a film vanishes,

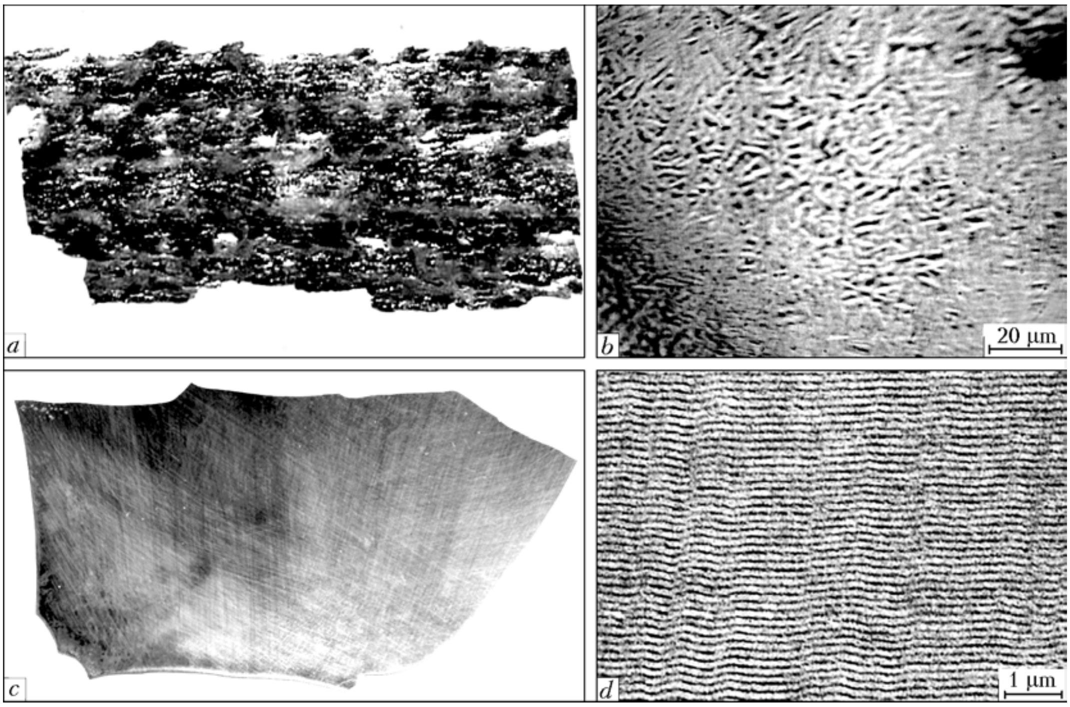

Figure 1. Appearance (*a, c*) and microstructure of the Ni_3Al intermetallic interlayer produced by super-rapid solidification (*b*), and microstructure of the Ni–Al system multi-layer film produced by vapour phase deposition in vacuum (*d*)

and its microstructure consists of individual grains of the partially ordered Ni_3Al phase. Along with monolithic films in a differing structural state, the process of vapour phase deposition makes it possible to produce multi-layer films by separate deposition of individual alloy components or individual phases [3]. Deposited non-epitaxially on a cold substrate, the multilayer films are characterised by a pronounced fibrous texture {111}, while those deposited epitaxially on substrate (001) have texture {001}.

Materials of the films consisting of alternating layers of individual elements are characterised by a high probability of occurrence of self-propagating high-temperature synthesis, which may result in formation of a new compound with increased diffusion activity. In this connection, the film-type materials in the amorphous and nano-structured state are of much current interest for use as an interlayer material for diffusion bonding.

Also, it should be noted that different heating methods can be employed to produce diffusion bonds using activating interlayers. As shown in [4], the use of the pulse current with peak values allows a very high plastic deformation to be achieved on the materials which cannot be deformed under conditions of conventional heating.

In this study, intermetallics Ni_3Al and $NiAl_3$, as well as a micro-layered film consisting of individual layers of nickel and aluminium, where the aluminium content was somewhat in excess of stoichiometric composition of intermetallic Ni_3Al, were chosen as materials of an interlayer for diffusion bonding of a heat-resistant nickel alloy.

Such films of intermetallics Ni_3Al and $NiAl_3$, up to 40 μm thick, in the nano-structured state were produced by the method of super-rapid solidification of the melt on the surface of a cooled copper drum*. Appearance of a film of intermetallic Ni_3Al and its microstructure are shown in Figure 1, *a, b*. Size of the structural element of such a material was not in excess of 40 nm, and size of the crystalline lattice was 0.3558 nm, which was a bit lower than the tabulated value of size of the crystalline lattice of compound Ni_3Al. Melting temperature of the Ni_3Al intermetallic film was 1385 °C.

Multi-layer film of the Ni–Al system produced by separate vapour phase deposition of nickel and aluminium in vacuum is shown in Figure 1, *c, d***. At a total thickness of the film produced by the above method equal to about 100 μm, thickness of an individual layer of nickel and aluminium was 1.0–1.5 μm. Parameters for deposition of the multi-layer film of the Ni–Al system were selected so that the content of nickel and aluminium in the film was close to stoichiometric composition of intermetallic Ni_3Al at a somewhat increased content of aluminium. Such films were used for diffusion bonding of heat-resistant nickel alloy of the Ni–Cr–W–Al–Ti–Nb system, in which the total content of aluminium, titanium and niobium was not in excess of 9 wt.%.

Diffusion bonding of the heat-resistant nickel alloy using an interlayer of the Ni–Al system alloy in dif-

---

*Nano-crystalline films of intermetallics Ni_3Al and $NiAl_3$ produced by super-rapid solidification were provided for investigations by Prof. Yu.V. Milman.

**Multi-layer films of the Ni–Al system in the nano-structured state, produced by separate deposition of elements, were provided for investigations by Prof. B.A. Movchan.

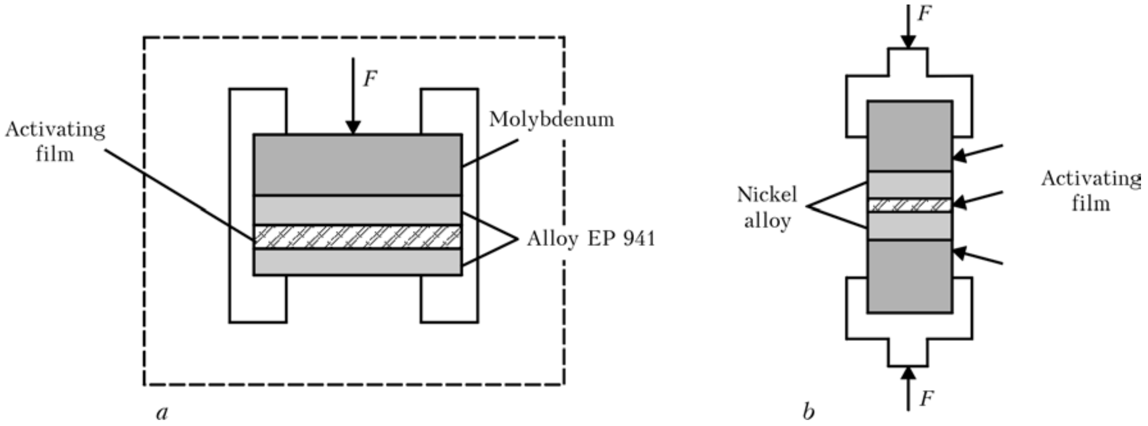

Figure 2. Schemes of heating the samples with one-sided electron beam (vacuum $1.3 \cdot 10^{-3}$ Pa) or electric arc (99.8 % Ar) (*a*), and current flow in vacuum (*b*)

ferent structural states was performed with the heating schemes shown in Figure 2. One-sided heating with a defocused electron beam in vacuum, or with a plasma arc in argon (Figures 2, *a*, and 3), fails to provide a sound bond. No bond at all was produced with an interlayer of crystalline intermetallics Ni_3Al in the nano-structured state. However, the bond was provided by using the multi-layer Ni–Al system with separate deposition of elements. In this case the exothermic reaction of interaction of nickel with aluminium to form intermetallic Ni_3Al occurred in this interlayer material in heating of the seam for welding. Also, it should be noted that with one-sided heating and using nano-structured intermetallics Ni_3Al and $NiAl_3$ as an interlayer, the bond can be produced only upon achieving a temperature of the seam close to melting point of the interlayer material. However, in this case as well the molten metal of the film fully wets the sample surface only on the side of heating, whereas in the other part of the sample only isolated islands of the bond are formed. It should be admitted that so far the one-sided heating method gives no way of producing a joint by diffusion bonding through an intermediate activating film.

Further experiments on diffusion bonding of heat-resistant nickel alloys were conducted using the heating scheme shown in Figure 2, *b*. In this case the alloy plates joined through an intermediate film were heated with a direct current flow by applying compression force *F*. Heating of the seam with a current flow in vacuum provides a uniform temperature field on the mating surfaces of the plates with an insignificant temperature gradient in the transition intermediate layer. This heating scheme makes it possible to control the temperature-time parameters of bonding, as well as the rates of heating and cooling of the plates joined. Also, it should be noted that the use of a peak value of the pulsed electric current for heating leads to a local increase in temperature to the required level particularly in the interlayer material, thus providing a substantial increase in its deformability and activating the process of formation of the solid-state diffusion bond.

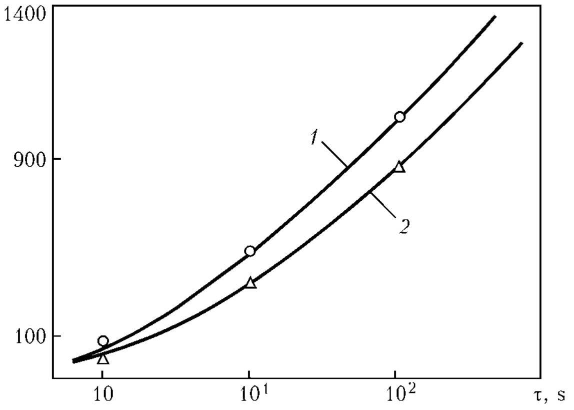

Figure 3. Dependence of temperature *T* of the sample surface upon time τ of holding in heating with electron beam in vacuum (*1*) and with electric arc in argon (*2*)

Figure 4 shows microstructures of the diffusion bonds produced on the nickel alloy using different interlayers of the Ni–Al system material. Crystalline intermetallics Ni_3Al and $Ni_xAl_yCe_zSc_v$ in the nano-structured state and multi-layer films of the Ni–Al system were used as interlayers.

As follows from the data presented, material of the Ni–Al system films both in the crystalline nano-structured state and in the form of multi-layers of individual elements can be used as an interlayer for diffusion bonding of heat-resistant nickel alloys.

Microstructure and chemical composition of different zones of the diffusion bond in the as-bonded condition and after subsequent annealing, produced by using the Ni–Al system multi-layer film consisting of separately deposited individual elements, are shown in Figure 5 and given in Table 1, respectively. Spontaneous exothermic reaction of interaction of nickel with aluminium to form chemical compound Ni_3Al occurs in the interlayer metal during heating of the seam with an intermediate multi-layer film of the Ni–Al system at 700–800 °C. In this case, a few layers of intermetallic Ni_3Al are formed from many thin layers of nickel and aluminium. Heating of the plates joined to a temperature of 1050 °C provides formation of a sound bond over the entire mating surfaces of the plates. Diffusion enrichment with alloying elements of the initial alloy can take place in the interface region on the side of the interlayer material, depending

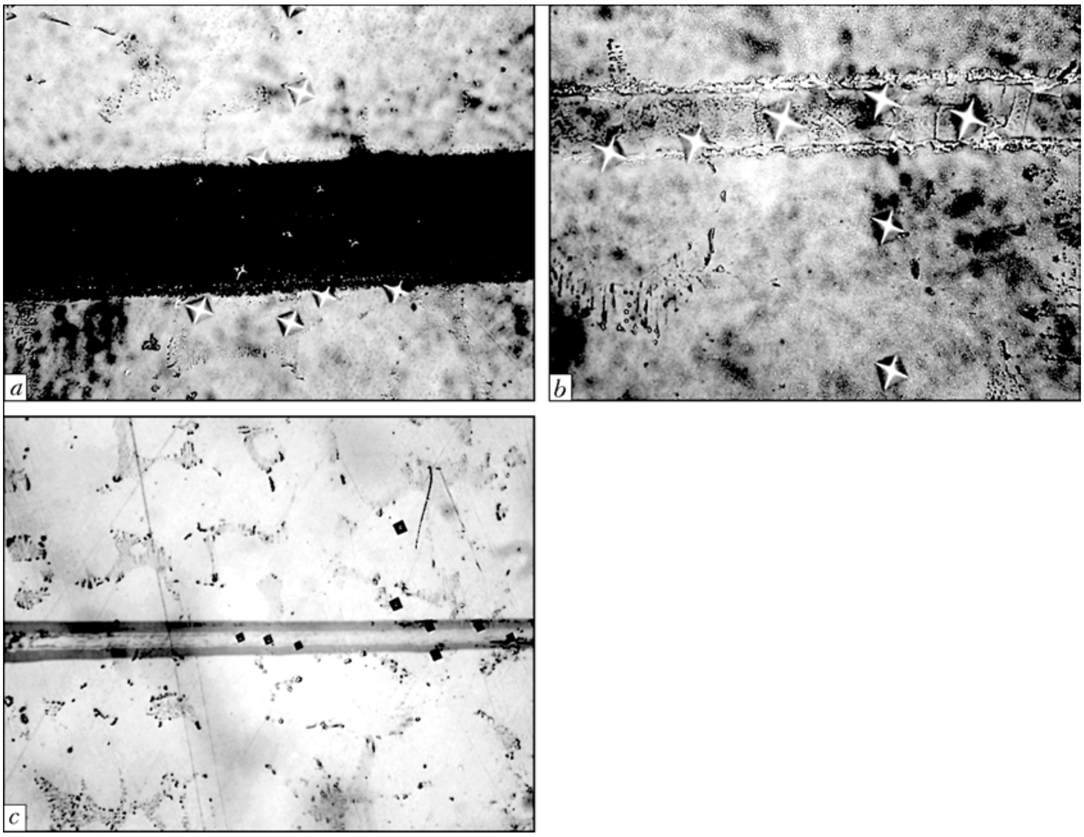

Figure 4. Microstructure of the diffusion bond on nickel alloy produced by using an interlayer: *a* — multi-layer film of the Ni–Al system (×500); *b* — crystalline intermetallic Ni_3Al in nano-structured state (×500); *c* — intermetallic $Ni_xAl_yCe_zSc_v$ (×200)

upon the bonding parameters. At the same time, no traces of diffusion of nickel and aluminium from the interlayer to the base metal during the bonding process were detected. Chemical composition of the interlayer after bonding corresponds to that of the initial multilayer film of the Ni–Al system. Microhardness of the bond zone in the as-bonded condition, and of the initial material is 5050 and 3730 MPa, respectively.

Annealing of the diffusion bond produced by using a multi-layer film of the Ni–Al system is accompanied by re-distribution of alloying elements of the alloy in the bond. Streakiness in the interlayer region disappears, and a large amount of precipitates with an increased tungsten content emerges (see Figure 5, *b*, and Table 1). Heat treatment leads to a uniform distribution of alloying elements across the section of the bond. And difference in values of microhardness between the bond and base metal decreases to 300 MPa.

Microstructure and chemical composition of different zones of the diffusion bond produced through the crystalline nano-structured film $Ni_xAl_yCe_zSc_v$ are presented in Figure 6 and Table 2, respectively. The melting temperature of material of this film is lower than the temperature used for diffusion bonding of nickel alloy.

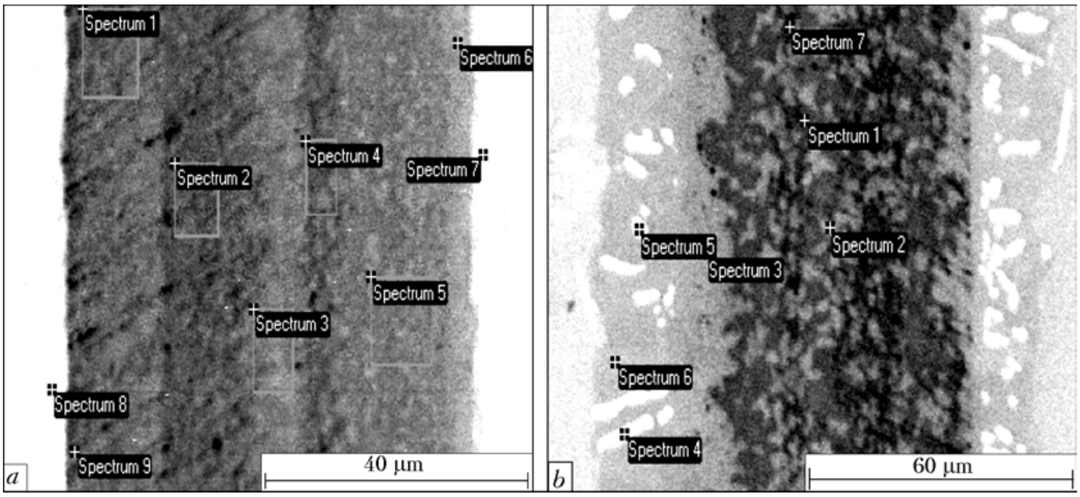

Figure 5. Microstructure of different regions of the diffusion bond on nickel alloy produced through a multi-layer film of the Ni–Al system in the as-bonded condition (*a*) and after subsequent annealing (*b*)

Table 1. Chemical composition of metal in different zones of the diffusion bond produced by using a multi-layer film of the Ni–Al system (as-bonded and after annealing)

Zone No.	Al	Ti	V	Cr	Co	Ni	Nb	Mo	W	Re
1	20.74/17.50	–/0.35	–	0.69/2.32	1.06/4.01	77.51/75.83	–	–	–	–
2	21.56/11.04	–/0.54	–/0.41	–/1.64	0.55/4.03	77.89/77.31	–/0.95	–/0.52	–/3.57	–
3	19.51/9.68	–/0.73	–/0.65	–/1.54	–/4.72	80.49/76.53	–/0.98	–/0.46	–/4.71	–
4	20.76/2.42	–/0.47	–/0.98	–/3.71	–/4.34	79.24/32.12	–	–/3.30	–/49.15	–/3.51
5	18.12/1.20	–/0.41	–/0.98	0.48/3.63	0.74/4.04	80.66/21.95	–	–/3.63	–/60.97	–/3.20
6	12.46/7.86	0.37/0.94	–/0.62	0.71/2.26	1.24/6.30	82.99/72.65	–/1.28	–/0.73	2.23/7.36	–
7	5.30/20.38	0.71/–	1.10/–	5.27/2.41	9.10/3.78	64.54/73.43	0.82/–	1.04/–	12.12/–	–
8	7.20/–	0.57/–	0.75/–	2.73/–	6.26/–	66.70/–	0.70/–	0.70/–	12.60/–	1.79/–
9	22.28/–	–	–	0.89/–	1.46/–	75.37/–	–	–	–	–

Note. Here and in Table 2, numerator gives chemical composition in the as-bonded condition, and denominator gives that after bonding and subsequent annealing.

Analysis of the data given in Figure 6 and in Table 2 shows that distribution of alloying elements in different zones of the bond immediately after bonding is more uniform than in the case of solid-state diffusion bonding using the multi-layer film of the Ni–Al system. However, whereas the regions rich in tungsten were formed after annealing of the bond, precipitation of the phases with a high content of tungsten took place immediately after bonding. The tungsten content of these phases was 13–26 wt.%. Annealing of the bond at a temperature of 1230 °C for 90 min was accompanied by enrichment of these phases with tungsten (50–65 wt.%).

Diffusion bonding through an interlayer of intermetallic Ni_3Al, produced by super-rapid solidification of the melt, did not provide a bond over the entire zone of contact of the interlayer. The bond was formed only in the regions where the reliable physical contact was ensured between the interlayer and mating surface of the initial material. Figure 7 and Table 3 give structure and chemical composition of different zones of the bond in nickel alloy produced by using an interlayer of rapidly solidified intermetallic Ni_3Al. As follows from these data, unlike the above cases, the bond here consists of clearly defined zones of the initial material and material of the interlayer. It should be noted that no traces of mutual diffusion of alloying elements in short-time heating were detected in the bond produced by using crystalline intermetallic Ni_3Al, although in the nano-structured state.

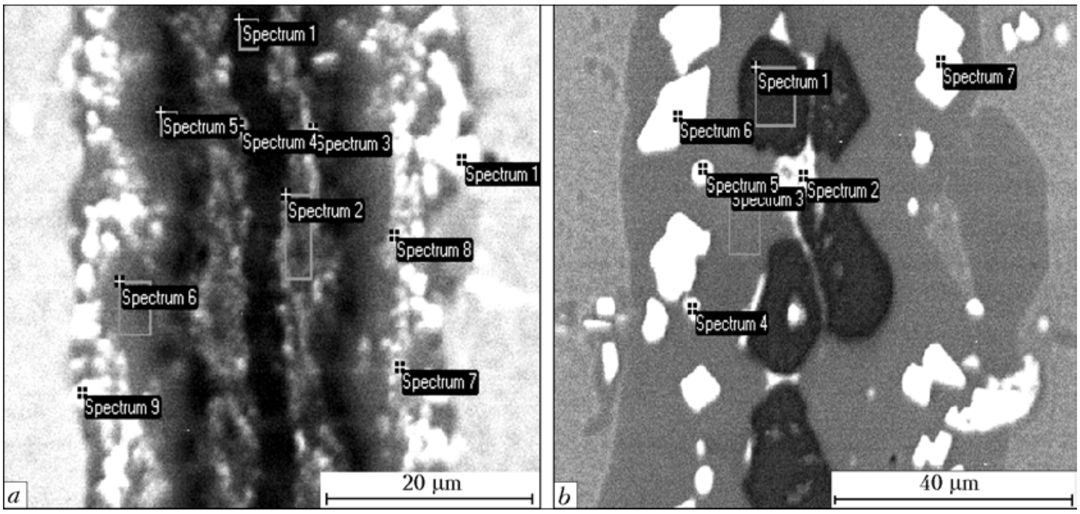

Figure 6. Microstructure of different zones of the diffusion bond produced by using the $Ni_xAl_yCe_zSc_v$ film in the as-bonded state (*a*) and after annealing (*b*)

Table 2. Chemical composition of metal of different zones of the diffusion bond produced by using the $Ni_{õ}Al_{y}Ñå_{z}Sc_{v}$ film

Zone No.	Al	Sc	Ti	V	Cr	Co	Ni	Nb	Mo	Ce	W	Re
1	29.12 15.31	–	0.27 0.50	– 0.52	1.45 4.29	5.49 8.13	63.67 69.17	– 0.47	–	–	– 1.61	--
2	22.51 4.06	– 0.82	–	0.57 –	1.93 --	5.53 5.12	60.59 59.32	--	0.30 --	0.20 29.71	8.38 0.96	--
3	19.30 8.49	–	– 1.06	0.55 0.65	2.10 3.06	5.40 8.41	56.89 71.37	– 1.10	0.49 --	1.15 –	14.12 5.86	--
4	20.82 1.83	–	0.35 0.63	– 1.16	2.25 4.61	5.21 5.86	57.63 24.19	– 2.89	0.30 3.38	0.37 –	13.07 53.01	– 2.44
5	25.55 1.14	–	0.40 0.65	– 1.36	1.69 4.41	6.56 5.57	64.75 21.35	– 4.37	-- 4.58	–	1.06 56.56	--
6	17.02 0.91	–	0.85 0.50	0.83 1.60	4.31 4.82	8.36 5.96	66.40 15.64	0.57 –	-- 2.28	–	1.67 65.35	– 2.94
7	11.48 --	–	1.15 0.58	0.98 1.48	4.61 4.84	7.77 5.83	53.57 16.94	--	0.61 3.20	–	19.83 63.90	– 3.24
8	14.23 --	–	1.05 0.34	1.05 4.11	4.51 21.81	9.03 2.72	59.89 6.50	0.98 –	0.41 13.02	–	8.84 48.14	– 3.36
9	6.66 3.08	0.17 0.42	1.10 –	1.09 –	5.09 --	7.84 6.31	47.40 56.18	1.16 –	1.20 --	2.18 32.28	26.09 1.72	--
10	2.24 --	–	0.88 –	1.43 –	5.82 --	7.14 –	27.33 --	5.43 –	3.86 --	3.49 –	42.40 –	--

Therefore, it can be concluded from analysis of the data shown in Figures 4–6 that the use of metal of the Ni–Al system in a certain structural state as an interlayer material allows producing a sound bond. In this case, the special effect on the temperature-time conditions of diffusion bonding are exerted not so much by chemical composition of the interlayer material as by its structural state.

In diffusion bonding using a crystalline film of intermetallic Ni_3Al as an interlayer, a higher temperature and a longer holding time are required to produce a bond than in bonding using the multi-layer Ni–Al system film of the same chemical composition produced by separate deposition of elements. In the last case, occurrence of a low-temperature exothermic interaction of nickel and aluminium in the multi-layer

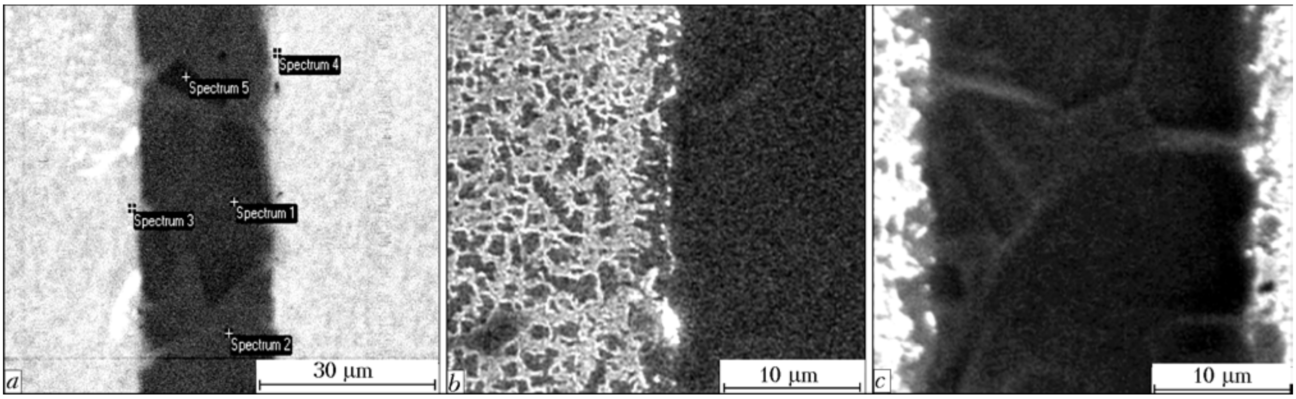

Figure 7. Microstructure of different zones of the diffusion bond produced by using the Ni_3Al intermetallic film: *a* — general view of the bond; *b*, *c* — different regions of the transition zone

Table 3. Chemical composition of metal of different zones of the diffusion bond produced by using the Ni_3Al film

Zone No.	Al	Ti	V	Cr	Co	Ni	Nb	Mo	W	Re
1	11.71	--	–	–	–	88.29	–	–	–	--
2	12.08	--	–	–	–	87.92	–	–	–	--
3	5.98	0.66	0.79	3.20	6.98	68.33	0.91	1.20	10.44	1.51
4	5.05	0.62	0.72	3.81	8.02	67.79	0.36	0.70	11.28	1.65
5	11.72	--	–	–	–	88.28	–	–	–	--

film at a heating stage is likely to lead to activation of the diffusion processes, which allows joining of materials structured in a certain way without violation of their phase composition, structural and crystallographic orientation by retaining properties of the initial material.

CONCLUSIONS

1. Conditions of formation of a diffusion bond in heat-resistant nickel alloys, based on the strengthening γ-phase, by using an interlayer are determined not as much by chemical composition of its material as by its structural state. The use of the multi-layer Ni–Al system film as an interlayer allows producing a sound bond.

2. In diffusion bonding using a multi-layer Ni–Al system interlayer or a low-melting point $Ni_xAl_yCe_zSc_v$ interlayer, the inter-diffusion of alloying elements takes place directly during the bonding process. Subsequent annealing leads to almost a uniform distribution of alloying elements across the section of the diffusion bond.

3. Using an interlayer of crystalline intermetallic Ni_3Al in the nano-structured state makes it possible to produce a sound bond by solid-state diffusion bonding.

1. Kolobov, Yu.R. (2003) Diffusion and properties of nano-structured materials. In: *Proc. of 15th Int. Conf. on Physics of Strength and Plasticity of Materials* (Toliatti, 30 Sept.–3 Oct., 2003). Toliatti: TolGU.
2. Zeldovich, V.I., Frolova, N.Yu., Pilyugin, V.P. et al. (2004) Amorphous and nano-crystalline structures in titanium nickelide produced by filamentary plastic deformation and postheating. *Fiz. Met. i Metallovedenie*, 97(**1**), 55–63.
3. Benerjee, R., Thompson, I.B., Anderson, P.M. et al. (2003) Sputter deposited nanocrystalline Ni--25Al alloy thin films and Ni / Ni_3Al multilayers. *Thin Solid Films*, 424(**1**), 93–98.
4. Frolov, K.V., Troitsky, O.A., Borisov, Yu.V. (2003) Metal can be kneaded as dough (Possibilities of new critical technologies). *Metallurgiya Mashinostroeniya*, **5**, 38–39.

STRUCTURAL HEREDITY IN THE INITIAL MATERIALS–METAL MELT–SOLID METAL SYSTEM (REVIEW)

I.A. RYABTSEV
E.O. Paton Electric Welding Institute, NASU, Kiev, Ukraine

Issues of structural heredity in the initial materials–molten metal--solid metal system are considered on the basis of literature data. It is shown that the solidified metal of ingot (deposited metal) inherits not only contamination of initial charge (electrode) materials by nonmetallic inclusions and other harmful impurities, but also elements of the crystalline structure of these materials. The use of ultrasonic treatment of the weld pool, as well as combined heat sources (hybrid technologies), such as arc-laser, plasma-laser, etc., is indicated to provide the equilibrium structure of the deposited metal.

Keywords: welding, surfacing, weld metal, metallurgical heredity, structural heredity, structure of melts, clusters, short-range order, long-range order, solid metal

General concepts of heredity in initial materials–metal melt--solid metal system. In metallurgy heredity in the broad sense of the word is understood as transfer from primary to subsequent substances of similarities either in their structure, external or internal, or in physical and chemical properties and features (metallurgical heredity) [1].

In foundry practice influence of initial charge materials on the melt, and through it on properties of the obtained solid metal, was noticed long ago. Such an influence, connected with presence and action of nonmetallic inclusions, gases and elements of crystalline structure of initial materials, depends on conditions of melting and post-furnace treatment of the melt: temperature and slag conditions, number of remeltings, degassing, etc.

Most fully the problems of transferring from primary to secondary substances of similarities in their structure, physical and chemical properties are considered in B.A. Baum's monograph [1], where it is noted that in metallurgy and materials science the term «heredity» has no commonly accepted meaning. In the opinion of the author, essence of the phenomenon, as applied to the processes of melting, is better rendered by the term «memory». As a result of such complex processes as charge preparation, remelting, deoxidation, alloying, casting and solidification, hereditary properties are seldom transferred unchanged. This phenomenon is most pronounced only in cast irons, at which melting graphite inclusions may not be dissolved. During solidification the form of graphite and depending on it properties of cast iron are restored [2]. In some cases transition of nonmetallic inclusions from charge into the crystallized metal is observed. Most often, especially in steels, the phenomenon in question is attributed to non-equilibrium of the melt structure.

Nevertheless, most researchers in this field for characterizing the processes of transfer of similarity from primary to secondary substances, all the same use the term «heredity» [3–6]. In the cases when chemical compositions, the impurities and nonmetallic inclusions content are close, at about identical conditions of the melt cooling, the casting metals differ in their micro- and macrostructure, as though passed on via the melt from the structure of initial charge materials, testify to the structural heredity [3].

The effect of technological parameters of melting on the quality of castings is usually considered from the point of view of changes in gases and nonmetallic inclusions content, solidification conditions, etc. The unfavorable heredity, as a rule connected with the presence of harmful impurities, is most often eliminated by application of rather high melt superheating temperatures, electroslag, plasma-arc and vacuum-arc remelting, intensive pool agitation, flux or slag treatment, etc. [6].

Though the problem of the influence of macro- and microstructures of initial charge materials on properties of the finished cast metal remains disputable, it is believed that some elements of the structure of the charge components influencing the process of solidification remain in the melts. The efficiency of external effects on the liquid metal (thermotiming and ultrasound treatments, agitation, laser and X-ray irradiation, etc.) can be linked with induced by them changes of precisely these structural elements. However the nature of the formations-carriers of structural attributes of the charge via liquid state to the end-product, is not yet quite clears [7].

The experience has shown that efficient control of hereditary processes is possible only in the case of differentiated account of the processes proceeding in the initial charge materials--metal melt--solid metal system. Structural state of metal melts in this system has been least studied.

Structure of metal melts. At melting of any alloy, are employed charge materials being either pure components, or enriched with these components alloying compositions, or recycled raw materials. In most cases any of many diverse charge components in solid state is internally essentially heterogeneous, due to the presence of eutectic colonies, precipitates of intermetallides and nonmetallic inclusions, as well as products of various segregation processes. At melting of such initial materials, macroscopically heterogeneous melt is formed.

In terms of their properties and structure, liquids are much closer to solids than to gases. Data on the structure of metal melts can be obtained either by indirect methods, based on measurements of various structure-sensitive properties (electrical conduction, viscosity, density, surface tension, magnetic susceptibility, etc.), or by direct diffraction methods (radiography and electron diffractometry, neutron diffractometry), allowing structural parameters to be experimentally defined (equilibrium interatomic distances, number of nearest neighbors, root-mean-square displacement of atoms, radiuses of correlation in the arrangement of particles) and by that to quantitatively characterize the structure of melt [8--12].

X-ray diffraction analysis has shown that at a temperature slightly exceeding the melting temperature, arrangement of particles in a liquid is not random; it is similar to that existing in a solid crystalline body. Instantaneous arrangement of particles in local volumes of a liquid resembles arrangement of atoms in a similar solid body [1]. However unlike solid crystalline bodies characterized by long-range order, basic characteristic of the structure of liquids is their short-range order. Regularity of atomic spacing in a liquid, peculiar to the given type of short-range order, concerns only a limited range of interatom distances. With increasing distance from any atom chosen as a reference one, deviations from the short-range order around it increase, which leads to disappearance at reasonable distances of any regularity in the arrangement of particles. Thus, short-range order is an ordered arrangement of atoms and molecules within the range of distances comparable with interatom distances, while long-range order is an ordered arrangement of atoms and molecules in the entire volume of a body.

Basic characteristics of the short-range order structure of liquid metals are the most probable interatom distances r and average coordination numbers Z. Z value is numerically equal to the number of the nearest neighbors around each melt atom. Approximate calculations have shown that ordered areas can cover 10 or more coordination spheres and reach the size of approximately 200 nm. It should also be remembered that initial solid state peculiarities can influence properties of the molten specimens. It is connected with the character of distribution, interaction of atoms of impurities, and lattice defects depending on the specimen history [1].

The affinity of structures of the liquid and solid metals can be confirmed by the following test: at slow melting and cooling a formed monocrystal of bismuth had the same orientation as the initial one, while at solidification of superheated liquid metal obtained by melting of a coarse-grained ingot, a newly-formed solid ingot also had a coarse-crystalline structure. The short-range order of iron after melting does not change, liquid iron retains body-centered cubical structure [13].

When comparing a liquid and a crystalline solid body, the following important point has to be stressed. Creation of the model of an actual crystalline solid body requires taking into account elements of disorder present in an ideal space lattice: displacements, vacancies, interstitial atoms, etc., while establishing structural pattern of any liquid requires taking account of elements of a certain short-range order or elements of ordering in a disorder [13, 14].

This circumstance is allowed for in the so-called sibotacsic model of liquids structure. Sibotacsics are areas with a certain type of spatial orderliness of particles. Later on a similar-sense term, «cluster» appeared. In multicomponent liquids clusters are rather steady formations with stronger in comparison with external, internal bonds. They have no physical interface, at which transition the state parameters and properties would change abruptly [13].

Proceeding from these concepts, the liquid metal model can be described as follows: the entire volume of liquid metal contains various in size groups of particles (clusters), within which the arrangement of atoms close to that in a solid body is preserved. The clusters change with time, continuously arising and disappearing. Atoms of one grouping pass into another having a different orientation of the axes of symmetry. In places of contact of clusters, some disordering of layers occurs. At each particular moment of time central part of a cluster in its structure is close to a solid, while external layers feature no strict symmetry.

Currently has gained ground a quasi-polycrystalline model of metal melts, being a peculiar combination of two structural components: clusters (microgroupings with ordered arrangement of atoms close to such in crystal bodies) and a disordered zone with a chaotic and, as a rule, more loose arrangement of particles, forming in melts a continuous three-dimensional cellular network enveloping the clusters. Clusters are structurally and genetically linked with solid metal [13].

In pure liquid metals one of the packings is usually packing of the initial crystal lattice type. The experience shows that transition from the crystalline state into liquid does not produce any essential rearrangement of the short-range order structure in such metals as iron, aluminum, nickel, copper, magnesium. So, iron and nickel at a temperature close to the temperature of solidification, have short-range order structure, which in its formal attributes most of all corresponds to BCC-type packing. Thus formation in the melt of clusters with a more dense packing of face-centered cubical structure and hexagonal close packing types is supposed [1].

In multicomponent melts at a small superheating over the liquidus, structural heterogeneity of initial charge materials is retained, which provides the basis to regard it as a non-equilibrium system. Solidification of such a non-equilibrium melt retaining of carbide and intermetallide type microgroupings, is accompanied by formation of a great number of structural and concentrational imperfections in the solidified metal.

Transition from non-equilibrium into equilibrium state can be achieved due to heating to a certain critical temperature (as is known, for each steel brand there is a critical temperature of melting, when liquid steel acquires a homogeneous structure resulting in a more homogeneous solid solution providing maximal plastic properties). Such a critical temperature of melting is defined by chemical compositions of the alloy and initial charge materials [13, 15].

Melting of metal can be considered, for the sake of simplicity, as a process of disintegration of a macroscopical solid body into individual clusters (or blocks) with growing distance between them, up to the point, at which interatom bonds connecting surfaces of the two neighboring clusters, break. Latent heat of melting is spent for breaking interatom bonds, not between individual atoms, but between neighboring clusters (blocks) [13].

A serious obstacle in the way of understanding the reasons of the observed temperature-concentrational changes of properties of metallic liquids, is the uncertainty in understanding the form of presence of impurities in them [13]. The character of interaction of the impurity with the surrounding particles defines also the form of its existence, surrounding it short-range order and its behavior, thus the properties of the melt. As a first approximation, we can restrict our consideration to the data on the relationship of energies of interaction of component atoms. Actually, irrespective of whether the added impurity is metallic or nonmetallic, structural changes occurring in the melt are usually reduced to formation of complexes whose centers are atoms of impurities. In other words, irrespective of differing nature of the impurities, there is no basic difference in describing the structure of their diluted solutions. In extra-pure specimens of iron, first additives of each of the investigated impurities, such as oxygen, sulfur, carbon, phosphorus, reduce the viscosity, in so doing the intensity of the impurities effect decreases in precisely the same sequence. Decreasing viscosity with increasing impurity content attests to microheterogeneity growth. Subsequent raising of concentration of a given impurity, and especially adding other elements into the melt, can either lower the rate of viscosity reduction or cause its growth.

In the context of quasi-polycrystalline model of melts, increase in viscosity of a molten medium containing nonmetallic inclusions, can be explained by increasing clusters content and corresponding reduction of relative proportion of the disordered zone. Increase in the proportion of clusters in adding to molten metal of disperse crystal particles is, apparently, a display of a sort of epitaxial effect. In insignificantly superheated melts, around foreign solid particles, stiff shells consisting basically of relatively large and relatively more stable clusters are formed. The orienting action of crystal lattices of inclusions on adjacent layers of metal shows itself in the increased degree of melt orderliness. Disperse inclusions of solid particles greatly facilitate solidification of melts. At constant overall content of nonmetallic inclusions, their effect on the viscosity of metal melts depends on their nature and dispersiveness.

Results of the investigations have enabled to establish the following basic peculiarities of transition from crystalline into the liquid state:

- essential reorganization of the short-range order of metals structure does not occur, rate of structural transformations in multicomponent melts is low;
- melts are characterized by their retention for long periods of time of microscopic ordered areas (clusters);
- dimensions and quantity of elements of melt structure, affect the kinetics of solidification and properties of castings, technology of melting of most casting alloys includes superheating to above melting

point temperature being much lower than that of liquids structure disordering [3].

Solidification of metal melts. Solidification is the process of transition of melt from liquid into solid state. The character of its progression to a great extent defines the structure and properties of the solidified metal. During solidification, structural heterogeneities of a liquid metal can be passed on to a solid body. In such a manner, in particular, takes place hereditary transfer of non-uniform distribution of impurities in an alloy being in liquid state at its transition into solid state.

In a number of works [3–5, 13, 15], correlation between properties of liquid alloys and mechanical, as well as functional characteristics of the resulting solid metal was reported. The most probable reason of the observed correlations connecting properties of liquid and solid metals is non-equilibrium of the melt before solidification. For full completion of the processes of establishment of equilibrium in a melt, sufficient time is required; therefore the degree of their completion by the moment of solidification can be different. Variation in the duration of the melt structure is reflected in its properties, while in the case of solidification from different states, in the properties of the solid metal.

It is assumed that not a single of the existing theories of solidification explains a whole variety of the observed phenomena. During solidification of metal melts simultaneously proceed the processes of micro- and macroscopical migration of particles and their groups, heat transfer and phase transformations are occurring.

Three mechanisms of crystal growth are applied more often:

- in-levels (nucleation and growth of two-dimensional nuclei of new crystalline layers on the atomically-smooth surface of crystals);
- dislocational (attachment of particles to the steps formed by emergence of screw dislocations on the crystal surface);
- normal (random attachment of particles to a rough crystal–melt interface [1]).

It is supposed that crystals of metals and alloys in usual industrial-practice conditions should have a rough interface and enlarge by normal mechanism of their growth. In the case of pure metals, in-levels mechanism of their growth is also not ruled out. The structure of melt, even equilibrium one, essentially influences the mechanism of solidification. In such cases, when the melt and the solid phase are quite close in their short-range order structure, normal growth of crystals occurs.

In existing theories of solidification, main attention is focused on the growing crystal surface; the liquid is thus conceived as a passive party, whose role is limited to transport of material and heat removal. Attention should also be paid to the state of liquid near the border with the solid phase. Thus the liquid can be considered as a superposition of atomic configurations in a crystal- and liquid-like environment, where transfer to the crystal of elements of disordering, mainly point and linear defects, is possible [1].

Motion of the solidification front in multicomponent microheterogeneous melts can take place due to attaching to it groups of particles-clusters. In this connection it is supposed that effects of ordering, shape and dispersivity of structural components in some solid alloys also depend on the melt structure. The melt structure, influencing the mechanism and other features of solidification, to a certain extent also conditions presence of defects in crystals. It is supposed that more microheterogeneous and non-equilibrium melts produce the most defective crystals [1].

Intentionally varying the structure of initial charge materials, it is possible to essentially improve the quality of castings and their properties. Structural information is put in by application of special methods of treating and making charge materials [3, 16, 17], such as:

- treatment of charge materials during melting (thermokinetic and thermotime treatment, modification, electroslag, plasma-arc and vacuum-arc refining, etc.);
- high-speed cooling of charge materials at solidification for obtaining fine-grained structure (cooling with water, pelletizing, centrifugal casting, etc.);

solid-phase treatment of charge materials (thermal, pressure, etc.) for obtaining non-equilibrium structures rich in displacements, having fine mosaic structure.

Thus, structural (metallurgical) heredity in initial charge materials–metal melt–solid metal system can be controlled by changing, firstly, composition, structure and shape of charge materials and, secondly, thermal, kinetic and slag conditions of the melting process.

Problems of structural heredity in system of initial electrode (filler) material–weld pool melt–solid metal in welding. Yet academician Evgeny O. Paton called attention to the fact that quality and properties of welded joints depend both on the electrode (filler), and the base metal. The higher the quality and the more homogeneous in composition are initial materials, the higher is the possibility of producing quality products. However, in welding, as a rule, attention is first of all paid to one aspect of structural heredity: contamination of initial materials with nonmetallic inclusions, other harmful impurities and their effect on properties of welds. No wonder that those were the welders who suggested such methods of improving quality of metals and alloys, as electroslag, vacuum-arc and electron-beam refining methods.

However in welding technical and scientific literature, practically unavailable are publications on the problem of relationship of crystalline structure of initial solid materials with similar structures of the weld pool and solidified metal of the weld, and the term «heredity» as applied to the system of initial electrode (filler) material–weld pool melt–solid metal in welding practice is not in common use.

Nevertheless, research of this problem is of great importance also for welding (surfacing) processes study. However research of structural heredity in welding in comparison with metallurgy is complicated by the following factors:

- heating, melting and transfer of electrode (filler) material at various methods of welding (surfacing) in respect of most physical-metallurgical parameters, differ very much;
- influence of the base metal which is remelted and gets into the weld pool; it can to a certain degree be classed with initial materials;
- temperature-time parameters of the weld pool (unlike metallurgical furnace) are not fixed and hardly give in to controlling, owing to it the structure of weld pool melt will apparently be far from equilibrium;
- solidification of the weld pool metal occurs on the solid substrate whose metal structure influences the structure of the metal being solidified.

As literary data show [18], for obtaining quality and homogeneous deposited metal, of great value are apparently methods of making charge (electrode, filler) materials. Use of impurities-free, homogeneous in composition and structure materials should ensure obtaining deposited metal with higher operational properties. For example, for widely applied for deposition highly alloyed flux-cored wires and strips, as well as sintered strips, promising is the use as a charge of alloying compositions made with application of refining remelts, fully or partially ensuring obtaining desired composition of the deposited metal.

Certain promise has ultrasonic treatment of weld pools. As it was established [19], inducing intense ultrasonic fluctuations in the weld pool before its soliditication, gives more ordered structure of the deposited metal, its friction coefficient decreases, wear resistance increases.

For controlling temperature-time parameters of weld pool, processes of its solidification, as well as structure of the deposited metal, it is apparently expedient to apply combined heating sources (hybrid technologies), such as arc-laser, plasma-laser, etc.

1. Baum, B.A. (1979) *Metal liquids*. Moscow: Nauka.
2. Girshovich, N.G., Ioffe, A.Ya., Zommer, L.R. et al. (1970) Influence of charge material nature on structure and properties of nodular and flake graphite cast iron. In: *Principles of cast alloy formation*. Moscow: Nauka.
3. Nikitin, V.I. (1988) Control of heredity of charge material and melt structure as an important reserve for improvement the quality of cast products. *Litejnoe Proizvodstvo*, **9**, 5--6.
4. Nikitin, V.I. (1982) About influence of charge metal quality on properties of light alloys. *Tsvet. Metally*, **8**, 73–75.
5. Prudovsky, P.P., Golyakov, V.D., Simonova, N.A. et al. (1986) Influence of heredity of charge material structure on mechanical properties of VAL8 alloy. *Litejnoe Proizvodstvo*, **11**, 7--8.
6. Elansky, G.N., Kudrin, V.A. (1984) *Structure and properties of liquid metal*. Moscow: Metallurgiya.
7. Popel, P.S., Baum, B.A. (1986) Thermodynamical analysis of one of the causes of metallurgical heredity. *Izvestiya AN SSSR. Metally*, **5**, 47–51.
8. Wilson, D.R. (1972) *Structure of liquid metals and alloys*. Moscow: Metallurgiya.
9. Tatarinova, L.I. (1983) *Structure of solid amorphous and liquid materials*. Moscow: Nauka.
10. Crockston, K. (1978) *Physics of liquid state*. Moscow: Mir.
11. Vatolin, N.A., Pastukhov, E.A. (1980) *Diffraction examinations of structure of high-temperature melts*. Moscow: Nauka.
12. Arsentiev, P.P., Koledov, L.A. (1976) *Metal melts and their properties*. Moscow: Metallurgiya.
13. Ershov, G.S., Chernyakov, V.A. (1978) *Structure and properties of liquid and solid metals*. Moscow: Metallurgiya.
14. Belashchenko, D.K. (1985) *Structure of liquid and amorphous metals*. Moscow: Metallurgiya.
15. Tyagunov, G.V., Kolotukhin, E.V., Avdyukhin, S.P. (1988) Relationship between melt properties and structure of solid metal. *Litejnoe Proizvodstvo*, **9**, 8–10.
16. Tretiakov, E.E., Tyagunov, G.V., Tsepelev, V.S. et al. (1992) Improvement of structure and properties of solid metal by action on metal melt. *Stal*, **7**, 31–34.
17. Popel, P.O., Baum, B.A., Kosilov, N.S. (1982) Interphase phenomena in displacement of metal melts. In: *Adhesion of melts and brazing of materials*. Issue 9, 8.
18. Eremeev, V.E., Strelyany, Yu.V., Korbut, V.A. et al. (1979) Chemical macroheterogeneity of metal deposited with different electrode materials. In: *Theoretical and technological principles of surfacing. Properties and tests of deposited metal*. Kiev: PWI.
19. Shilyaev, A.S., Ivinsky, V.I., Stukin, S.A. (1986) Electric arc surfacing of machine parts with application of ultrasonic field. In: *Surfacing in manufacture of machine parts and equipment*. Kiev: PWI.

FEATURES OF δ-FERRITE FORMATION ON THE FUSION BOUNDARY IN WELDING HEAT-RESISTANT CHROMIUM MARTENSITIC STEEL

V.Yu. SKULSKY
E.O. Paton Electric Welding Institute, NASU, Kiev, Ukraine

Possible mechanism of formation of decarburized δ-ferrite grains in the fusion zone was studied by simulating the thermodeformation cycle of welding in a rigidly-restrained sample of heat-resistant steel P91 through heating with passing electric current up to surface melting, and by comparing the resulting structure with that of the actual welded joints. The suggested mechanism attributes formation of the above grains to appearance of regions depleted in carbon and rich in ferritizing elements, which results from liquation redistribution of alloying and impurity elements, as well as regions depleted in carbon in the grain bulk, resulting from its migration towards the weld.

Keywords: chromium martensitic steel, welded joints, fusion zone, grain surface melting, liquation, carbon diffusion, δ-ferrite

When studying the weldability of heat-resistant steels with 9 % Cr it is established [1] that δ-ferrite in the form of light-coloured grains forms in the fusion zone (FZ) of welded joints in the martensite matrix (Figure 1). Ferrite grains are not prone to hardening or formation of carbide precipitations at tempering, and have a low microhardness in as-welded and as-tempered condition (δ-ferrite after welding / tempering: *HV*0.2-199--258 / 202–248; martensite: *HV*0.2-378–415 / 288–324). An assumption has been made [1] that δ-ferrite formation can be associated with metal overheating in the HAZ up to grain surface melting and carbon migration.

This work has been performed in order to more precisely determine the mechanism of ferrite phase formation in welded joints of martensitic steels with 9 % Cr. During the studies the welding thermodeformational cycle was simulated in a unit which allows heating rigidly fixed cylindrical samples by passing current up to the specified temperature with the specified rates of heating, cooling and soaking at the selected temperature T_h [2]. In order to provide stress concentration, the samples have a V-shaped groove in their working part, similar to a notch in Charpy samples. Sample material is P91 steel, wt.%: 0.1C–0.34Si–0.47Mn–0.003S–0.018P–8.5Cr–0.28Ni–0.93Mo–0.2V–0.072Nb–0.06N. X-ray microprobe analysis was performed in «Camebax» unit, and «Neophot-32» light microscope and microhardness meter PMT-3 were used for metallographic investigations.

Heating rate in the experiments was 79, cooling rate was 39 °C / s (adjustable by additional heating in the range of T_h = 1200–550 °C, followed by natural cooling of the specimen), at T_h = 1200 °C / s — 10 s soaking. Sample overheating in the undercut zone led to its partial melting. This resulted in simulation of the welded joint structure, including the melting zone and the adjacent overheated zone (Figure 2, *a*). Shrinkage (solidification) cracks formed in the melting zone, which is inevitable under such experimental conditions (Figure 2, *b*).

A coarsening of the grain structure and formation of a carbide ridge on the base metal (BM)–melting zone boundary is observed in the HAZ metal. Closer to the melting zone the metal microhardness increases, which is caused by increased content of carbon in this direction (Figure 3). In the fusion zone (beyond the zero line 0--0) the hardness drops abruptly. A pro-

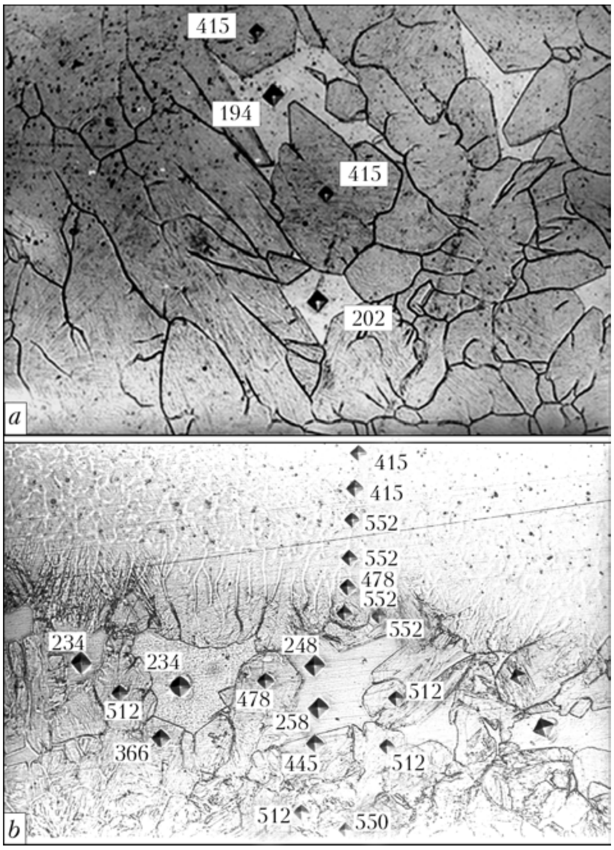

Figure 1. Microstructure of the near-weld zone in automatic submerged-arc deposition of a bead (as-deposited condition) on steel with 9 % Cr: *a* — deposition with flux-cored wire of a composition similar to steel; *b* — deposition with Sv-04Kh19N9T wire (numbers are microhardness values *HV*0.2) (×400)

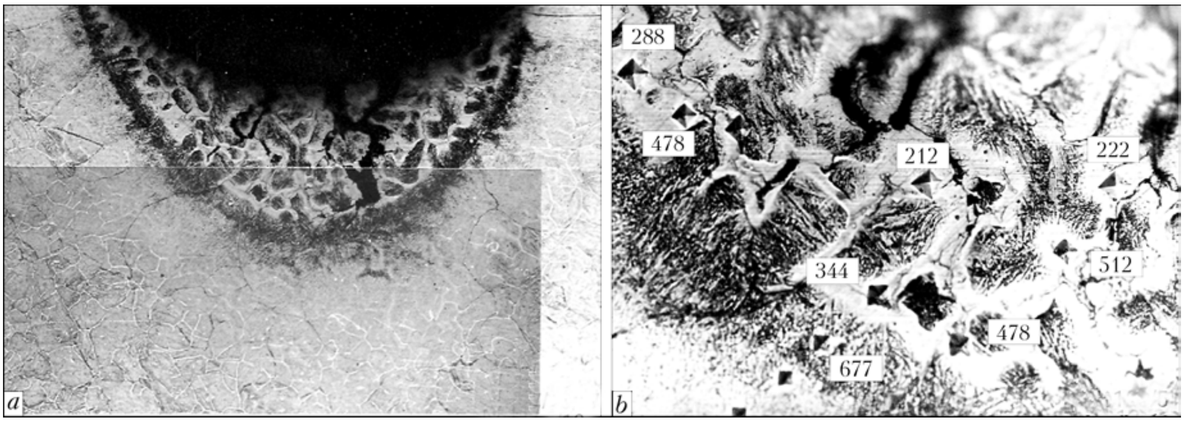

Figure 2. Microstructure of sections in a simulated welded joint: *a* — general view (×200); *b* — melting zone (×800)

nounced structural inhomogeneity and scatter of microhardnes values are found here (Figure 2, *b*): there are sections with martensite hardness (*HV*0.2-478–512) and soft sections corresponding to the hardness of δ-ferrite (*HV*0.2-212–222).

Results of the processes running in the considered experimental sample are similar to those, which develop in the actual welded joints.

Processes of carbide phase dissolution and development of homogenization ran in the HAZ metal (without partial melting) in high-temperature region due to diffusion redistribution of the elements present in the dissolved particles. This is seen by uniform etching of the grains near the melting zone. Diffusion displacement of carbon and its «ousting» into the high-temperature zone leads to enrichment in carbon of a region at the BM–melt interphase. Dissolution of grain boundary particles and depletion of part of the grains in carbon ensure a lowering of the resistance to dislocation motion, associated with dynamic recrystallization and migration of boundaries [3–5], which results in grain growth. Partial decarbonization of the solid solution due to its motion towards the weld, observed in this experiment, was a condition for easier grain growth (in the actual joints there is usually not enough time for such a growth to occur, because of the fast temperature change). However, despite carbon migration no δ-ferrite forms in the HAZ metal overheated section.

In the FZ at surface melting of the grains the liquation mechanism is in place for chemical element redistribution, of which sulphur, phosphorus and carbon have high liquation ability. Liquation redistribution of the alloying and impurity elements leads to development of microsections with considerable compositional variations in the melting zone (Table). In the region of the light-coloured sections of the microstructure (Figure 2, *b*) an increased sulphur content is found, which is related to its liquation, and which additionally confirms the liquation origin of these sections. Local increase of chromium and molybdenum content is also found. As a result, at additional separation of carbon, detected along the dark interlayers formed after sample tempering, conditions are in place for formation of low-carbon δ-ferrite with minimum hardness.

Thus, in the zone of overheating of welded joints on steels with 9 % Cr, welded by a similar weld, a tendency is observed to carbon displacement into the weld zone, this leading just to grain growth without formation of grains of δ-ferrite, stable up to room temperature. A more noticeable redistribution of alloying elements and carbon, leading to residual structural changes, is observed at the stage of grain surface melting, having reached temperatures corresponding to the intermediate solidification region (L + δ).

These results confirm that δ-ferrite in the welded joint FZ on steels of P91 type is formed after reaching temperatures of the start of grain melting.

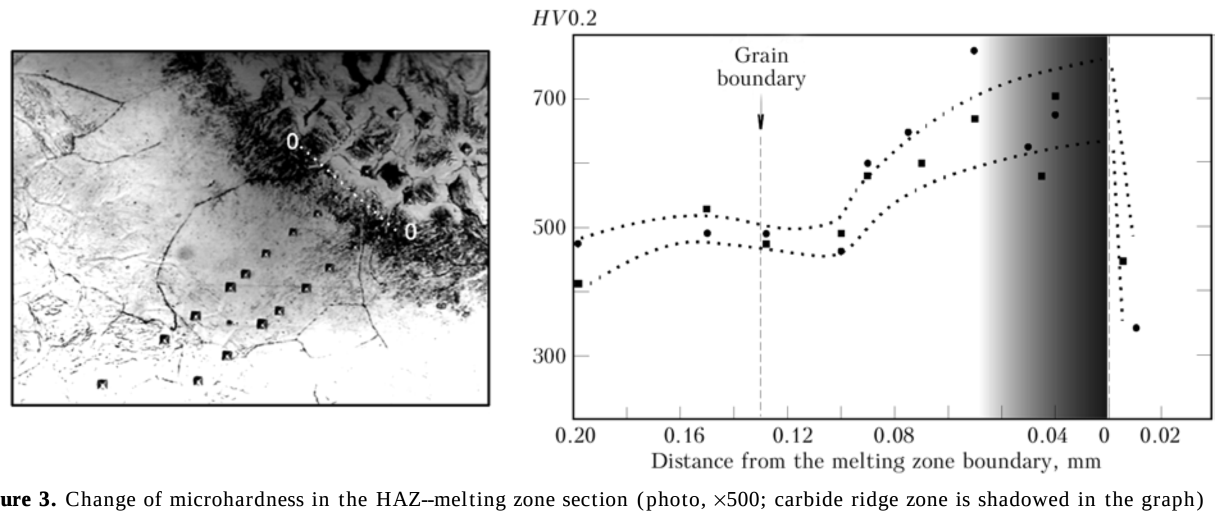

Figure 3. Change of microhardness in the HAZ–melting zone section (photo, ×500; carbide ridge zone is shadowed in the graph)

Investigations performed in [1, 6] allow suggesting the following mechanism of δ-ferrite formation in the FZ. In steel with 9 % Cr (by analogy with the diagram of equilibrium structural transformations in steels with 12 % Cr (Figure 4) [7] $\gamma \rightarrow \gamma + \delta$ transformations should proceed at heating above 1360–1400 °C, followed by $\gamma + \delta \rightarrow \delta$ transformations in the subsolidus interval. Under the conditions of a fast temperature rise, the transformation can be restrained and can shift into the region of higher temperatures close to T_S temperature. In the absence of considerable local changes in the composition, in the high-temperature region at subsequent cooling the HAZ metal again undergoes polymorphous transformations: first $\delta \rightarrow \gamma$, then $\gamma \rightarrow \alpha$ with formation of the martensitic structure. This is valid for the overheated section, in which carbon migration caused just formation of a carbon-enriched ridge near the weld, which turned out to be insufficient for appearance of residual δ-ferrite phase.

Rows of grains located at the weld are heated up to temperatures of the level of effective solidus T_S and higher, i.e. up to the intercritical interval $T_S - T_L$ (Figure 5). Here grain boundary partial melting also develops in addition to carbon migration (Figure 5, *a*). The cause for earlier partial melting can be accumulation of elements along the boundaries, which were earlier present in the composition of the dissolved grain-boundary carbides. Closer to the weld and at higher temperature accordingly, the degree of grain body melting rises developing over the surface and inner subboundaries. At this stage carbon liquation into the liquid channels on the former grain boundaries [8–10] at its continuing displacement to the boundaries from the in-depth regions of the grain and its fast migration along these channels into the region of higher temperatures (towards the weld) will lead to depletion in carbon (compared to the nominal composition) of grain sections at the surface-melted boundaries. Carbon diffusion in the grain towards the weld and its shifting into the melt on the subgrains also promote widening of the dimensions of the zones with its lower content.

Reduction of carbon concentration in the grain sections adjacent to the molten channels, should cause an increase of T_S, i.e. in some places at a stationary temperature distribution in the HAZ metal the already started surface melting of the grains will stop, and carbon outflow along the channels will bring about the conditions for the start of intergranular melt solidification (Figure 5, *c*). Channel solidification, accompanied by carbon release from the new solid solution into the liquid ahead of solidification front, will promote formation of stable δ-ferrite in a certain intergranular section, until carbon accumulation in the channel leads to loss of stability of the forming δ-solid solution at cooling or causes solidification of carbon-enriched austenite. In addition, depletion of some volumes of grain bodies in carbon as a result of its liquation and removal through diffusion should also lead to formation of sections of δ-ferrite in them, decarbonized to the degree of ensuring its stability at cooling to room temperature (Figure 5, *d*).

Distribution of chemical elements in HAZ metal and melting zone in a sample of steel P91 after simulation of thermodeformational welding cycle

Analyzed zone	Weight fraction of elements, %					
	Cr	Mo	Ni	Si	S	Mn
HAZ metal	8.39	1.19	0.26	0.48	0	0.23
Melting zone	7.50	0.50	0.38	0.54	0	0.136
	9.60	0.88	0.32	0.58	0.021	0.33
	12.99	1.67	0.28	0.52	0.054	0.25

An additional factor of local stabilization of δ-ferrite is increase of the concentration of ferritizers (chromium, molybdenum) and reduced content of austenitizers — nickel and manganese in the zone of surface-melted boundaries, which was established experimentally. Carbon as an austenitizer should also separate from these microsections. It is possible that the nuclei of stable δ-ferrite form exactly in these sections with an increased content of ferritizers and «deep» depletion in carbon and other autenitizers. Furtheron, including the cooling stage, additional diffusion outflow of carbon and δ-ferrite grain growth start developing from them, as separation of ferritizers from austenitizers occurs more readily in the metal with the initial two-phase ($\gamma + \delta$) than single-phase structure [11, 12]. Such a mechanism is probable also in the case, if there is not enough time for $\gamma \rightarrow \gamma + \delta \rightarrow \delta$ transformation to proceed at fast heating in welding with a low heat input, and intergranular partial melting starts at preservation of overheated austenite. Then formation of δ-ferrite can occur by a reaction, similar to reverse peritectic reaction $\gamma \rightarrow L_C + \delta$, i.e. austenite melting,

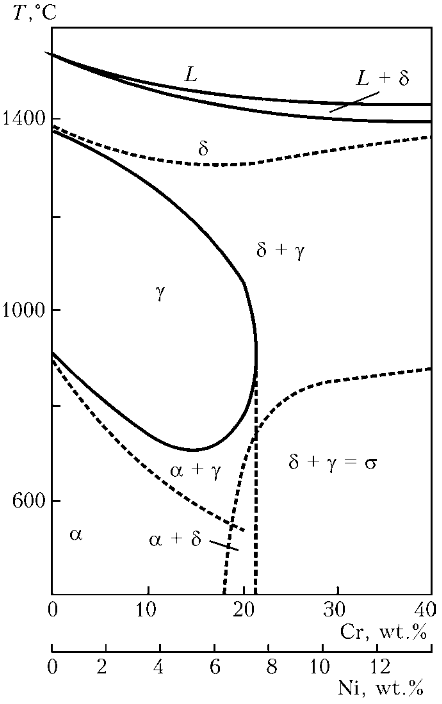

Figure 4. Diagram of equilibrium transformations in steel Fe–12Cr–Ni at the proportion of Cr / Ni = 3 / 1 [7]

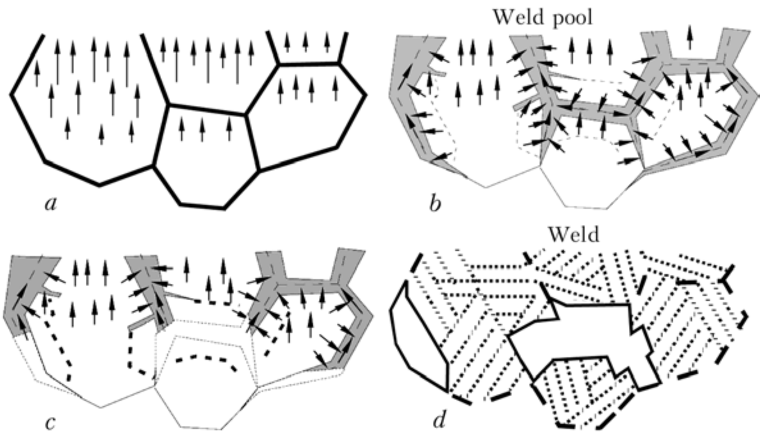

Figure 5. Schematic of the assumed mechanism of δ-ferrite formation in the FZ metal of welded joints on steel with 9 % Cr: *a* — heating and carbon diffusion towards high temperatures; *b* — stage of intergranular partial melting, liquation and migration of carbon along liquid channels; *c* — solidification of intergranular zones with formation of stable δ-ferrite nuclei and their growing into the adjacent grain sections; *d* — resulting structure of martensite with δ-ferrite grains

carbon liquation with formation of carbon-enriched liquid L_C and nucleus of decarbonized δ-ferrite. Further redistribution of carbon, and, to a certain degree, of ferritizers and austenitizers leads to «growing-through» of stable δ-ferrite in the initial grain bulk, as described above.

At liquid solidification, a new boundary forms in the intergranular channel in the zone of abutting of the formed solid phase and «old» grain. Later on this boundary migrates in-depth of one of the grains and takes up the position of δ/γ interphase, while the formed δ-ferrite grain will include parts of adjacent grains, which existed separately before the start of intergranular surface melting (Figure 5, *b*). Boundaries of ferrite grains have the shape of irregular polyhedrons with even regions, which must be associated with the process of polymorphous transformation of the crystalline lattice along certain crystallographic directions. By their chemical composition the ferrite grains almost do not differ from the surrounding martensite [1, 6], so that their growth is associated chiefly with carbon migration. It follows that formation and dimensions of δ-ferrite grains should be determined by overheating temperature and duration of its impact on the FZ metal, which depends on the arc thermal power and resulting thermal cycle of welding.

Carbon accumulation at BM–weld interphase prevents decarbonization, sufficient for δ-ferrite formation, which may cause absence of this phase directly along the boundary with the weld.

In welding of steel with 9 % Cr with high-alloyed austenitic chromium-nickel welding consumables, the highly mobile carbidizers present in them promote carbon outflow into the weld [4, 13, 14]. Apparently, formation of a larger number of δ-ferrite grains in dissimilar joint FZ than in that of a similar joint, is associated with it (see Figure 1). At tempering carbon migration from the FZ into the weld may possibly lead to a certain increase of the dimensions of such grains.

CONCLUSIONS

1. Analysis of experimental observations of structural changes in welded joints on steel with 9 % Cr allowed suggesting a possible mechanism of formation of δ-ferrite grains in the base metal sections adjacent to the welds.

2. An assumption has been made that formation of δ-ferrite in the near-weld zone of welded joints on steel with 9 % Cr is associated with metal overheating up to an intercritical temperature range ($T_S - T_L$) and includes two possible stages: initiation — formation of nuclei in the form of zones with an increased content of ferritizers and lower carbon content due to liquation and migration of carbon towards the weld along the liquid channels; and diffusion depletion in carbon of grain sections adjacent to the nuclei up to the stage of ensuring ferrite stability at lower temperatures.

1. Skulsky, V.Yu. (2005) Metal structure in the fusion zone and HAZ of high-chromium heat-resistant steel welded joints. *The Paton Welding J.*, **5**, 10–18.
2. Kasatkin, B.S. (1991) Micromechanism of cold cracking in welding of medium-alloy steels. In: *Proc. of Int. Seminar on Metallurgical Requirements of Manufacturers and Customers to Weldability of Steel Products* (Kiev, Sept. 10–20, 1991).
3. Gorelik, S.S. (1978) *Recrystallisation of metals and alloys*. Moscow: Metallurgiya.
4. Zemzin, V.N. (1966) *Dissimilar steel welded joints*. Moscow: Mashinostroenie.
5. Likhachev, V.A., Myshlyaev, M.M., Senkov, O.N. (1987) About role of structural transformations in superplasticity. *Fizich. Mekhanika Materialov*, **63**, 1045–1060.
6. Skulsky, V.Yu. (2006) Influence of alloying of filler material and welded steel on fusion zone structure. *The Paton Welding J.*, **1**, 9–15.
7. Akselsen, O.M., Rorvik, G., Kvaale, P.E. et al. (2004) Microstructure-property relationships in HAZ of new 13 % Cr martensitic stainless steels. *Welding J.*, 83(**5**), 160--167.
8. Vogel, H.J., Ratke, L. (1991) Instability of grain boundary grooves due to equilibrium grain boundary diffusion. *Acta Metal. Mater.*, 39(**4**), 641–649.
9. Petelin, A.L. (2003) Model of growing of liquid metal channels on grain boundaries in metals. *Fizika i Khimiya Obrab. Materialov*, **2**, 21–23.
10. Petelin, A.L. (2005) Formation of liquid metal channels on triple grain junctions in metals. *Tekhnologiya Metallov*, **1**, 18–19.
11. Guttmann, M. (1991) Intermediate temperature aging of duplex stainless steels. A review. In: *Proc. of Conf. on Duplex Stainless Steels* (Beaune, France, Oct. 28–30, 1991), Vol. 1, 79–92.
12. Wang, X.G., Dumortier, D., Riquier, Y. (1991) Structural evolution of zerron 100 stainless steel between 550 and 1100 °C. *Ibid*., Vol. 1, 127–134.
13. Livshits, L.S. (1979) *Metals science for welders*. Moscow: Mashinostroenie.
14. Gotalsky, Yu.N. (1992) *Welding of pearlitic steels by austenitic consumables*. Kiev: Naukova Dumka.

INFLUENCE OF STRUCTURAL TRANSFORMATIONS IN WELDING OF ALUMINIUM ALLOY B96 ON FRACTURE RESISTANCE PARAMETERS

T.M. LABUR, T.G. TARANOVA, V.A. KOSTIN, A.Ya. ISHCHENKO, G.M. GRIGORENKO and **V.E. FEDORCHUK**
E.O. Paton Electric Welding Institute, NASU, Kiev, Ukraine

The nature of structural transformation occurring in aluminium alloy B96 during heating in welding was studied by scanning electron microscopy. The composition of the phases and their morphological peculiarities were estimated quantitatively and qualitatively, depending on the thermophysical conditions of nonconsumable electrode and electron beam welding. Effect of the volume content of phases on the processes of initiation and propagation of cracks under the conditions of off-centre fracture of samples of welded joints was evaluated.

Keywords: high-strength aluminium alloy, thermal cycle of fusion welding, heat-affected zone, cooling rate, fracture resistance, microstructure, inclusions, investigations

Structural transformations running in aluminium alloys at the thermal cycle of welding, cause metal softening in the near-weld zone, as well as embrittlement of individual structural components [1--5]. Judging by publications, there is no unambiguous opinion on the influence of slag inclusions and particles on the strength and fracture toughness of welded joints. It is noted that the particles lower the rupture resistance, promote metal fracture ahead of the crack tip, delamination of their surface from the contact boundary with the matrix, etc. For a more complete understanding of the phenomena occurring at the thermal cycle of welding, B96 alloy was studied, which is characterized by high values of mechanical properties, but is difficult to weld [6].

The method of simulation of the thermal cycle of welding by a nonconsumable electrode and electron beam was used for determination of the volume fraction of phases precipitating during the thermal cycle of welding, establishing the features of their morphology and chemical composition, influence on the processes of crack initiation and propagation in the near-weld zone structure. For this purpose flat samples of 36 × 57 mm size with a sharp notch 11 mm deep with 0.1 mm radius in the tip were cut out of a 3 mm sheet. Sample heating modes were selected proceeding from the thermokinetic diagram of transformations of the studied alloys [7]. As a result of heating samples were produced with different structural components identical to those forming in the local sections of HAZ metal in welding of aluminium alloys. Subsequent testing of the processed samples was conducted under the conditions of off-center tension, this allowing in addition to studying the structure, also determining the fracture resistance properties of individual sections. Structural analysis of the particles, precipitating in the alloy at heating and cooling, was performed using a scanning electron microscope JSM-840. Having studied the change of fracture surface relief, features of structural fragments of the fracture in the crack propagation path were noted. Determination of volume fraction of particles located along the grain boundaries, dimensions, shape and topology of distribution allowed establishing the influence of their dependence on the main physicomechanical properties of welded joints in the HAZ metal.

Quantitative assessment of volume fraction of particles in the structure of the studied samples was conducted using a computer program Image Pro 30, which helps isolating the characteristic structural elements based on the colour contrast with subsequent mathematical processing. In combination with Statistica 5.0 program it allows processing the obtained results by one of the statistical approaches, and plot graphic dependencies on their basis.

As shown by the results of investigation of the volume fraction of inclusions, the nature of their distribution is non-uniform at different distances from the notch by sample height (Figure 1). During the thermal cycle of nonconsumable-electrode arc welding, it is equal to 2.0–7.2, electron beam — 0.8–4.0 %. Maximum amount of precipitations in arc welding is observed in as-annealed condition, under the conditions of electron beam welding — in the hardening section. In the overheated condition (550 °C) which simulates the metal of the welded joint fusion boundary, their volume fraction changes in the range of 2.11–3.58 % (minimum compared to other conditions of heating and cooling at the welding cycle), this corresponding to 10 and 18 mm distance from the notch. Heating of B96 alloy up to the hardening temperature (460 °C) in both the welding processes, leads to increase of volume fraction of the inclusions.

Under the conditions of fast cooling of the metal in water, the greatest amount of inclusions (3.9 %) is noted in the section located at 10 mm distance, and the smallest (2.1 %) — at 18 mm from the notch. At cooling in air this value is equal to 6.44 and 2.34 %, respectively. Such a regularity of phase precipitations in the studied alloy is noted at cooling from annealing

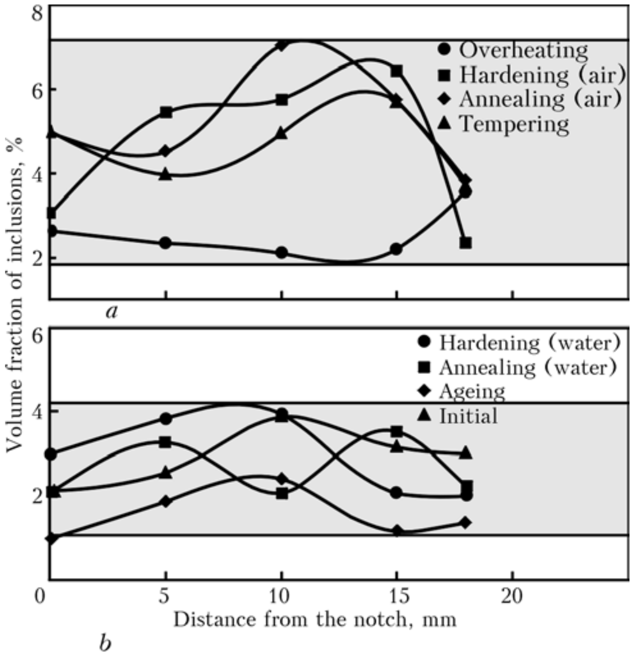

Figure 1. Nature of variation of volume fraction of inclusions by sample height depending on the condition of the metal at heating simulating the conditions of nonconsumable electrode arc (*a*) and electron beam (*b*) welding

temperature (360 °C). Quantity of precipitations at cooling in water is preserved, and in air it increases 2--2.5 times compared to the as-hardened condition of the metal. In as-tempered condition of the metal, the value of volume fraction of the inclusions is close to their values in the annealed condition at cooling in air, and in the ageing condition an abrupt reduction of the phase volume fraction at their coarsening is observed. In the metal section at the notch the amount of volume fraction of the inclusions is 0.77 %, and at 10 mm distance it is 2.42 %, being 2--3 times smaller compared to other heating sections in the HAZ metal. Thus, the established regularities of variation of the volume fraction of inclusions in B96 alloy, depending on heating temperature show that compared to the initial condition, the greatest amount of the phases precipitates at heating up to the annealing condition with cooling in air. This fact can be related to the intensity of processes at coagulation of nonmetallic inclusions in this alloy.

Table 1. Influence of heat treatment and cooling medium on the quantity of inclusions in the metal

Kind of heat treatment	Cooling medium	Volume fraction of inclusions (max / min), %
Hardening (460 °C)	Water	3.97 / 2.00
	Air	6.48 / 2.35
Annealing (360 °C)	Water	3.54 / 2.08
	Air	7.15 / 3.92

Let us consider the influence of heat treatment and cooling medium on the amount of inclusions in the metal (Table 1). From the comparison it is seen that the lower limit of values at hardening is constant and equal to approximately 2 %. Upper limit changes from 3.97 up to 6.48 %, which is indicative of the high sensitivity of B96 alloy to the cooling rate. In as-annealed condition the cooling rate influences both the lower and upper limit. At cooling in water the volume of inclusions is the same as in as-hardened condition, and is equal to 2.08 %, and at cooling in air it is 3.92 %. Upper limit of variation of the volume fraction of inclusions is here equal to 7.05 %, which is practically close to the as-hardened condition.

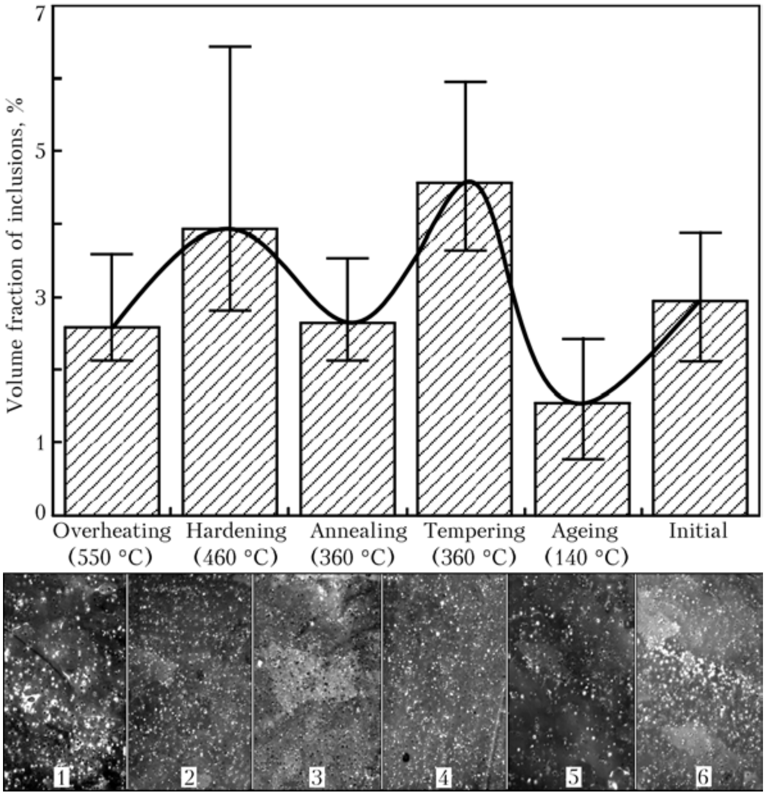

Figure 2. Nature of variation of volume fraction of inclusions and microstructure of B96 alloy depending on thermophysical properties of heating simulating the process of electron beam welding (×200)

The same regularity of phase precipitation is also noted for the upper limit values in samples cooled in air. However, the range of values of volume fraction of phase precipitates in as-hardened condition is wider than at annealing, which is attributable to different rate of phase formation under the studied cooling conditions.

Figures 2 and 3 give the dependence of volume fraction of phase precipitates and microstructure of the studied alloy on the heating conditions in EBW and nonconsumable electrode welding of B96 alloy in different sections of HAZ metal. As is seen from the data in the Figures, the nature of phase distribution in the structures is non-uniform, which is related to temperature-time differences in the processes running at heating and cooling of the studied alloy. Under the conditions of heating in EBW the maximum values of phase precipitation are observed for as-hardened and as-tempered conditions, and minimum ones — in the aged condition. This may lead to deterioration of welded joint properties in the respective section of HAZ metal. Volume fraction of inclusions at overheating and annealing is the same as in the base metal (see Figure 2). Under the conditions of heating simulating nonconsumable electrode welding (see Figure 3), the maximum amount of phase precipitates (5.21 %) is observed in as-annealed condition, which is 2 times higher than after EBW. A reverse regularity is observed in the metal in as-hardened condition. The noted features of the microstructure are due to a difference in the rate of metal cooling after the respective welding heating. In welding of samples by the electron beam change of volume fraction of inclusions is of a sinusoidal nature, under the conditions of nonconsumable electrode process the noted dependence is disturbed due to increase of the duration of the thermal cycle in welding.

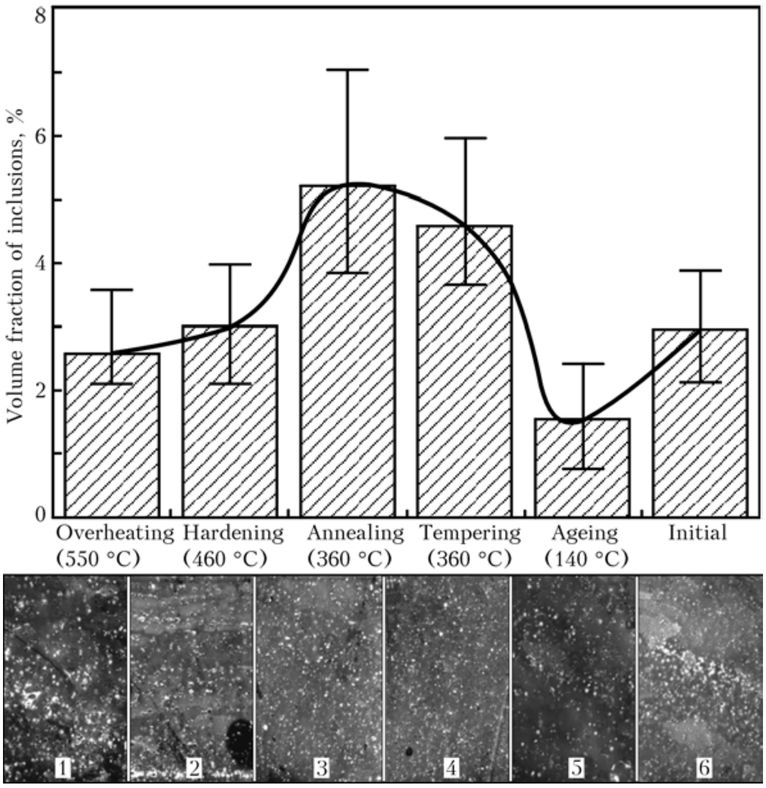

Figure 3. Nature of variation of volume fraction of inclusions and microstructure of B96 alloy depending on thermophysical conditions of heating simulating the process of nonconsumable electrode arc welding (×200)

During investigation of the morphology of arrangement of particles precipitating at welding heating, it is established that impact of the thermal cycle leads to formation of three to five different kinds of precipitations in the alloy, in addition to the undissolved inclusions of intermetallic phases.

The used computer procedure of determination of volume fraction of inclusions contained in the studied samples, did not allow identifying them separately, which is associated with insufficient resolution of Image Pro program by colour contrast. In this connection when studying the features of structure morphology, samples were cut out of the crack propagation zone in the section transverse relative to the rolling direction, as this is exactly the direction in semi-finished products of aluminium alloys which is characterized by the lowest level of properties. According to [8], B96 alloy contains phase inclusions, the composition of which consists of compounds of the main alloying elements, %: 26–28 Cu; 38–40 Zn; 11–14 Mg. Their shape and dimensions in the structure are determined by the heating temperature and cooling conditions of the metal in the HAZ. Under the thermophysical conditions simulating EBW, phase dimensions vary in the range of 1.77–4.94 μm, and in nonconsumable electrode welding — 2.50–7.82 μm. They are located in cluster form predominantly along the boundaries of grains oriented along the rolling direction.

Microstructure of B96 alloy in overheated condition typical for base metal along the fusion boundary, is characterized by the presence of three kinds of phase precipitations (Table 2). Stoichiometric formula of the white-coloured phase can be identified as $MgZn_2$. It has the predominantly round shape of 0.5–20 μm size and is located in the solid solution volume (Figure 2, 3, position 1). Grey-coloured particles of an

Table 2. Influence of the heating and cooling conditions on the kind of inclusions

Phase colouring	Over-heating (550 °C, 3 s)	Hardening (460 °C, 1 h, water)	Hardening (460 °C, 1 h, air)	Annealing (360 °C, 20 min, water)	Annealing (360 °C, 20 min, air)	Tempering (360 °C, 3 min)	Ageing (140 °C, 7 h)	Base metal (20 °C)
White	$MgZn_2$							
Grey	Fe_2SiAl_8							
Dark	Mg_2Si							
Dark with white fringe	--	$Mg_3Zn_3Al_2$						
Grey with black fringe	--	--	Al–$Mg_3Zn_3Al_2$--$MgZn_2$	--	Al–Mg3Zn_3Al_2–$MgZn_2$	–	Al--Mg3Zn_3Al_2--$MgZn_2$	
Total quantity of phases	3	4	5	4	5	4	5	

acicular shape, may belong to Fe_2SiAl_8 compound. Dark-coloured particles, which have much smaller dimensions, can be regarded as Mg_2Si phase. All the enumerated phases are in the solid solution. Eutectic formations 2–15 μm long and 0.3–0.7 μm wide, probably, of $Mg_3Zn_3Al_2$ composition are clearly seen along the grain boundaries [8]. After hardening and cooling in air five varieties of round-shaped phases are found in the alloy microstructure (Figure 2, position 2), which are non-uniformly located in the grain bulk and along their boundaries. Unlike the previous condition, complex phases (grey-coloured with a white fringe) are present in the metal bulk, which are coarser compared to other types of inclusions.

Increase of cooling rate of the metal heated up to the hardening temperature, reduces the amount of phase precipitations to four kinds. They are smaller in size (1.77–4.94 μm) and the nature of their location is non-uniform. No dark-coloured particles with a white fringe, which are an eutectic, have been detected, which is indicative of the influence of the metal cooling rate not only on the precipitation volume, but also on the diversity of the kinds of phase precipitates at the thermal cycle of aluminium alloy welding. Similar to the as-hardened condition, four kinds of phases can be singled out in the metal structure in the condition after annealing and cooling in water (Figure 2, position 3). Three of them belong to the basic composition of the studied alloy given above. Grey-coloured phase with a dark fringe is absent in the structure, which is, probably, due to the heating temperature and cooling medium. Action of such a temperature for a relatively long time at metal cooling in air is sufficient for precipitation of five kinds of phases (Figure 3, position 2). Coarse coagulated particles are chaotically located in the grain bulk, and finer particles are located in the form of stringers along the boundaries. A feature of this structure is presence of complex grey-coloured particles with a black fringe. In the aged condition the metal contains all the five types of the coarser phases, their quantity being greater than under other heating conditions (Figures 2, 3, position 5). Five types of phases were also observed in the base metal (Figures 2, 3, position 6), their string arrangement relative to the direction of rolling, non-uniform distribution of phases, as well as a large amount of complex precipitates being clearly visible in the microstructure.

Thus, the conducted investigations provide convincing proof that during heating inherent to the welding cycle, aluminium alloy B96 contains different amounts of phases dependent on temperature and cooling medium. At overheating only three phase types are present, consisting of the main alloying elements. As this condition is characterized by a high temperature, the process of surface melting of the grains predominates, compared with the phase precipitation process.

Four types of phases are associated with the conditions of temperature (tempering) and cooling rate at hardening and annealing. In this case, a complex dark-coloured phase with a white fringe appears, which forms at metal cooling at a high rate or under the conditions of a short-term (3 min) heating (see Table 2). Five types of phases are associated with appearance of additional complex grey-coloured phase with a black fringe. It is possible that they have a eutectic composition, as under the conditions of off-center tension of the sample they behaved as brittle fracture sites.

Results of mechanical testing for off-center tension of samples of B96 alloy in different thermal conditions showed (Table 3) that increase of the volume fraction of the phases at heating and unfavourable shape of their precipitates along the grain boundaries facilitate crack initiation and propagation, this lowering the alloy ability to develop local plastic deformation.

Metal cooling rate has the strongest influence on the level of crack propagation energy (LCPE), the value of which in the overheated condition is equal to 4.3 J / cm^2. At fast cooling (in water) after hardening, this index is equal to 2.2–2.7 J / cm^2. Its lowest values (0.5 J / cm^2) correspond to the base metal in the initial condition, and to the sample after cooling in air simulating the conditions of nonconsumable electrode welding. Maximum values of LCPE (5.4 J / cm^2) are found in the alloy structure after heating up to the tempering temperature (360 °C). In the HAZ metal section, where ageing occurred during welding heating, this index is equal to 1.1 J / cm^2.

Table 3. Influence of heating conditions on fracture toughness characteristics of B96 alloy in different temperature sections of the HAZ metal of welded joints

Heating conditions	σ_f, MPa	$\hat{E}_{ñ}$, MPa$\sqrt{m}$	J_c, J / cm^2	LCPE, J / cm^2
Overheating (FZ) (550 °C, 3 s)	415	22.1	6.3	4.3 / 2.0
Hardening (460 °C, 1 h)	499 / 427	12.9 / 12.9	8.6 / 8.0	2.2 / 2.7
Annealing (360 °C, 20 min)	343 / 401	15.1 / 5.5	8.0 / 6.3	2.7 / 0.5
Tempering (360 °C, 3 min)	373	26.8	10.6	5.4
Ageing (140 °C, 7 h)	251	8.1	3.5	1.1
Initial condition	453	5.5	3.6	0.5

Note. Numerator gives the results of testing after heating and cooling in water, simulating the EBW conditions, denominator — after heating and cooling in air, the modes of which simulate the heating conditions in arc welding.

Value of critical stress intensity factor, K_c, is also determined by the metal cooling rate, particularly after heating up to the annealing temperature. In this case value K_c decreases 3 times.

Structural changes occurring at artificial ageing of B96 alloy lead to lowering of not only the values of the rated breaking stress 1.5 times, but also other fracture toughness indices (K_c = 8.1 MPa$\sqrt{\text{m}}$, J_c = = 3.5 J / cm^2, LCPE = 1.1 J / cm^2).

Thus, the obtained investigation results give an idea about the structural changes occurring in B96 alloy during process heating, and their influence on the ability of the alloy welded joints to resist crack initiation and propagation at fracture. The fact that the observed phenomena run within the bounds of certain thermophysical conditions points to the need to allow for them in development of the joining technology.

CONCLUSIONS

1. Regularities of formation of structural inhomogeneity in the HAZ metal of B96 alloy under different thermophysical conditions of fusion welding have been established. It is shown that at welding heating the formed structure of welded joints determines the physicomechanical properties, depending on the welding process and mode. Degree of property change depends on the volume fraction of the phases and inclusions, associated with the initial condition of the alloy and welding process.

2. Quantitative and qualitative evaluation of phases precipitating in the near-weld zone of B96 alloy under the impact of the thermal cycle of welding has been conducted. Influence of volume fraction of the phases on the processes of crack initiation and propagation at fracture has been established.

3. Heating and cooling conditions have been investigated, at which a uniform structure with a minimum volume of brittle precipitates of intergranular interlayers forms, the interlayers providing high values of the characteristics of metal resistance to crack initiation and propagation at fracture of a welded joint on B96 alloy.

1. Davydov, V.G. (1997) Metals science and technological researches of aluminium-lithium alloys at the current stage. *Tekhnologiya Lyog. Splavov*, **5**, 15–25.
2. Fujiwara, T. (2001) Technologies of joining of light metals in aircraft and space engineering. *Keikinzoku Yosetsu*, 39(**3**), 1–11.
3. Kiyoto, S. (1993) Materials and joining technologies for rocket structures. *J. JWS*, 62(**8**), 46–52.
4. Ishchenko, A.Ya., Sklabinskaya, I.E. (1979) Peculiarities of transformations in heat-affected zone during welding of some high-strength aluminium alloys. *Avtomatich. Svarka*, **5**, 26–29.
5. Rabkin, D.M. (1986) *Metallurgy of fusion welding of aluminium and its alloys*. Kiev: Naukova Dumka.
6. (1974) *Aluminium alloys. Structure and properties of aluminium-alloy semi-finished products*: Refer. Book. Ed. by V.A. Livanov. Moscow: Metallurgiya.
7. (1979) *Aluminium alloys (properties, treatment, application)*: Refer. Book. Ed. by H. Nilsen et al. Moscow: Metallurgiya.
8. Mondolfo, L.F. (1979) *Structure and properties of aluminium alloys*. Moscow: Metallurgiya.

ABRASIVE WEAR BEHAVIOUR OF Fe–Cr–C OVERLAYS

K.B. SHAH[1], **S. KUMAR**[1] and **D.K. DWIVEDI**[2]
[1]National Institute of Technology, Hamirpur, India
[2]Indian Institute of Technology, Roorkee, India

Present paper describes the influence of number of passes on abrasive wear resistance of Fe–Cr–C hardfacing on mild steel. Overlays were deposited by a gas metal arc (GMA) welding processes using a commercially available surfacing electrodes of 4.0 mm diameter. Overlays were deposited using welding current of 160 A. One, two and three pass coatings were developed using DCSP at constant welding speed of 15 cm / min. The abrasive wear resistance of overlays was evaluated on a pin on disc system against a 320 grade SiC abrasive medium at two normal loads of 2 and 10 N. Wear pin of 6 × 6 × 20 mm size was used for abrasive wear test. Optical microscopy was used to study the microstructure of overlays. SEM studies of wear surface were carried out to analyze the wear mechanism. Increase in number of welding passes increases the abrasive wear. Variation in the hardness across the interface was noticed.

Keywords: chromium carbide, welding current, number of passes, microstructure, abrasive wear, micro-cutting, hardness, dilution, overlays

Hardfacing involves the application of good quality wear-resistant overlays by welding on comparatively cheaper substrate. Surfacing needs controlled melting of base metal and deposition of good quality wear resistant layer on substrate [1–3]. The less sensitive control of deposition of overlays during the welding causes penetration of weld metal into the base metal which, in turn, dilutes the quality coating [4, 5]. Wear resistance of hardfacing alloys is largely governed by its microstructure. Wear of iron-base hardfacing alloys to a great extent depends on hard phases like metal carbide (MC, i.e. M_7C_3 and M_3C) and borides (MB_2, i.e. M_3B_2, M_2B and $M_{23}C_3$ type) [3, 6]. According to the microstructure hardfacing alloys can be divided into five categories, i.e. carbide-, boride-, silicide-, intermetallic- and solid solution type [3]. Recently many studies have been reported on the influence of alloy compositions [5, 7–9], heat treatment [10], welding parameters [2, 4], sliding conditions [3, 5, 10–15] and microstructure [10, 16] on the abrasive wear behaviour of Fe–Cr–C hardfacing. Authors of [7, 14] studied the effect of chromium content on abrasive wear behaviour of Fe–Cr–C coating. Dwivedi [4] has reported the influence of welding procedure on abrasive wear behaviour of low carbon and low chromium iron-base hardfacing and found that increase in welding current lowers the wear resistance and increases the dilution of hardfacing alloys.

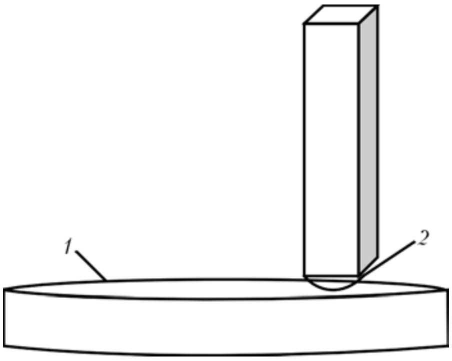

Figure 1. Principle diagram of wear testing set up: *1* — counter surface covered with 320 grade SiC paper; *2* — wear pin 6 × 6 × × 20 mm with hardfaced end

In the present work, attempts have been made to investigate the influence of number of passes on microstructure, hardness and abrasive wear behaviour of Fe–Cr–C hardfacing deposited on the mild steel substrate. Effect of the sliding parameters, like sliding distance, and normal load on the abrasive wear has also been investigated.

Experimental procedure. An iron-based hardfacing alloy (Table) was used for overlaying the mild steel using GMA welding. Overlays were produced by DCEN GMA welding using 160 A welding current. Multipass coatings (1–3 layered) were deposited. Transverse section of the hardfaced steel was metallographically polished using standard metallographic polishing techniques and etched in 0.1 % Nital solu-

Chemical composition (wt.%) of base metal and electrode used for hardfacing

Metal Chemistry	C	Si	Mn	S	P	Cr	V	Mo
Electrode	3.0–4.0	0.5–0.7	0.4–0.6	–	–	30–32	0.10–0.15	0.18–0.24
Base	0.15–0.20	0.8–1.2	0.7–0.9	0.04	0.05	–	–	–
Note. Fe — balance.								

tion. A Reichert Jung (MEF-3) optical microscope was used for the examination of microstructure of overlays. Scanning electron microscope (Leo-435-VP, England) was used to study the worn out surface of wear pins. The samples were cleaned with acetone and fixed on the studs meant for the purpose in the SEM. Rockwell hardness test (HRC) was conducted to measure the hardness of overlays.

Abrasive wear test (two-body) was carried out using the pin on disc wear friction monitor (TR-20L, DUCOM) (Figure 1). Rectangular-shaped specimens having dimension 6 × 6 × 40 mm were cut from the

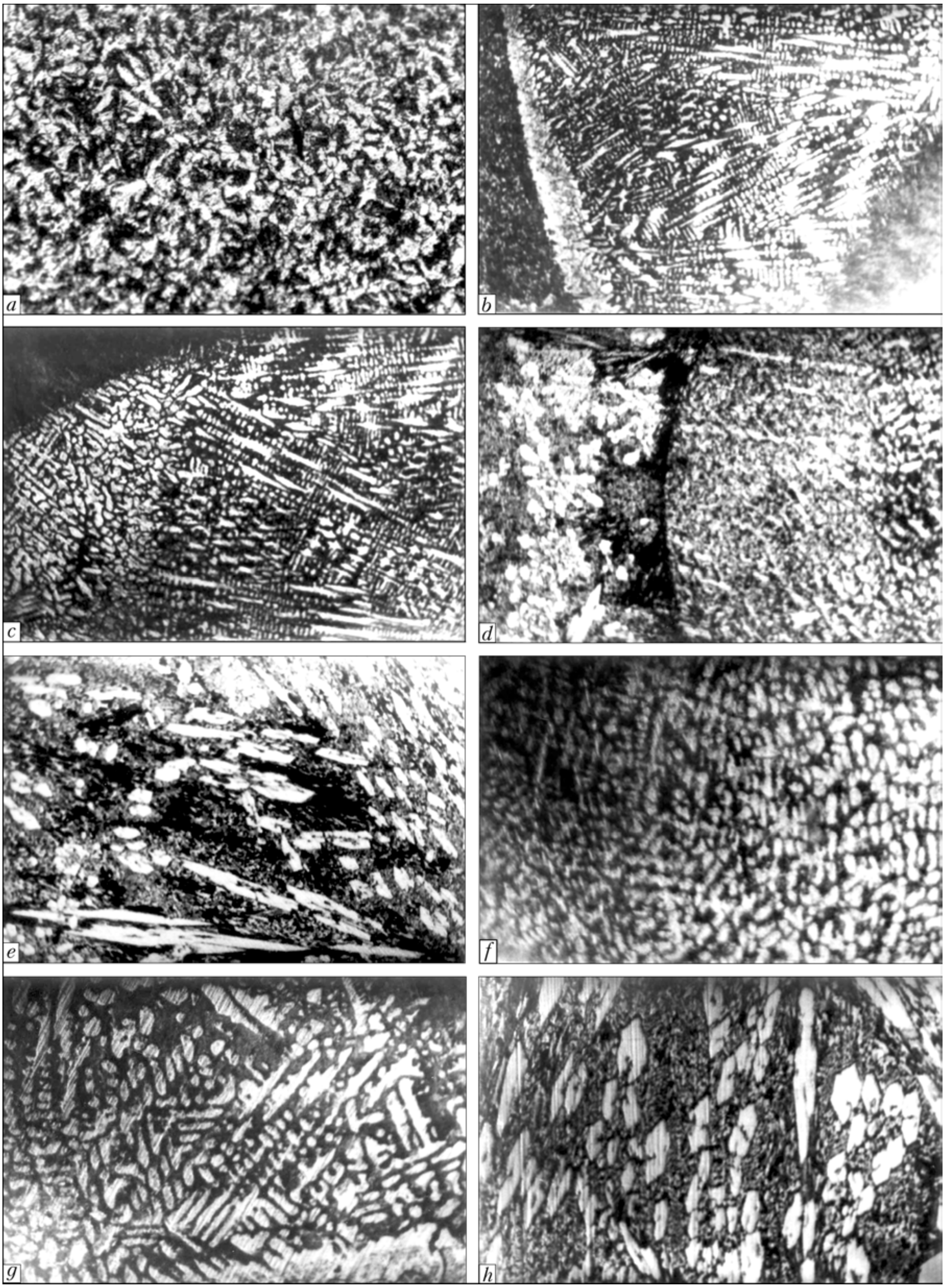

Figure 2. Optical micrographs of steel substrate (*a* — ×200), interfaces of base metals and first layer showing the good bonding (*b* — ×100), of first and second layers (*c* — ×100), of second and third layers (*d* — ×100), microstructure of third (*e* — ×100), first (*f* — ×250), second (*g* — ×250) and third layers (*h* — ×250)

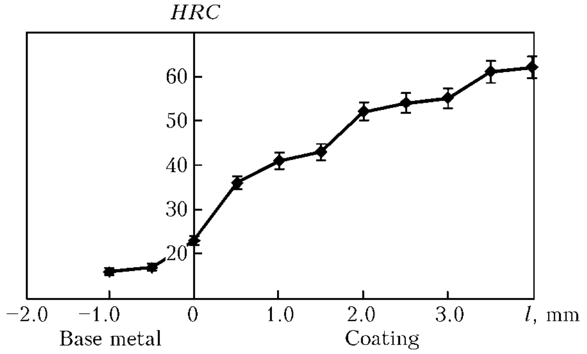

Figure 3. Variation in hardness across the interface and in the 3-layered coating

hardfaced samples of steel. The samples were ground to remove the sharp edges before sliding tests. Emery paper embedded with the desired size of SiC particles (320 grade) was used as abrasive medium. The specimen was fixed with a locking arrangement against the abrasive medium. Load was applied on the specimen by cantilever method. The sample was made to slide at two normal loads of 2 and 10 N at constant sliding speed of 1.0 m / s against abrasive medium fixed on the counter surface. A Mettler microbalance (accuracy 0.1 mg) was used for weighing the specimens before and after the sliding. Weight loss was used as a measure of wear. Wear rate was calculated using weight loss per unit sliding distance. The specimen was cleaned with acetone prior to and after the wear test. Each test was conducted with fresh abrasive paper. Tests were carried out up to a sliding distance of 200 m. Wear rate was calculated from weight loss measurement after every 50 m sliding distance.

Results and discussion. Microstructure of structural steel substrate (Figure 2, *a*) shows that there are two mainly phases in the steel substrate, i.e. ferrite and pearlite. Coating showed good bonding with the substrate and in the inter-passes (Figure 2, *b*–*d*). Microstructure at the interface of single (Figure 2, *b*), double (Figure 2, *c*) and third layer (Figure 2, *d*) at low magnification shows the structural variation, i.e. gradually reducing proportion of austenite metallic cells and increasing the content of eutectic of carbides and austenite. Third layers showed entirely different microstructure of overlays compared to the two earlier overlays in terms of presence of large elongated and polyhedral shape primary carbide particles in the matrix of eutectic (Figure 2, *e*). Columnar dendritic structure was observed in overlays close to the interface. Constituents of eutectic are austenite and carbide along the grain boundary of austenite. Closer look of overlays at higher magnification of coating produced using single (Figure 2, *f*), double (Figure 2, *g*) and three (Figure 2, *h*) layers. Structure is finer in case of single layer (Figure 2, *f*) than double layer (see Figure 2, *g*) overlay and amount of primary metallic cells of austenite is dominating over the eutectic in the inter-dendritic regions. Microstructure of third layer mainly exhibits the primary carbide particle in the matrix of the eutectic and independent austenitic phase appears to absent in structure. These structural variations are attributed to two factors, i.e. difference in cooling rate and extent of dilution with increasing number of layers. These coatings are known to have poor thermal conductivity as compared to the mild steel matrix, therefore would produce low cooling rate during the solidification of second and third overlays. Reduced dilution in case of second layer and third layer can attributed to the presence of higher amount of eutectic in second layer and primary carbide particles in the third layer.

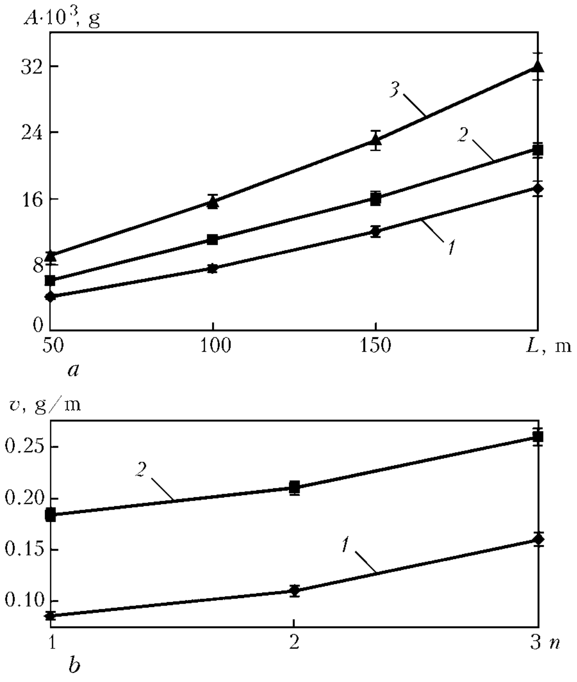

Figure 4. Hardfacing weight loss *A* versus sliding distance *L* relationship at 2 N normal load for first (*1*), second (*2*) and third (*3*) layer (*a*), and wear rate of overlays *v* as a function of number of passes *n* at 2 (*1*) and 10 N (*2*) normal loads (*b*)

Microstructural features, such as amount of massive primary or secondary carbides, tempered or untempered martensite, retained austenite; internal notches are important factors which should be considered in the analysis of wear behaviour of these overlays [17]. Phases of iron-base alloys systems, such as austenite, chromium carbide, eutectic of austenite-carbide, martensite, predominantly affect the abrasive wear. Most abrasion-resistant phase in these alloys is primary carbide with austenite-carbide eutectic. Second most abrasion-resistant phase in these alloys is near-eutectic austenite-carbide.

Hardness of coating produced under different welding conditions was tested on Rockwell hardness tester. Increase in number of passes increased the hardness of coatings. Variation of hardness across the interface is shown in Figure 3. It can be seen that hardness of overlays increases with the distance *l* from the interface in the coating and is primarily attributed to dilution. Dilution decreases with increase in number of passes and, therefore, increases hardness. Dilution produces overlay having the composition different from that of electrode. Microstructure of overlays is known to influence the mechanical properties such as strength, hardness, and toughness. Hardness is defined as measure of abrasive wear but in fact it is not the only characteristics controlling the loss of material under abrasive conditions.

Wear behaviour of overlays at different normal load, sliding distance and number of passes is shown in Figure 4. Variation of weight loss with sliding distance at 2 N normal loads is shown in Figure 4, *a*. It can be seen that the weight loss increases with increase in sliding distance irrespective of number of passes. Wear behaviour of overlays as a function of number of pass exhibits (Figure 4, *b*) that the increase in number of passes increases the wear rate under identical conditions. Increase in normal load as expected increases the wear rate.

The worn surfaces of samples after completion of the tests under varying conditions were studied under SEM to explain the mechanism responsible for material removal under different abrasive wear conditions. SEM images of wear surface show the uninterrupted continuously running abrasive scoring marks (Figure 5, *a, d*). It appears that increase in number of passes reduces the penetration but reduced toughness of the overlays which can promote micro cutting and brittle fracture especially at high load. It can be seen that ridges formed due to abrasion are subjected plastic deformation in the direction perpendicular that of scoring marks also leads to detachment of material in form debris, as evident from the Figure 5, *b, c*. Some interruption in scoring marks can be seen in three layer coatings (Figure 5, *e, f*) and, probably, it is due to presence polyhedral shape primary carbide particle in the comparatively soft matrix. Material under abrasive wear conditions is primarily removed by abrasion and micro cutting, and both these mechanisms need penetration of materials by hard abrasive particle which in turn in depend the hardness of material. So, hardness of overlays plays a significant in controlling the wear during the sliding [17].

Dilution reduces the amount of eutectic carbides and primary carbide which, in turn, adversely affects

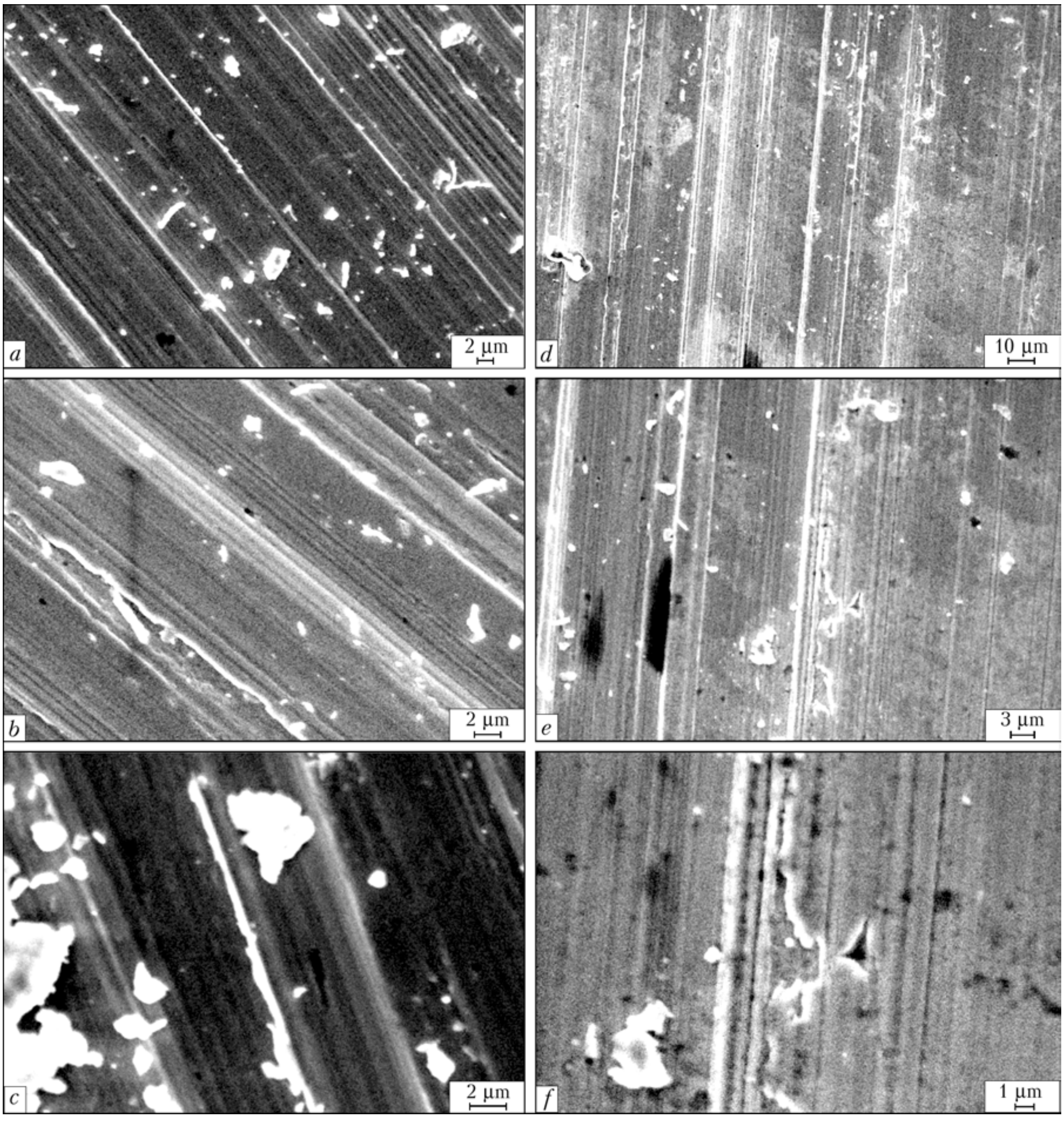

Figure 5. SEM images of wear surface of overlays after sliding at 10 N of single (*a*–*c*) and three pass overlays (*d*–*f*)

the wear resistance and therefore can also be attributed to variation in hardness of the coating across the interface (see Figure 3). Dilution changes the composition of overlays and hence the microstructure. Intermixing of low carbon steel with electrode material during the welding reduces the actual content of carbon and alloying elements in overlays which, in turn, can reduce hardnenability, and increase the amount of soft phases due to that wear resistance may adversely affected [4, 5, 10]. Observation reported in [11, 12] that with low carbon and high chromium offers better wear resistance than the one consisting of more carbon but less chromium supports to the results obtained in this study. Carbon content is an important factor determining microstructure of iron-based hardfacing electrodes and therefore its wear resistance. These results are also in line of work [2] that abrasive wear resistance is not simply related to the hardness of the overlays but is largely determined by toughness of overlays specially when abrasive particle are large in size.

CONCLUSIONS

High chromium and high carbon overlays deposited using varying number of layer on steel substrate were investigated for variation in microstructure, hardness, wear behaviour and surface morphology of wear surface and following points were concluded:

1. Even first layer of hardfacing on steel substrate showed good bonding with substrate. Microstructure in the first and second layer primarily exhibited eutectic in the inter-dendritic region of metallic cells of austenite. However, third layer showed the presence of polyhedral shape primary carbide particles in the matrix of eutectic (carbide and austenite).

2. Variation in hardness across the interface was observed. Increase in distance from the interface has shown improvement in the hardness. Increase in number of passes has shown increase in hardness of respective layers.

3. Weight loss has been found to increase with sliding distance. Moreover, highest weight loss was noticed with overlays deposited using three of layers / passes compared to one- and two-layer overlays.

4. SEM study has revealed that loss of materials from the overlays primarily takes place by scoring, micro cutting and plastic deformation and fracture of ridges formed by abrasion. One-pass overlay showed uninterrupted abrasive marks while three-layer overlays showed some interruption in these marks. Plastic deformation of ridges was noticed only with one-layer overlays not with three-layer ones especially at high magnifications.

1. Ghosh, P.K., Kaushal, O.P., Sharma, S.K. (1992) *ISIJ*, 32(**2**), 250.
2. Chatterjee, S., Pal, T.K. (2003) *Wear*, 255(**1**), 417–425.
3. Su, Y.L., Chen, K.Y. (1997) *Ibid*., **209**, 160–170.
4 Dwivedi, D.K. (2004) *Surface Eng*., 20(**2**), 87–92.
5. Dwivedi, D.K. (2004) *Materials Sci. and Technology*, 20(**10**), 132
6. Berns, H., Fischer, A. (1997) *Materials Characterization*, 39(**2 / 5**), 11, 499–527.
7. Dasgupta, R., Prasad, B.K., Jha, A.K. et al. (1997) *Ibid*., 209(**1**), 255–262.
8. Dasgupta, R., Thakur Rashmi, Yadav, M.S. et al. (1999) *Ibid*., 236(**1**), 368–374.
9. Lee, K., Lee, S.H., Kim, Y. et al. (2003) *Ibid*., 255(**1**), 481–488.
10. Dwivedi, D.K. *ISIJ* (accepeted).
11. Jha, A.K., Prasad, K., Dasgupta, R. et al. *J. Materials Eng. and Performance*, 8(**2**), 190–196.
12. Jha, A.K., Gachake, A., Prasad, B.K. et al. (2002) *Ibid*., 11(**1**), 37–45.
13. Dasgupta, R., Prasad, B.K., Jha, A.K. et al. (1998) *Materials Transact. JIM*, 39(**12**), 1191–1196.
14. Kumar, S., Mondal, D.P., Khaira, H.K. et al. (1999) *J. Materials Eng. and Performance*, 8(**6**), 711–715.
15. Colaco, R., Vilar, R. (2003) *Wear*, 255(**1 / 6**), 643–650.
16. Buytoz, S., Mustafa, M., Eren, H. *Materials Letters* (in press).
17. Francis, J.A. (2002) *Sci. and Techn. of Welding and Joining*, 7(**5**), 331–338.

SELECTION OF STEEL FOR CRITICAL BUILDING WELDED STRUCTURES

V.A. KOVTUNENKO[1], **A.M. GERASIMENKO**[1] and **A.A. GOTSULYAK**[2]
[1]E.O. Paton Electric Welding Institute, NASU, Kiev, Ukraine
[2]Ukrainian R&D Institute of Structural Materials «Prometej», Mariupol, Ukraine

High-strength sparsely-alloyed steel 06G2B meets the current requirements to materials for critical metal structures applied in construction and mechanical engineering. Comparative analysis of steel 06G2B and other steels usually used in the local metal structures has been performed. Results of investigation of service properties of 06G2B rolled stock and welded joints are presented. It is shown that the steel has a certain potential for application in fabrication of critical metal structures.

Keywords: high-strength sparsely-alloyed steel, microalloying, strength properties, cold resistance, weldability, critical building metal structures

For a number of years Ukrainian R&D Institute of Structural Materials «Prometej» and the E.O. Paton Electric Welding Institute have been jointly working on development of a new steel for bridge and other critical building metal structures. A series of studies on optimizing the steel composition allowed lowering the content of carbon (≤ 0.09 %), sulphur and phosphorus (≤ 0.03 %), and absence of nickel is compensated by microadditives of carbide- and nitride-forming elements. As a result of studies, a steel was proposed, which combines a high strength and impact toughness due to limitation of the content of carbon, sulphur and phosphorus, and microalloying with niobium, vanadium and molybdenum in an optimum proportion, modifying treatment with calcium-containing reagents, as well as maximum refinement of the structure at thermal improvement or heat treatment [1, 2].

Due to its chemical and structural homogeneity 06G2B steel has high strength properties in directions x, y and z. Metal does not lose its properties after mechanical ageing, has good weldability, is readily adaptible to fabrication when used in site.

Low susceptibility of steel to mechanical ageing was achieved as a result of limitation of carbon and nitrogen content and their complete binding into carbides, nitrides, carbonitrides at deoxidation and microalloying. Refining of liquid steel up to a low sulphur content, reducing the quantity and dimensions of nonmetallic inclusions and diffusion degassing during the sheet cooling by special modes after their rolling, provide a high resistance of the rolled sheets to lamellar cracking (Z-properties) and guaranteed continuity indices.

Results of investigation of physico-mechanical properties and weldability of test and pilot-production batches were the basis for development and approval of specifications for rolled sheets of weldable quality steels 06GB of strength class 355–390 and 06G2B of strength class 440-490 (TU U 14-16-150–99).

Sparsely-alloyed steel 06G2B of a higher strength and cold resistance for metal structures (including bridge structures), offers certain advantages compared to steels usually used in local metal structures.

Chemical analysis of the compared steels in keeping with the specification is given in Table 1, mechanical properties and impact toughness — in Table 2. Steel 06G2B ensures impact toughness indices KCV at –20, –40 and –60 °C equal to 98, 78 and 59 J / cm^2, respectively.

Good weldability of steel 06G2B is the result of minimum required total alloying, providing the value of carbon equivalent $C_{eq} < 0.41$ %. Calculation was conducted to European standard by IIW formula, Table 3:

$$C_{eq} = C + \frac{Mn}{6} + \frac{Cr + Mn + V}{5} + \frac{Ni + Cu}{15}.$$

Reduction of carbon content in 06G2B steel promotes grain refinement, lowers the sensitivity to stress concentration, which is favourable both for endurance and cold resistance of the material and structures made of it, particularly welded structures.

Low content of impurities is an indubitable advantage of 06G2B steel. It leads to lowering of susceptibility to hot cracking in welding, improvement of corrosion and cold resistance.

PWI has conducted comprehensive studies of a commercial batch of 06G2B steel 30 mm thick of 440 strength class (supplied to TU U 14-16-150–99 by «Azovstal» Metallurgical Works), as well as optimization of welding technology and technique.

Steel was produced in an oxygen-blown vessel of 360 t capacity with subsequent treatment by liquid synthetic slag and blowing with powder-like silica-calcium in an argon jet, this providing a low content of sulphur, phosphorus and non-metallic inclusions. Pouring was conducted in a continuous-casting machine.

Tables 4, 5 give the results of mechanical testing of 06G2B steel rolled stock. Strength properties along and across the rolled stock are practically on the same level, and correspond to the norms of TU U 14-16-

Table 1. Composition of steels applied for critical metal structures

Steel grade	Standard document	Strength class	Weight fraction of elements, %						
			C	Si	Mn	Cr	Ni	Cu	S
09G2S	GOST 19281–89	295 325 345	≤ 0.12	0.50–0.80	1.30--1.70	≤ 0.30	≤ 0.30	≤ 0.30	≤ 0.040
10KhSND	GOST 19281–89	390	≤ 0.12	0.80–1.10	0.50--0.80	0.60–0.90	0.50–0.80	0.40–0.60	≤ 0.040
16G2AF	GOST 19281–89	440	0.14--0.20	0.30–0.60	1.30--1.60	≤ 0.40	≤ 0.30	≤ 0.30	≤ 0.040
09G2SYuCh	TU U 322-16-127–97	325 390	0.08--0.11	0.30–0.60	1.90--2.20	≤ 0.30	≤ 0.30	< 0.30–0.60	≤ 0.015
06GB	TU U 14-16-150–99	390	0.04--0.08	0.15–0.35	1.10--1.40	≤ 0.20	≤ 0.35	0.15–0.30	≤ 0.010
06G2B		440	0.04--0.08		1.30--1.60				
		490	0.05--0.09		1.50--1.60				

Table 1 (cont.)

Steel grade	Weight fraction of elements, %						
	P	Nb	Ti	Mo	V	N	Other
09G2S	≤ 0.035	–	≤ 0.03	–	–	–	–
10KhSND	≤ 0.035	–	≤ 0.03	–	–	–	–
16G2AF	≤ 0.035	–	–	–	0.08–0.14	0.015–0.025	–
09G2SYuCh	≤ 0.020	–	–	–	–	–	REM 0.002–0.005
06GB	≤ 0.020	0.01–0.03	≤ 0.20	0.01–0.03	0.04–0.07	≤ 0.01	≥ 0.001 Ñà 0.02–0.05 Al
06G2B		0.03–0.05		0.05–0.08			
		0.03–0.05		0.05–0.08			

Table 2. Mechanical properties of steels applied for critical metal structures

Steel grade	Standard document	Strength class	Metal thickness, mm	σ_y, MPa	σ_t, MPa	δ, %	KCU, J / cm^2, at T, °Ñ			
							–40	–70	Mechanical ageing	
									+20	–20
09G2S	GOST 19281–89	295	20–32	295	430	21	29	24	29	–
		325	10–20	325	450	21	34	29	29	–
		345	Up to 10	345	490	21	39	29	29	–
10KhSND	GOST 19281–89	390	Up to 10 10–15 15–40	390	510	19	44 39 39	34 29 29	29	–
	GOST 6713–91	390	8–15 16–32 33–40	390	530–685 530–670 510–670	19	39	29	29	29
16G2AF	GOST 19281–89	440	20–32	440	590	19	39	29	29	–
09G2SYuCh	TU U 322-16-127–97	325 390	8–20 21–30 31–40	450 430 400	570 560 530	19	39 39 –	29	39	29
06GB 06G2B 06G2B	TU U 14-16-150–99	390 440 490	8–50	390 440 490	--	22 22 20	–	–	–	–

Table 2 (cont.)

Steel grade	*KCV*, J / cm^2, at *T*, °Ñ				
	0	–20	–40	–60	–70
09G2S	–	--	--	–	--
	–	--	--	–	—-
	–	--	--	–	--
10KhSND	– 40 40	-- -- 40	--	–	--
	–	--	29	–	--
16G2AF	–	--	--	–	--
09G2SYuCh	–	39	29	–	29
06GB 06G2B 06G2B	–	98	78	59	--

Table 3. Value of carbon equivalent of steels applied for critical metal structures

Steel grade (standard document)	C_{eq}, %	
	min	max
09G2S (GOST 19281–89)	0.42	0.49
10KhSND (GOST 19281–89)	0.38	0.52
16G2AF (GOST 19281–89)	0.36	0.61
09G2SYuCh (TU U 322-16-127–97)	0.49	0.59
06G2B (TU U 14-16-150–99)	0.34	0.46

150--99. The steel has good ductility properties, relative elongation and reduction of metal being not less than 30 and 80 %, respectively.

Steel structure is a fine-grained ferrite-pearlite mixture with prevalence of the ferritic component (low-pearlite structure), steel hardness being equal

Table 4. Mechanical properties of rolled stock of 06G2B steel 30 mm thick at test temperature of 20 °C

Sample type acc. to GOST 1497–84	σ_y, MPa	σ_t, MPa	δ, %	ψ, %	Note
Type I	484–488 486	548–554 551	23.5--23.5 23.5	71.1–72.1 72.1	Across rolling direction
	484–498 491	548 548	24.5--26.5 25.5	74.4 74.4	Along rolling direction
Type III	499–503 500.6	569–579 574	29.3--30.7 30.0	82.6–84.0 83.5	Across rolling direction
	479–496 487	570–576 572	30.3--32.3 31.3	82.6–84.0 83.5	Along rolling direction
	440–458 452	555–569 559.3	25.3--31.3 28.1	74.8–84.0 81.5	In *Z*-direction

Table 5. Impact toughness of 06G2B steel rolled stock 30 mm thick*

KCU, J / cm^2 (type I acc. to GOST 9454–78) at *T*, °Ñ						*KCV*, J / cm^2 (type IV acc. to GOST 9454–78) at *T*, °Ñ			
+20		–40		+20	–40	+20		–40	
along	across	along	across	as-aged		along	across	along	across
430	434	432	429	345	346	429	431	433	433
431	430	432	429	347	347	430	433	431	434
432	431	431	430	347	346	432	434	429	432
*Samples of types I and IV could not be broken completely at *T* = +20 and –40 °C, tough fracture share was 90 %.									

Table 6. Standard and calculated resistance of steel 06G2B 30 mm thick

Steel grade (strength class)	Rolled stock thickness, mm	Standard resistance, MPa		Calculated resistance, MPa	
		by yield point	by tensile strength	by yield point	by tensile strength
06GB (390)	10–20	3900	5230	3550	4750
	21–50	3850	5170	3500	4700
06G2B (440)	10–20	4400	5690	4000	5180
	21–50	4350	5610	3950	5100

Table 7. Mechanical properties of welded joints on steel 06G2B 30 mm thick and of weld metal

Welding process	Welding consumables	Welded joint*		Weld metal			
		σ_t, MPa	Bend angle, deg	σ_t, MPa	σ_y, MPa	δ_5, %	ψ, %
Automatic submerged-arc	Sv-10NMA, AN-47	527 538	180 180	624 638	537 572	23 23	66 66
Automatic CO_2 (horizontal welds on a vertical plane)	Sv-08G2S, CO_2	540 532	150 62	690 693 600	624 636 492	19 22 20	64 67 67
Semi-automatic CO_2	Sv-08G2S, CO_2	–	--	575 563	461 445	27 29	73 69
Manual arc	UONI-13 / 55 electrodes	542 531	148 150	568 617	454 541	25 20	73 75
	FOX EV 50 electrodes	585 627	180 180	577 604	471 514	28 32	76 77

*Rupture location ---- base metal.

Table 8. Impact toughness of the metal of weld and HAZ of welded joints on 06G2B steel 30 mm thick

Welding process	Welding consumables	KCV, J / cm^2, at T, °Ñ			
		+20		–40	
		Weld center	HAZ	Weld center	HAZ
Automatic submerged-arc	Sv-10NMA, AN-47	125 142 100	431 226 285	34 36 36	233 195 195
Automatic CO_2 (horizontal welds on vertical plane)	Sv-08G2S, CO_2	164 182 132	432 433 431	114 89 41	432 429 430
Semi-automatic CO_2	Sv-08G2S, CO_2	189 172	244 302	99 107 76	143 119 131
Manual arc	UONI-13 / 55 electrodes	118 141 158	107 299 431	55 50 29	208 302
	FOX EV 50 electrodes	--	355 369 362	–	324 373 352

Figure 1. Preparation of ESW-joined blocks for check assembly of tank shell section of DP-9 at «Krivorozhstal»

Figure 2. Tank of 75000 m^3 capacity with application of 06G2B steel stock of 440 strength class, Brody town (construction was performed by incremental method)

to HV 170–180. Value of the carbon equivalent to European standard $C_{eq} = 0.357$ %. Relative reduction across the rolled stock thickness ($\psi_z \geq 79$ %) characterizes the high lamellar fracture resistance. Impact toughness KCV of the studied rolled stock is significantly higher than the specification requirements.

In keeping with the program of studying steel 06G2B, metal behaviour after thermodeformational ageing was evaluated to GOST 7268–82. Ageing was performed by deformation of the billet by 10 ± 0.5 % tension and heating of the samples up to the temperature of 250 ± 10 °C, soaking for 1 h with subsequent cooling in air. Testing results compared to those of testing 06G2B steel 30 mm thick for impact bending in the initial condition are given in Table 5.

Values of impact toughness of 06G2B steel 30 mm thick after thermomechanical ageing are somewhat decreased, but remain on a high level.

Stability of investigation results of mechanical properties of rolled sheets of steel 06GB (strength class 390) and 06G2B (strength class 440) allows establishing the coefficient of reliability for material $\gamma_m = 1.10$. The specified and calculated resistances are given in Table 6.

Welded butt joints of 06G2B steel were made by manual arc welding with electrodes of UONI-13 / 55 and FOX EV 50 grade, automatic submerged-arc welding in the downhand position and CO_2 welding (horizontal weld on a vertical plane), tee joints were made by gas-shielded semi-automatic welding. Tables 7 and 8 give the results of tensile and impact toughness testing of welded joints.

On the whole, the conducted investigations showed that sparsely-alloyed low-pearlite steel 06G2B of 440–490 strength class has stable mechanical characteristics and impact toughness. The high cold resistance of this steel ($KCV_{-40} \geq 300$ J / cm^2) should be particularly noted. The steel has good resistance to lamellar fracture, is insensitive to hydrogen embrittlement and features a high resistance to cold cracking in the HAZ metal [3].

It is established that the strength, ductile properties and impact toughness of the weld and HAZ metal of steel welded joints meet the requirements of TU U 14-16-150–99.

Production of rolled sheets of 06G2B (06GB) steel has been mastered in OJSCs «Metkombinat «Azovstal» and «Metkombinat im. Ilyicha». In 2003 these enterprises manufactured 1700 t of rolled sheets 12–45 mm thick all in all. The metal was used in overhauling of blast furnace 9 (Figure 1) of Krivoj Rog Metal Works «Krivorozhstal» [4], construction of a unique tank for oil storage of 75000 m^3 capacity (Figure 2) and a tank farm for 2000 m^3. In 2005 rolled stock of 06G2B steel 50 mm thick was used in construction of DP-2 blast furnace (Figure 3) in «Metkombinat «Azovstal». The rolled sheets fully meet the specification requirements, and in terms of impact energy, impact toughness after strain ageing, transverse reduction and transverse reduction across the thickness, the actual results are much higher than the specified level. At present structures of a bridge spanning the harbor entrance in Kiev are being manufactured from 06GB(D) steel of strength class 390.

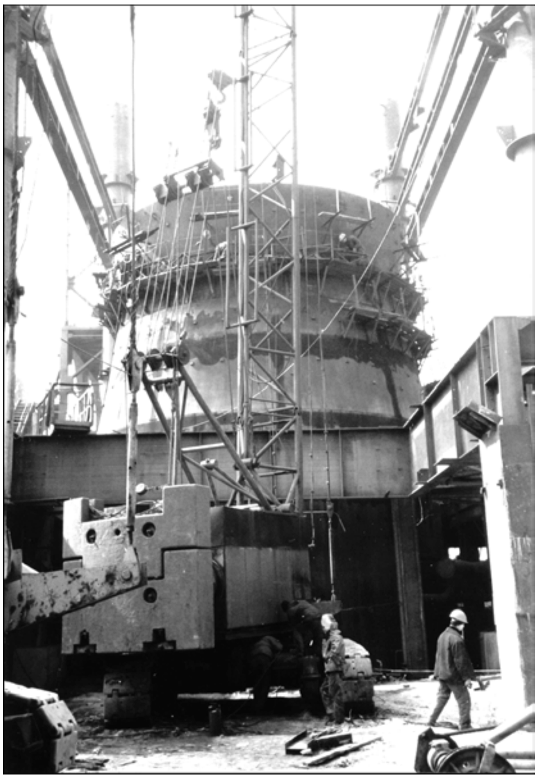

Figure 3. Construction of blast furnace DP-2 at «Azovstahl»

Considering that the issues of corrosion resistance are the main ones in terms of service life of bridges, the Ukrainian R&D Institute of Structural Materials «Prometej» together with PWI are working to develop a steel of a similar strength class of a higher atmospheric resistance.

1. Kovtunenko, V.A., Gerasimenko, A.M., Sineok, A.G. (2004) High-strength sparsely-alloyed steel 06G2B with $\sigma_y > 440$ MPa for bridge engineering. *Avtomobilni Dorogy i Dor. Budivnytstvo*, **69**, 106–113.
2. Kovtunenko, V.A., Gerasimenko, A.M., Gotsulyak, A.A. (2004) High-strength sparsely-alloyed steel 06G2B with $\sigma_y > 440$ MPa for critical products of mechanical, shipbuilding, bridge engineering and building structures. In: *Proc. of Int. Colloquium on Steel Tanks: Structures, Welding, Diagnostics, Repair, Resource* (Varna, May 18–20, 2004).
3. Mikhoduj, L.I., Kirian, V.I., Poznyakov, V.D. et al. (2003) Sparsely-alloyed high-strength steels for welded structures. *The Paton Welding J.*, **5**, 34–37.
4. Lobanov, L.M., Kovtunenko, V.A., Gerasimenko, A.M. et al. (2003) Welding technology in major repair of blast furnace 9 of KGMK «Krivorozhstal». In: *Proc. of Int. Conf. on Current Problems in Welding and Life of Structures* (Kiev, Nov. 24–27, 2003).

TECHNOLOGICAL CHARACTERISTICS OF LASER BEAM FOR CUTTING AND WELDING

V.P. GARASHCHUK
E.O. Paton Electric Welding Institute, NASU, Kiev, Ukraine

An analytical expression of depth resolution was derived through the beam parameter product and its angle of convergence with the assumption that the caustic surface of the focused beam has the shape of a single-cavity hyperboloid of revolution. For practical use of the derived relationship, formulas of the beam parameter product in resonators and lasers applied in practice are given.

Keywords: *laser welding, laser cutting, focusing, laser beam, beam parameter product, depth resolution*

Technologically important characteristics of laser irradiation in laser thermal technologies of metal treatment are not only its power, but also the ability of focusing to small sizes using long-focus objectives with great depth resolution. We shall interpret the latter as the length of the focused beam in the vicinity of its throat, within which its cross section area changes insignificantly. Depth resolution $2l_R$ in work [1], where it is called Relay length, is determined as the distance between the cross sections of focused beam, the area of which is 2 times greater than the area of the throat cross section. It is obvious that the greater is the depth resolution at the same beam power and throat cross sectional area, the deeper is metal penetration in welding, if the penetration mode is deep. In cutting the thickness of cut metal is greater and the cut walls have smaller rounding. In other laser processes the requirements to focusing accuracy are lowered.

In the approximation of paraxial optics, which is practically fulfilled in operation with laser radiation, the depth resolution is determined by a complex parameter of the light beam:

$$Q = nuh, \tag{1}$$

where n is the index of refraction of the medium, in which the beam is focused; u is the angle between the extreme beam in the converging focused beam and the main optical axis (convergence angle); $2h$ is the throat size, if it has axial symmetry, then its radius $r(0) = h$ (Figure). The meaning of Q for the given beam is constant in all of its transformations by optical systems. This parameter is called Lagrange–Helmholtz invariant by some authors [2], and Smith–Helmholtz invariant by other authors [3], although other authors were also involved in its derivation [3]. This parameter is called the product of beam parameters in foreign literature sources, and we suggest the term «beam parameter product». As the majority of laser technologies are implemented in the air, the refraction index is $n = 1$, and the correlation (1) is simplified:

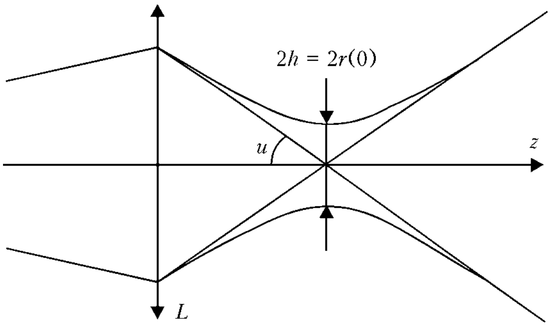

Focused laser beam: L — focusing optical objective

$$Q = uh.$$

The aim of this work is to derive an analytical dependence of the depth resolution of the focused beam on the parameter product.

For determination of the depth resolution, let us assume that the caustic surface of the focused beam, as well as the laser beam, formed in a stable resonator, has the form of single-cavity hyperboloid of revolution, in which the throat radius and asymptote slope are equal to the throat radius $r(0)$ and angle of convergence u of focused beam, correspondingly. Evidently, such a hyperboloid should describe the real caustic surface rather precisely.

Let us use the cylindrical system of coordinates for solving this problem. Let the light beam spread along axis z, and coordinate r reflect the change of beam radius. Let us assume that the distribution of intensity by beam radius does not depend on azimuth. Then the caustic surface of the focused beam will be described as

$$\frac{r^2(z)}{r^2(0)} = 1 + \frac{z^2}{b^2},$$

where b is the parameter that is necessary to determine. Let us use the criterion of the depth resolution adopted in work [1]. Then the equality $2l_R = 2b$ will be valid. From hyperbola parameters it follows that

$$\lim_{z \to \infty} \frac{r(z)}{r(0)} = \frac{z}{b},$$

where $\frac{r(z)}{z} = u = \frac{r(0)}{b}$ and $b = \frac{r(0)}{u}$. Multiplying the numerator and denominator by u we get the required expression

$$b = \frac{r(0)}{u}\frac{u}{u} \equiv \frac{Q}{u^2}, \quad (2)$$

from which it is possible to calculate the depth resolution $2b$ using the angle of convergence of focused beam and the given laser beam parameter product. The latter, as a rule, is available in the laser certificate. It is easy to find angle u experimentally as the ratio of the beam thermogram radius on the focusing element $r(z_f)$ to the distance from it to the throat of focused beam z_{th}, that is practically equal to focal distance f of the focusing element. Then the equation (2) can be written in the following way:

$$b = \frac{Q}{u^2} = \frac{Q f^2}{r^2(z_f)}. \quad (3)$$

From relationships (2) and (3) it follows that the greater is the depth resolution, the larger is the radius of the throat and the parameter product, that is proportional to the square of focal distance of the focusing optical objective and inversely proportional to the square of the beam radius in it.

The obtained relationships allowed predicting the change of geometrical parameters of the cut or penetration in the case of extended items, for example, using the Cartesian manipulator, in which the focusing optical objective moves relative to a stationary item. The radius of the laser beam, as a rule, becomes greater at its spreading in space. So, the depth resolution of the focused beam will be greater in the closest position of focusing objective to the laser, then in the most remote position that will surely influence the treatment parameters. Will these changes within the limits of tolerance, depend on the angle of laser beam divergence, namely, the smaller it is, the smaller are the differences of the treatment zones in the extreme positions of the manipulator focusing objective.

Analytical expressions for beam parameter product for resonators and lasers that are known in practice are given below for practical use of correlation (2).

In work [1] the expression for parameter product of the laser beam formed in stable resonator of TEM_{00} mode, was given:

$$Q_{00} = \theta w_{00} = \lambda/\pi,$$

where $\theta \equiv u$; $w_{00} \equiv h$; λ is the irradiation wave length. In work [4] it is shown that the beam parameter product of TEM_{pq} mode for round mirrors is equal to

$$Q_{pq} = Q_{00}(2p + q + 1).$$

Here p and q are mode indices.

For a beam formed in an unstable resonator with its output bypassing a round mirror (that is the most widely spread) the parameter product is equal to

$$Q \approx 0.55\lambda M / (M - 1), \quad (4)$$

where M is resonator magnification.

Laser beam formed in a single fiber of a fiber laser with optic fiber diameter $d_{o.f} < 10\lambda$ is characterized by parameter product

$$Q \approx 0.25\lambda,$$

and for the beam transmitted by optic fiber,

$$Q \le 0.5\, A_N d_{o.f},$$

where $A_N = \sqrt{n_c^2 - n_{sh}^2}$ is its numerical aperture; n_c and n_{sh} are the indices of refraction of the core and the shell, respectively.

During the last years the power of slotted lasers reached several kilowatt. This is quite enough for application of laser thermal technologies. Laser beam at the output from the resonator has the shape of an extended rectangle in its cross section. Its shape is transformed into a square or round shape by the optical system. Such a beam is characterized by the parameter product that can be described by relationship (4), where $M = \infty$; then (4) becomes

$$Q = 0.61\lambda. \quad (5)$$

Multibeam lasers make up a considerable part of the technological lasers, in which a multitude of lower-power beams are integrated to achieve a higher power of the laser beam, for example, CO_2-lasers [5], as well as semiconductor [1] and fiber [6] lasers. Separate beams can be mutually coherent or incoherent. When focusing such compound beams by identical focusing systems, different radii of focused beam throat were obtained with the same intensity as on its axis, as well as average ones over the throat cross-section.

For derivation of the formula for determination of multibeam laser parameter product, let us take that the axes of all components of the beams are strictly parallel to one another and their divergence is equal. In lasers designed for direct use in thermal technologies, the component beams are arranged in such a way that the component beam has minimum dimensions in the transverse direction. When calculating the throat radius of the focused compound beam and its intensity, we will assume that focal distance F of focusing element is not less than 5 times greater than diameter D of the compound beam, i.e. $F \le 5D$. Realization of this criterion minimizes the influence of the spherical aberration.

Case 1. Component beams are mutually incoherent. Let component beams be generated by a laser running in the waveguide mode, and the diameter of active element be $2a$. Then half of the angle of divergence of an individual beam is $\alpha = 0.61\lambda / a$, and the throat radius of the focused beam made up by a multitude of incoherent beams is equal to

$$r^{inc}(0) = \alpha F \equiv h. \quad (6)$$

Angle $u = D / 2F$. Therefore, the composite beam parameter product will be

$$Q = r^{inc} u = 0.61\lambda D / 2a.$$

Ratio $D / 2a = \sqrt{N}$, where N is the number of sources in the set. Finally

$$Q = 0.61\lambda\sqrt{N}.$$

Case 2. Component beams are mutually coherent. The throat of the focused composite beam is the result of interference of the focused component beams. Simple relationship of the type of (6) for the composite beam is absent. Therefore, let us use the expressions for average intensity of the focused beam in the throat for calculation of beam radius. As follows from [2], the intensity of total irradiation from incoherent light sources I_Σ^{inc} is equal to the sum of intensities of individual sources $I_\Sigma^{\mathrm{inc}} = NI_1$, where I_1 is the intensity generated by the light beam of an individual laser. The total intensity for coherent sources I_Σ^{c} is equal to the square of component beams $I_\Sigma^{\mathrm{c}} = N^2I_1$ or $I_\Sigma^{\mathrm{c}} = NII_\Sigma^{\mathrm{inc}}$. If the total power of both the component beams (coherent and incoherent) is equal, then throat radius of the coherent beams can be described by the following relationship:

$$r^{\mathrm{c}}(0) = \frac{1}{\sqrt{N}}\, r^{\mathrm{inc}}(0).$$

Then the parameter product will be

$$Q = r^{\mathrm{c}}(0)u = \frac{1}{\sqrt{N}}\, r^{\mathrm{inc}}(0)u = 0.61\lambda,$$

i.e. it coincides with (5). Strictly speaking, relationship $I_\Sigma^{\mathrm{c}} = N^2I_1$ is not fulfilled, as at interference of individual laser beams diffracted on the aperture, additional side lobes will appear, and at focusing the side maximums — throats, which is proved in the work [7]. It is evident that their intensity is the lower, the smaller the number of component beams and the larger their diameter $2a$. The position of side maximums is determined by the law of component beam arrangement in the composite beam.

1. (2002) *Einfuehrung in die industrielle Lasermaterialbearbeitung*. Hamburg: Rofin.
2. Landsberg, G.S. (1976) *Optics*. Moscow: Nauka.
3. Born, M., Wolf, E. (1973) *Principles of optics*. Moscow: Nauka.
4. Garashchuk, V.P. (2005) *Principles of laser physics. Lasers for thermal technologies*: Manual. Kiev: PWI.
5. (1991) *Technological lasers*: Refer. Book. Vol. 1. Ed. by G.A. Abilsiitov. Moscow: Mashinostroenie.
6. Nakatani, H. (2004) Development of powerful fiber lasers and their applications. *Yosetsu Gijutsu*, **3**, 108–114.
7. Hergenhan, G., Schull, M., Brauch, U. (2001) Kohaerente Vertikalemitter — Arrays. *Laser Opt.*, 33(**3**), 68–75.

EFFECT OF HEAT TREATMENT ON STRUCTURE OF AMORPHISED DETONATION Fe--B COATINGS

E.A. ASTAKHOV, Yu.S. BORISOV, G.S. KAPLINA, N.N. KOKORINA, Z.G. IPATOVA and **O.F. CHERNYAKOV**
E.O. Paton Electric Welding Institute, NASU, Kiev, Ukraine

The effect of heat treatment (HT) in a range of 200–650 °C on the process of crystallisation of the amorphous phase (AP) in detonation coatings deposited from powders of amorphising Fe–B alloy with a particle size of < 40 and 40–63 μm was investigated. It is established that the AP content of a coating deposited from a fine powder is 32 vol.%, and that of a coating deposited from the powder with a particle size of 40–63 μm is 57 vol.%. Heating to 500 °C leads to complete crystallisation of AP in both cases. Microstructure of coatings was investigated, and they were tested to gas-abrasive wear resistance after HT at different temperatures. Maximal increase in wear resistance (by 35–40 %) was achieved at a structural state of the coatings corresponding to crystallisation (~ 3 % AP).

Keywords: detonation spraying, amorphous phase, nano-crystalline structure, crystallisation, gas-abrasive wear resistance

Increasing requirements to properties of coatings make it necessary to seek new ways of improving them in order to achieve the increased values of hardness, wear and corrosion resistance. One of such ways is deposition of thermal spray coatings with nano-crystalline structure. Much experimental data have been accumulated up to now that confirm the increased values of hardness, wear and corrosion resistance of thermal spray nano-composite coatings containing nano-sized phases, compared with properties of coatings of the identical composition but having a conventional crystalline structure [1–3].

Three basic approaches to formation of thermal spray nano-composite coatings are available now [4]:

- utilisation of initial spraying materials with a nano-crystalline structure. They include nano-crystalline powders (WC–Co, stainless steel, Ni alloys, etc.), colloidal solutions and suspensions (Al_2O_3–ZrO_2, etc.);
- combination of the process of thermal spraying with synthesis of nano-structured materials through vapour phase deposition in a gas flame or plasma jet, or reactive spraying of composite powders (e.g. Ti–Al–B);
- heat treatment (HT) of thermal spray coatings with a meta-stable structure, where decomposition of the amorphous structure or oversaturated solid solutions leads to formation of nano-sized phases.

New types of thermal spraying machines were developed to realise these approaches. They allow using such non-traditional types of materials as colloidal solutions and suspensions for deposition of coatings, and employing hybrid deposition processes that combine thermal spraying and gas phase processes.

In terms of producing nano-composite coatings by spraying initial nano-crystalline powders, of practical interest are detonation spraying (DS), plasma spraying (PS) and HVOF spraying. With the above technologies a short-time dwelling of powder particles in the spraying process allows the growth of grains to be avoided or limited, and nano-sized phases to be retained in a coating layer.

On the other hand, application of these processes for spraying powders of amorphising alloys provides the high rates of cooling of the spraying material particles and the possibility of forming the amorphous state in the resulting coatings [5–8]. As indicated above, HT of such coatings may serve as a basis for formation of nano-composite structures.

Data on properties of thermal spray heat-treated coatings from amorphising alloys evidence that HT results in increase in hardness and corrosion resistance. For example, as reported in study [9], amorphous coatings produced by PS of powder Fe–17Cr–38Mo–4C had hardness HV 10,000 MPa in the as-deposited condition, whereas after crystallisation at a temperature of 650 °C their hardness was HV 14,500 MPa, and it remained high (> HV 13,000 MPa) after crystallisation at 1000 °C. Corrosion resistance of these coatings after crystallisation also remained high and comparable with that of plasma coatings produced from stainless steel.

The purpose of this study was to determine a temperature range for crystallisation of the amorphous phase (AP) in detonation coatings sprayed from alloy of the Fe–B system, investigate its quantitative variation depending upon the HT temperature, and relationship between wear resistance of the coatings and their structural state.

DS was performed using powders with a particle size of <40 and 40–63 μm, detonation unit «Perun-S», and a detonation mixture consisting of oxygen, acetylene and nitrogen (shooting rate was 6.6 Hz / s, thickness per shot was 15–20 μm, and spraying distance was 110 mm).

Material of the initial samples was steel St.3. The choice of parameters for HT of the AP-containing coatings was based on the results of differential thermal analysis (DTA) of coatings separated from the substrate, X-ray phase analysis (XPA) of these coatings,

Table 1. Thickness of coating of Fe–B system alloy and its AP content after spraying

Spraying powder particle size, μm	Coating thickness, μm	AP content, %
< 40	300–330	32
40–63	300–320	57

Table 2. Variation in AP content of coatings as a result of HT, %

Spraying powder particle size, μm	Heating temperature, °C						
	Without HT	200	300	330	360	450	500
< 40	32	32	32	28	21	18	0
40–63	57	57	57	54	27	15	0

and analysis of the data available in literature on crystallisation of amorphous coatings and strips of the same composition ($Fe_{20}B_{80}$) produced by spinning [10]. Conditions required for amorphisation of metal alloys in DS, and selection of rational spraying parameters providing a 50–80 % content of AP are described in studies [5–8].

To conduct HT, the coated samples were placed in a muffle of stainless steel, after preliminary purging

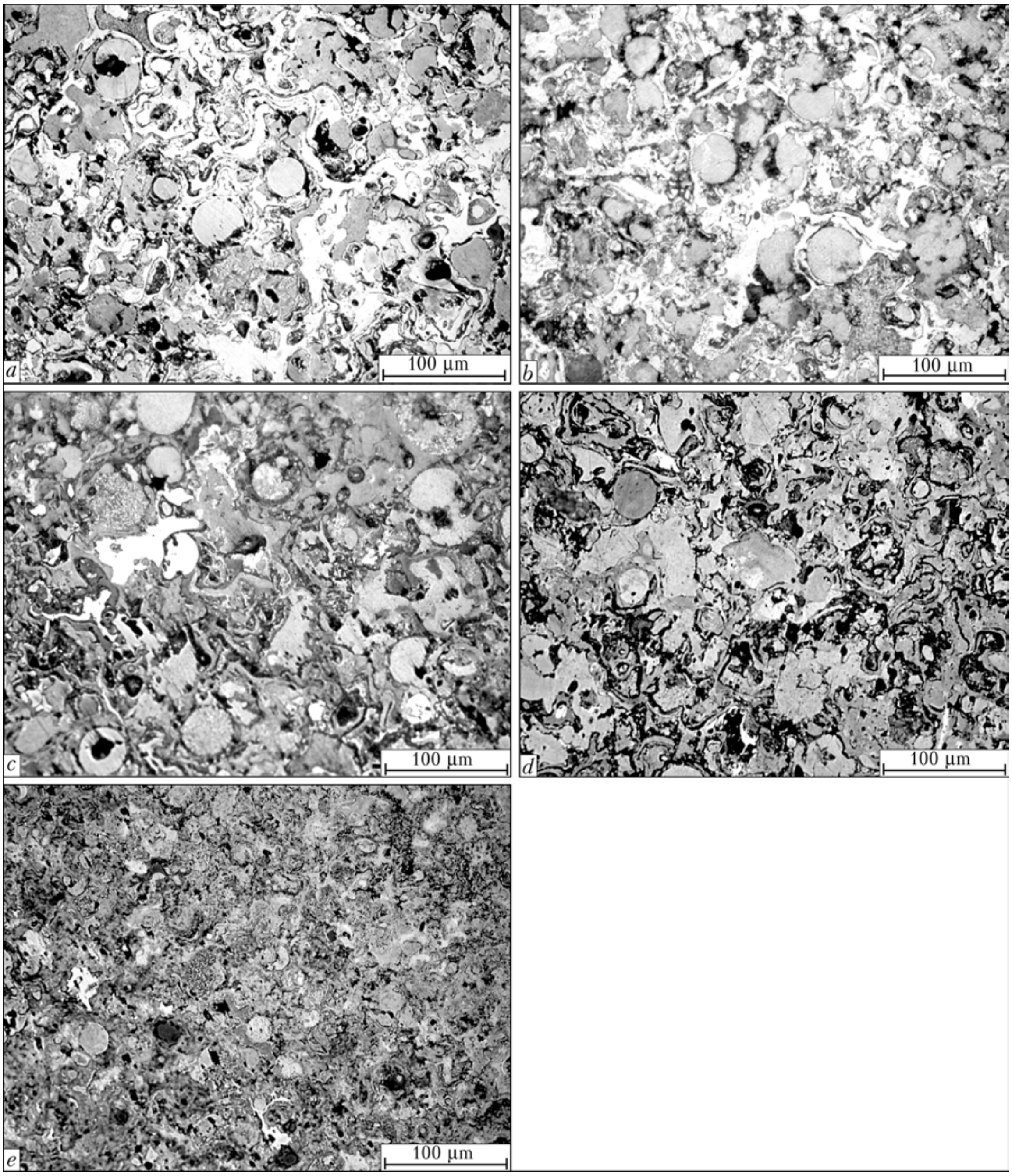

Figure 1. Microstructure of detonation coatings sprayed from powder $Fe_{80}B_{20}$: *a* — without HT, 57 % AP; *b* — HT temperature 300 °C, 52 % AP; *c* — 360 °C, 40 % AP; *d* — 500 °C, 0 % AP; *e* — 650 °C, 0 % AP

with high-purity argon its flow rate was set at a level of 20–30 cm^3 / min, then the muffle was placed in a work space of the shaft heating furnace, heating in argon was conducted at the HT temperature at a rate of 20–22 °C / min, and holding at this temperature was 30 min.

X-ray diffraction examinations were carried out using diffractometer «DRON-3» in CuK$_\alpha$-radiation. The volume content of AP in the case of an amorphous-crystalline structure of the coatings was determined by the procedure based on separation of diffraction reflections from the amorphous and crystalline phases and comparison of areas under the curves of X-ray radiation scattering intensity [11]. Metallography examinations of the coatings were conducted using optical microscope «Neophot-32» at up to ×1000, and using electron microscope at up to ×100,000. Wear resistance tests of the coatings under gas-abrasive wear conditions were performed using centrifugal accelerator TsUK-3 M at an accelerator disk rotation speed of 100 rpm and abrasive attack angles of 45 and 60°, according to GOST 23.201–78 [12]. Quartz sand with a particle size of 0.5–0.9 mm was used as an abrasive. Wear was evaluated from the loss of weight of the test samples, which were weighted using analytical balance VLA-200. Table 1 gives characteristics of the initial coatings in the as-deposited condition.

Results of DTA of the coatings separated from the substrate allowed determining the range of crystallisation of AP in continuous heating at a rate of 80 °C / min: crystallisation beginning temperature 400 °C (beginning of the crystallisation heat release), maximal crystallisation temperature 500 °C (maximal exothermic effect), and crystallisation completion temperature 600 °C (end of crystallisation heat release).

The HT range differing from that determined by DTA, i.e. 200–650 °C, was chosen to investigate the process of crystallisation of AP. This can be explained by several reasons:

- kinetics and temperature of beginning of crystallisation of AP in continuous heating differ from those observed in isothermal annealing (crystallisation beginning temperature is higher by about 70 °C) [13–15];
- crystallisation temperature range shifts towards a region of higher temperatures with increase in the heating rate [10];
- DTA fails to detect changes in a period preceding crystallisation, when the zones enriched with a corresponding alloy component are formed in locations of precipitation of future crystals, which may affect properties of the coatings;
- DTA does not account for the crystalline phase grain growth phenomenon.

As seen from Table 2, the intensity of lines of meta-stable borides Fe_3B (tetragonal and orthorhombic) decreases with increase in the HT temperature. Figure 1 shows microstructures of the detonation coatings before and after HT conducted at different temperatures (investigation of crystallisation of AP was conducted on samples with the coatings sprayed from the powder with a particle size of 40–63 μm). Structure of a coating not subjected to HT (Figure 1, *a*) contains an amorphous component in the form of non-etchable deformed particles. The oxide component in the form of thin interlayers is located along the grain boundaries, and the crystalline one, having the form of etchable grains of a round shape about 50 μm in size, has a characteristic fine configuration of eutectic colonies inside the grains. Etchability of the structure, especially of AP (white regions after spraying), rises with increase in the HT temperature, and the content of the amorphous component decreases (Figure 1, *b*, *c*), whereas after annealing at 500–650 °C (Figure 1, *d*, *e*) there is no AP at all, and particles with the pronounced eutectic structure are scarce.

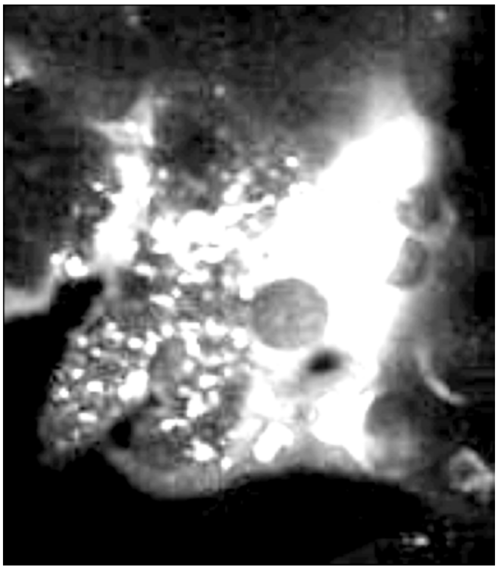

Figure 2. Electron microstructure of a coating with nano-crystalline inclusions (10–20 nm), which are the Fe_3B phase (×100,000)

Electron microscopy examination of structure of a sample containing 52 % AP, subjected to HT at 330 °C, allowed detection of nano-sized (10–20 nm) crystal-

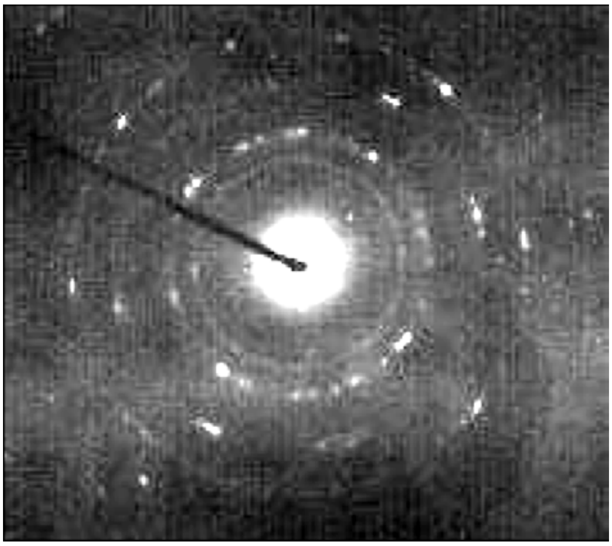

Figure 3. Diffraction pattern of a coating sample after HT at 330 °C

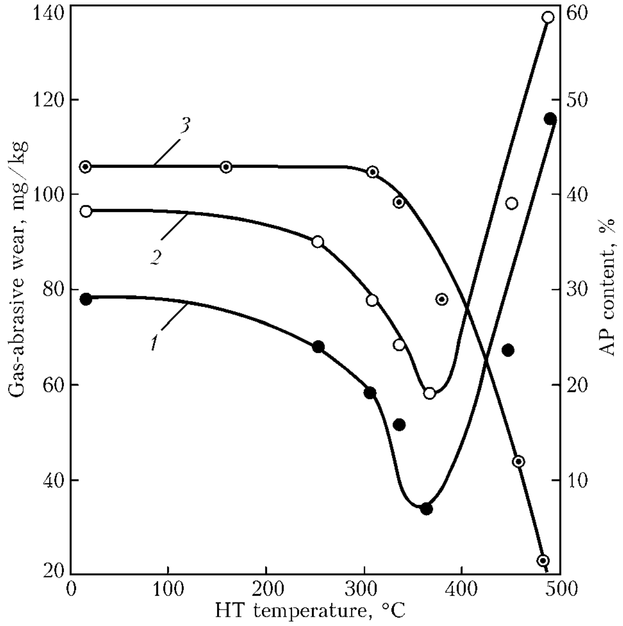

Figure 4. Effect of HT temperature on AP content and gas-abrasive wear resistance of a detonation coating: *1*, *2* — abrasive attack angle 45 and 60°; *3* — AP content

line inclusions of iron borides in locations of decomposed AP (Figure 2)[*].

The diffraction pattern obtained on this sample turned out to be characteristic of a nano-structure with gradually changing disorientation of grains (Figure 3). Results of abrasive wear resistance tests of the detonation coatings depending upon the HT temperature, as well as an additional superposition of the curve of variations in the AP content depending upon the HT temperature, are shown in Figure 4. Analysis of these curves suggests a conclusion that variations in gas-abrasive wear resistance are not unambiguously related to variations in the AP content of the coating fixed by XPA. This characteristic is known to be in direct dependence upon the AP content of a coating layer [5, 6, 16, 17], i.e. the higher the AP content of the coating, the higher the wear resistance of the layer. The results obtained evidence that HT in a temperature range of 200–300 °C does not lead to a detectable (using the selected procedures) decrease in the AP content, whereas wear decreases to a substantial degree. With the HT temperature increased to 330 °C, the AP content decreased only by 3 %, whereas wear resistance grew by 20–25 %. A minimal wear was achieved after HT at a temperature of 360 °C, where the AP content of a coating was still substantial (~45 %), and only after HT in a temperature range of 400–500 °C the decrease in gas-abrasive wear resistance became to be directly related to the decrease in the AP content of the coating.

CONCLUSIONS

1. As established, the temperature range of crystallisation of AP in detonation coatings of alloy of the Fe–B system in isothermal heating is 300–500 °C.

2. Increase in gas-abrasive wear resistance of coatings takes place after the HT temperatures, when no change in the AP content, resulting from beginning of the process of fine structural transformations, is not fixed as yet.

3. Maximal increase in wear resistance (by 35–40 %) is achieved after HT within a temperature range of 300–360 °C, which is likely to be related to the fact that a structure hardened with fine (nano- and micro-sized) products of AP decomposition is formed instead of a decomposed AP. Further increase in the HT temperature is accompanied by growth of grains of the crystalline structure, which leads to decrease in wear resistance.

1. Jiang, H.G., Lau, M.L., Lavernia, E.J. (1998) Synthesis of nanostructured engineering coatings by high velocity oxygen fuel (HVOF) thermal spraying. *J. Thermal Spray Technology*, **7**, 412–413.
2. Scholl, M., Becker, M., Atteridge, D. (1998) Microstructure and properties of plasma sprayed nanoscale tungsten carbide-cobalt coatings. *Ibid.*, **7**, 425–426.
3. Usmani, S., Sampath, S., Houck, D. et al. (1997) Effect of carbide grain size on the sliding and abrasive wear behaviour of thermally sprayed WC–Co coatings. *Tribol. Transact.*, 401(**3**), 470–478.
4. Borisov, Yu.S. (2004) Thermal spraying of coatings with nano-crystalline phases. Nano-sized systems. In: *Abstr. of NANSIS 2004 Conf.* Kiev.
5. Kunitsky, Yu.A., Korzhik, V.N., Borisov, Yu.S. (1988) *Nonocrystalline metal materials and coatings in engineering*. Kiev: Tekhnika.
6. Astakhov, E.A., Korzhik, V.N., Chernyshev, A.V. (1990) *Detonation spraying of amorphous and microcrystalline coatings*. Moscow: Znanie.
7. Korzhik, V.N. (1992) Theoretical analysis of conditions of amorphisation of metal alloys in thermal spraying. *Poroshk. Metallurgiya*, **10**, 11–15.
8. Borisov, Yu.S., Korzhik, V.N. (1995) Amorphous thermal coatings: Theory and practice (Review). *Avtomatich. Svarka*, **4**, 3–12.
9. Kishitake, K., Era, N., Otsubo, F. (1996) Characterization of plasma sprayed Fe–17Cr–38Mo–4C amorphous coatings crystallizing at extremely high temperature. *J. Thermal Spray Technology*, **5**, 283–288.
10. (1987) *Amorphous metal alloys*. Ed. by F.E. Luborsky. Moscow: Metallurgiya.
11. Grigorenko, G.M., Borisova, A.L., Adeeva, A.I. et al. (1995) Application of methods of quantitative X-ray analysis for examination of phase composition of thermal spray coatings. *Problemy SEM*, **2**, 63–71.
12. Kulu, P. (1988) *Wear resistance of powder materials and coatings*. Tallinn: Valgus.
13. Shmyreva, T.P., Mukhin, A.P., Khlyntsev, V.P. et al. (1995) Features of structure and solidification in sprayed massive amorphous layers. *Metallofizika i Nov. Tekhnologii*, 17(**4**), 74–78.
14. Naberezhnykh, V.P., Tkach, V.I., Limanovsky, A.I. et al. (1991) Crystallisation of amorphous alloy $Fe_{80}B_{20}$ in constant-rate heating. *Fizika Metallov i Metallovedenie*, **2**, 157–164.
15. Shmyreva, T.P., Bereza, E.Yu. (1990) *Rapidly cooled eutectic alloys*. Kiev: Tekhnika.
16. Astakhov, E.A., Astakhov, I.E. (1998) Detonation spraying of microcrystalline coatings. In: *Proc. of 5th Int. Conf. on Films and Coatings*. St.-Petersburg.
17. Koziakov, I.A., Borisov, Yu.S., Korzhik, V.N. (1996) Resistance of amorphised flame coatings of Fe–B system under gas-abrasive wear conditions. *Avtomatich. Svarka*, **9**, 27–29.

---

[*] Examinations were conducted by Dr. P.S. Britun at the Institute for Materials Science Problems, NASU.

FORECASTING CAVITATION-CORROSION RESISTANCE OF DEPOSITED METAL OF Fe–Cr–Ni–(Mo) ALLOYING SYSTEMS IN 92 % SOLUTION OF SULFURIC ACID

À.V. PATYUPKIN and **D.A. ANTONYUK**
Zaporozhie National Technical University, Zaporozhie, Ukraine

An empirical dependence is proposed of the influence of the main alloying elements in complex-alloyed stainless alloying systems (Fe–Cr–Ni–(Mo)) on cavitation-corrosion resistance of the deposited metal in the concentrated solutions of sulfuric acid.

Keywords: cavitation-corrosion resistance, stainless steels and alloys, sulfuric acid, tests, mathematical model, statistical processing

The commercial equipment of the systems of evacuation of anodic chlorine (chlorine compressors, centrifugal pumps, stop valves, etc.) of titanium-magnesium plants mainly operates in 92–98 % solution of sulfuric acid, which hasan essential bearing on the intensity of the process of cavitation failure of the important parts of the mechanisms involved [1]. Therefore in selecting a wear-resistant material for manufacturing fast-wearing parts, joint effect of cavitation and corrosion should be taken into account. In connection with the extensive range of stainless steels and alloys recommended for operation in acid media, and their high alloying degree, its influence on cavitation-corrosion resistance of metals [2] depending on nickel and chromium equivalents was investigated. Cavitation-corrosion tests were carried out on a special shock-erosion test rig according to a technique described in [3].

Based on the results of statistical processing of laboratory research data of cavitation-corrosion resistance of steels and alloys of Fe–Cr–Ni, Fe–Cr–Ni–Mo and Fe–Cr–Ni–Mo–Cu systems, optimum range of Ni_{eq} = 24–31 % and Cr_{eq} = 23–26 and 30–31 % was determined [2]. Within the range of increased resistance are the following of steels and alloys: 06Kh23N18, 08Kh23N18 Ì 5, 08Kh23N28 Ì 2Ò, 06Kh23N28 Ì 3D3Ò and 06Kh24N21. Thus cavitation-corrosion resistance of 08Kh23N18 Ì 5 steel is of the same order as that of the 06Kh23N28 Ì 3D3Ò alloy (Table), inspite of the high degree of alloying of the latter. On this basis a necessity arose for studying the influence of concrete alloying components on cavitation-corrosion resistance of metals. Basic chemical elements in the given stainless steels and alloys, controlling their resistance, are carbon, chromium, nickel and molybdenum. Carbon expands γ-range and is a very active austenite-forming element, whose austenizing coefficient equals 30 (with nickel it is 1) [4]. According to [5], in the presence of austenitic-ferritic structure, the failure will develop in ferrite, thus will increase cavitation resistance of steels with a reduced content of the ferrite phase due to austenitic phase growth. In [5] it is also shown that increasing content of carbon in the hardened steel from 0.023 to 0.8 wt.%, reduces the loss of mass in 5-hour test from 0.650 to 0.180 g, while its hardness increases. However increase in the carbon content results in chromium depletion of steels or alloys, and accordingly decreased resistance of metal to intercrystalline corrosion, therefore the content of carbon in tested stainless steels and alloys was below 0.08 %; so further on we focused our study on the effect of chromium, nickel and mo-

Cavitation-corrosion resistance of deposited metal

Sample No.	Deposited metal	Element content, wt.%			Loss of sample mass, g, in 92 % H_2SO_4 solution
		Ñr	Ni	Mo	
1	10Kh18N10T	18.1	10.5	–	1.96
2	07Kh14N20	14.0	20.5	–	1.65
3	07Kh15N21	15.0	20.9	–	1.63
4	08Kh15N21M6	15.1	20.9	5.4	0.79
5	08Kh17N24M3D	17.0	24.2	3.0	1.37
6	08Kh18N24M3D	18.2	24.3	2.9	1.31
7	12Kh18N25M3	18.0	25.1	3.2	0.82
8	10Kh15N21M6	15.3	21.1	5.9	0.68
9	10Kh14N29M5	14.0	29.1	5.3	0.61
10	10Kh14N29M6	14.4	29.0	5.9	0.57
11	08Kh15N30	15.2	30.1	–	1.26
12	07Kh16N30	16.0	29.8	–	1.37
13	14Kh19N25M3D	19.0	24.9	3.0	0.92
14	06Kh23N18	22.8	18.0	–	0.65
15	08Kh23N18M5	22.9	18.2	5.3	0.50
16	08Kh23N28M2T	23.2	28.0	1.9	0.71
17	06Kh23N28M3D3T	23.1	28.0	2.9	0.46
18	06Kh24N21	24.0	21.0	–	0.59

Note. Tests were carried out in 92 % H_2SO_4 solution at 60 °C for 10 h.

lybdenum additives on cavitation-corrosion resistance of metals.

Based on experimental data, the regression-correlation analysis was carried out, and a mathematical dependence demonstrating the influence of the above components on the loss of mass of samples under cavitation-corrosion attack ($P_{H_2SO_4}$) was derived:

$$P_{H_2SO_4} = f(\mathrm{Ni, Cr, Mo}).$$

The empirical dependence was derived using the least squares method [6--8]. According to laboratory research data (see the Table), was found the closest theoretical curve, whose equation describes functional and correlational dependences between the values in question. In solving this problem we used the same approach as in studying the influence of Ni_{eq} and Cr_{eq} on cavitation and cavitation-corrosion resistance using the technique of [2], but in our case elements of the matrixes constituted values representing chromium, nickel and molybdenum content in the deposited metal and data of the laboratory research (see the Table).

As a result of mathematical analysis was derived the equation describing cavitation-corrosion resistance (losses of the mass of samples, g) of the metal depending on the weight content (%) of the basic alloying components:

$$P_{H_2SO_4} = 12.8419 - 0.5648\mathrm{Cr} - 0.6057\mathrm{Ni} + 0.8264\mathrm{Mo} + 0.0235\mathrm{CrNi} + 0.0393\mathrm{CrMo} - 0.0277\mathrm{NiMo} - 0.0016\mathrm{CrNiMo} + 0.0025\mathrm{Cr}^2 + 0.0062\mathrm{Ni}^2 - 0.1649\mathrm{Mo}^2 + 0.0002\mathrm{Ni}^2\mathrm{Mo}^2.$$

Mean absolute error for the given case does not exceed 5 % (0.56), while correlation coefficient exceeds 0.7, which gives proof to the adequacy of the suggested model. Based on the experimental and calculated values of cavitation and cavitation-corrosion resistance parameters of the studied steels and alloys, a statistical data processing was carried out: thus the correlation coefficient was 0.86; adequacy variation was 0.007; reproducibility was 0.006; estimated Fisher criterion was 1.25; tabular one was 1.99; estimated Cochren criterion was 0.06, tabular one was 0.219. Values of estimated Fisher criterion for two cases were below tabular data, which testifies that empirical dependences are plausible. As the variations were more than two and one of them being much higher than others, Cochren criterion was used for determining their uniformity [4--6]. Estimated values of Cochren criterion for both cases do not exceed tabular ones, which gives proof to the hypothesis of uniformity of variations.

Based on our statistical analysis, it is possible to state that the regression equation holds for high correlation relationships, and it is expedient to use it in

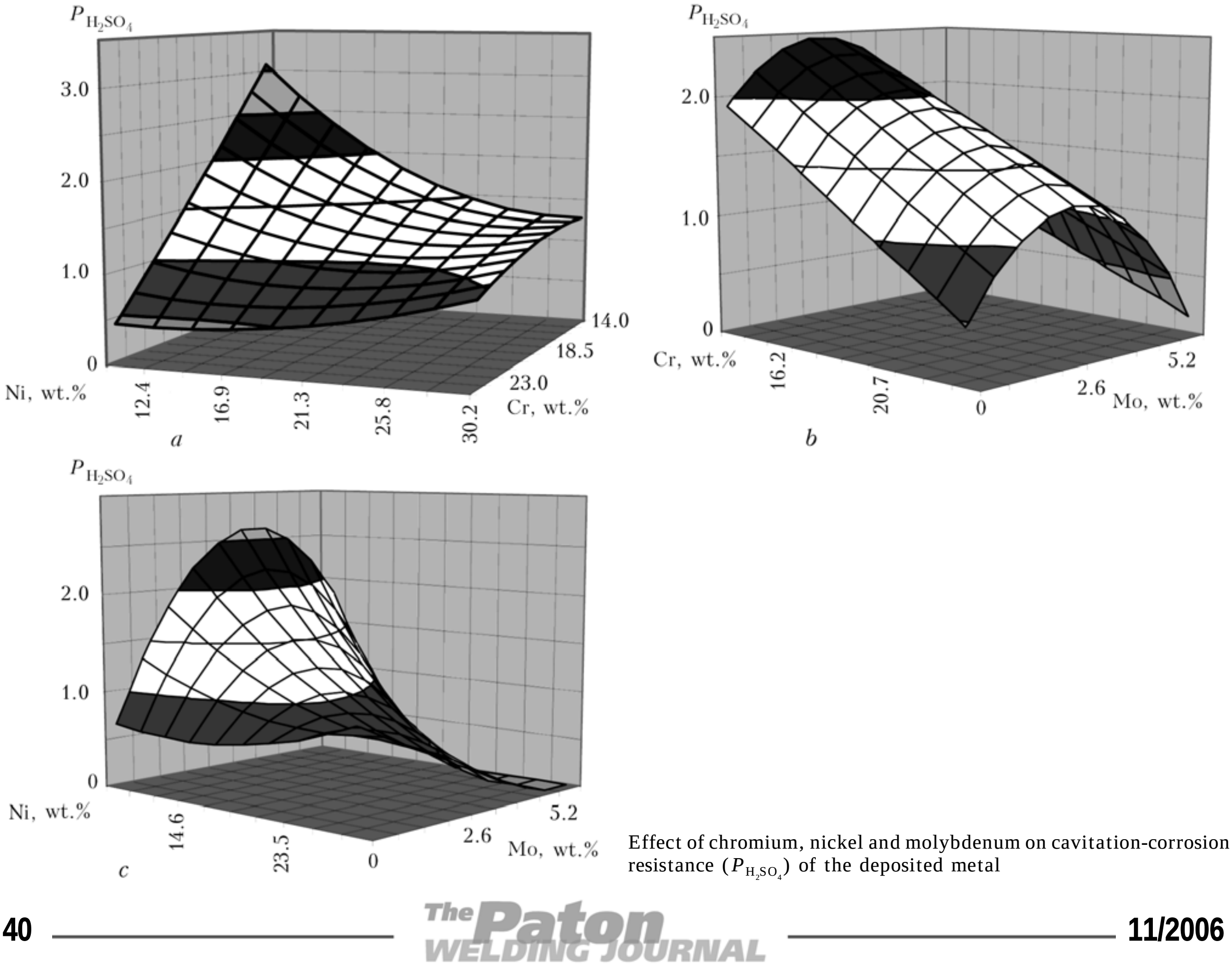

Effect of chromium, nickel and molybdenum on cavitation-corrosion resistance ($P_{H_2SO_4}$) of the deposited metal forecasting cavitation-corrosion resistance of Fe--Cr--Ni and Fe--Cr--Ni--Mo alloy systems.

With regard for joint effect of cavitation and corrosion, on the basis of the laboratory research data, hyperplanes demonstrating the effect of chromium, nickel and molybdenum content variation on cavitation-corrosion resistance of the deposited metal (Figure) were constructed. The increase of the content of chromium actually in the entire range of nickel concentrations results in appreciable increase in cavitation-corrosion resistance of metal (see the Figure, *à*). Increasing the content of chromium for conditions of corrosive attack is recommended by many authors [7--10], as it reduces propensity of metal to intercrystalline corrosion. Addition to the deposited metal of up to 27 % Cr increases by the order of magnitude the minimal time for the intercrystalline corrosion onset [9].

Corrosion resistance of Fe--Cr--Ni alloy system also depends on the content of nickel. So, with the increase of the content of the latter from 10 to 15 %, corrosion resistance first grows, reaching a maximum, then decreases at concentration of nickel of 25 and 35 % [9], which correlates with the data of laboratory research (see the Figure, *à*). Addition of up to 2 % Mo to steel with 23 % Cr and 18--20 % Ni, degrades cavitation-corrosion resistance of the metal (Figure, *b*), which is explained by poor resistance of such steels in the concentrated solutions of sulfuric acid at elevated temperatures of [9]. At molybdenum content of up to 6 %, the propensity of metal to passivation grows (the passivation current and the passive-condition current diminish) which, in turn, promote passive condition stability. In the opinion of the authors of [9], plastic deformation with the degree of reduction up to 50 %, does not have any appreciable effect on the corrosion rate in sulfuric acid solutions of steels and alloys containing 18--20 % Cr, 12--28 % Ni and alloyed with up to 5--6 % Ì î.

06Kh23N28 Ì 3D3Ò (06KhN28 Ì DÒ) alloy, widely used in the domestic industry for operation in various-concentration solutions of sulfuric acid, features good cavitation-corrosion resistance. High resistance at its alloying with 3 % Ì î is due to addition to the alloy of copper reducing the surface of the anodic areas as it accumulates on the surface layer. The process proceeds in the range of potentials of active dissolution of copper. During the exchange process (electrochemical reaction), the latter passes from the electrolyte, depositing on the surface of the alloy and forming a protective shielding layer [11]. Data of the laboratory research are confirmed by the research data reported in [12].

As is evident fromthe hyperplane showing the influence of nickel and molybdenum on cavitation-corrosion resistance of the deposited metal (see the Figure, *c*), the smallest losses of samples mass are observed at alloying the metal with 18--20 % Ni, either without molybdenum at all, or at the content of the latter in the range of 5--6 %. The above mathematical and statistical results of laboratory research conducted on a series of complex-alloy stainless steels and alloys, allow choosing for the deposition a sparsely alloyed metal having better cavitation-corrosion resistance.

Optimum cavitation-corrosion properties under the attack of 92 % solution of H_2SO_4 features steel 08Kh23N18 Ì 5, being not inferior to 08Kh23N28 Ì 2Ò and 06Kh23N28 Ì 3D3Ò alloys. A more thorough explanation of the phenomena accompanying the improvement of the resistance of 08Kh23N18 Ì 5 steel requires conducting their further study.

The empirical dependence of the effect of basic alloying components (chromium, nickel and molybdenum) in complex-alloy stainless steels and alloys on cavitation-corrosion resistance of the deposited metal, allows choosing optimum composition of a wear-resistant metal for making parts of chemical plants operated in sulfuric acid solutions. Compositions containing, wt.%: 23--25Cr; 18--20Ni; 5--6 Ì î and 23--25Cr; 25--28Ni; 3--5 Ì î, belong to the optimum range of alloys.

Of special interest is steel 08Kh23N18 Ì 5, whose cavitation-corrosion resistance is of the same order as that of the 06Kh23N28 Ì 3D3Ò alloy, while nickel content in the former is reduced (10 %).

1. Patyupkin, A.V., Rudychev, A.S., Bykovsky, O.G. (2000) Cavitation-corrosion resistance of some deposited stainless steels and alloys. *The Paton Welding J.*, **8**, 37–39.
2. Patyupkin, A.V., Antonyuk, D.A. (2005) Effect of alloying on cavitation-corrosion resistance of stainless steels and alloys. *Ibid.*, **4**, 14–16.
3. Patypkin, A.V. (2004) Effect of corrosion factor on kinetics of cavitation-corrosion wear of stainless steels and alloys. *Novi Materialy v Metalurgii ta Mashynobuduvanni*, **1**, 143–145.
4. Kakhovsky, N.I. (1975) *Welding of high-alloy steels*. Kiev: Tekhnika.
5. Adler, Yu.P., Markova, E.V., Granovsky, Yu.V. (1976) *Experiment planning in search of optimum conditions*. Moscow: Nauka.
6. Hartman, K., Letsky, E., Schefer, W. (1977) *Experiment planning in investigation of technological processes*. Moscow: Mir.
7. Myshkis, A.D. (1967) *Higher mathematics lectures*. Moscow: Nauka.
8. Bogachev, I.N. (1972) *Cavitation fracture and cavitation-resistant alloys*. Moscow: Metallurgiya.
9. Ulianin, E.A., Svistunova, T.V., Levin, F.L. (1987) *Corrosion-resistant high alloys*. Moscow: Metallurgiya.
10. Chigal, V. (1969) *Intercrystalline corrosion of stainless steels*. Leningrad: Khimiya.
11. Tufanov, D.G. (1990) *Corrosion resistance of stainless steels, alloys and pure metals*. Moscow: Metallurgiya.
12. Chukalovskaya, T.V., Tomashov, N.D., Majskaya, V.D. (1984) About mechanism of anodic dissolution of molybdenum in water electrolytes. *Zashchita Metallov*, **6**, 864--871.

CHARACTERISTICS OF PULSED PLASMA FLOW IN PLASMA-DETONATION GENERATOR AT DIFFERENT FLOW RATES OF FUEL MIXTURE

M.L. ZHADKEVICH, Yu.N. TYURIN, O.V. KOLISNICHENKO and **V.M. MAZUNIN**
E.O. Paton Electric Welding Institute, NASU, Kiev, Ukraine

Thermal and gas-dynamic characteristics of a supersonic pulsed plasma flow depending upon the degree of filling of an inter-electrode gap with a fuel mixture were calculated on the basis of analysis of the results of theoretical studies of the plasma-detonation unit.

Keywords: plasma detonation spraying, pulsed plasma, geometry of accelerator, fuel mixture, flow rate

Quality formation of coatings or hardened layers using a pulsed-plasma generator depends upon many factors. Experimental evaluation of optimal geometric parameters of the generator, which is based on acceleration of the fuel gas mixture (C_3H_8, O_2, air) detonation products between coaxial electrodes, is a complicated task. A mathematical model of the magnetic gas-dynamic flow of the combustion products in a coaxial gap [1, 2] was used to evaluate parameters of the plasma at outlet of the generator. Study [2] describes evaluation of the effect of electric characteristics of the discharge circuit on parameters of the plasma at a preset geometry of electrodes. The most important parameters of heat treatment and spraying technologies using the pulsed-plasma generator are the composition of a fuel gas mixture and degree of filling of the inter-electrode gap with this mixture. Based on the investigations described in study [2], below we consider numerical evaluation of thermal and gas-dynamic characteristics of a supersonic plasma flow depending upon the degree of filling of the inter-electrode gap with a detonation mixture at constant parameters of a power supply and geometry of the plasma-detonation unit generator. Parameters of the plasma-detonation unit are given below.

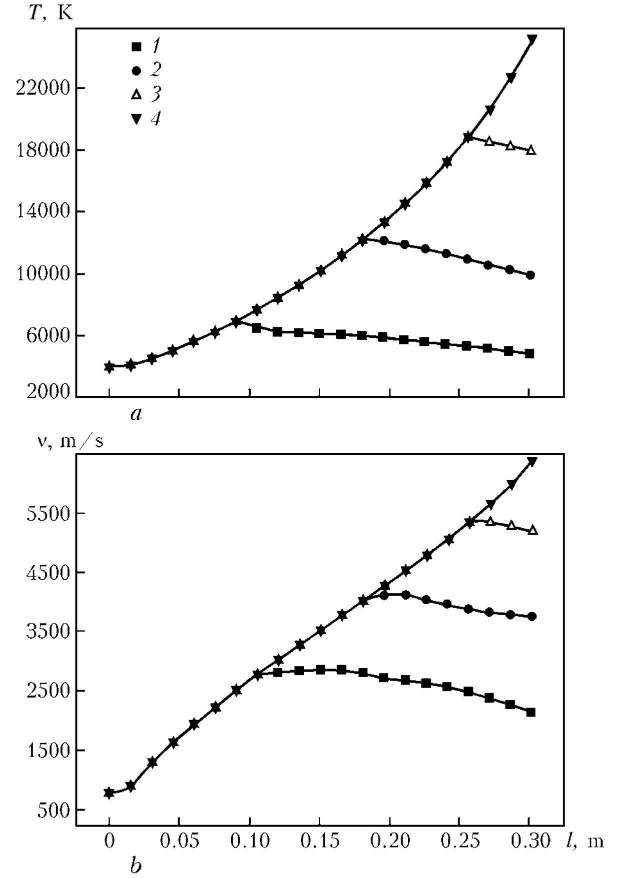

Dependence of averaged temperature (*a*) and velocity of the gas mixture (*b*) in a trace behind the detonation wave upon the flow rate of the fuel mixture (1--4 — modes, see the Table)

Parameters of generator oscillation circuit

Inductance of circuit, μH	7.5
Capacitance of capacitor bank, μF	800
Initial voltage between electrodes, kV	3.2
Calculated active resistance of circuit (resistance of plasma in inter-electrode gap) according to decay curves, Ohm	0.01–0.09

Geometric parameters of accelerator

Initial diameter of internal electrode, mm	65
Initial diameter of external electrode, mm	81
Length of internal electrode, mm	300
Taper angle of internal and external electrodes, deg	15

The inter-electrode gap was filled with a detonation mixture according to the modes given in the Table. The calculations were made following the proce-

Modes of filling of inter-electrode gap with a detonation gas mixture at a temperature of 294 K

Mode No.	Flow rate of detonation gas mixture at 2 Hz frequency, cm^3	Degree of filling of inter-electrode gap, %
1	274.4	25
2	550	50
3	825	75
4	1100	100

dure suggested in study [2]. The modes were traced on the basis of variations in velocity and temperature of the plasma near the detonation wave propagating through the inter-electrode gap.

Analysis of the results obtained (Figure) allows the following conclusions: velocity and temperature of the ionised combustion products in the plasma-detonation accelerator vary with the degree of filling of the inter-electrode gap with the detonation mixture. Increase in the latter leads to increase in temperature and velocity of the detonation products immediately behind the wave. This is caused by the fact that the electric current starts flowing through the detonation products at the presence of the external magnetic field, resulting in formation of an extra ponderomotive force, as well as an additional inflow of energy to a gas due to Joule heat dissipation, this exerting a substantial effect on propagation of the detonation wave.

The calculation results are in good agreement with the experimental data obtained, in particular, for conditions of thermochemical treatment of the surfaces of tools and machine parts. The detonation mixture was fed to the inter-electrode gap, and surfaces of the plates were subjected to heat treatment in accordance with the above modes. Increase in volume of the detonation mixture was found to change properties of the heat-hardened layer, which is directly related to a heat flow and its duration. In turn, the latter depends upon the temperature and velocity of the plasma jet.

In general, the investigations conducted allow a conclusion that thermal and gas-dynamic parameters of the plasma in the plasma-detonation unit, immediately behind the detonation wave, vary with the degree of filling of the inter-electrode gap with the detonation mixture, which, in turn, affects properties of the heat-hardened layer on pieces being treated.

1. Gurovich, V.Ts., Desyatkov, G.A., Spektrov, V.L. (1987) Peculiarities of movement of current envelope and shock wave in pulse high-pressure accelerator. *Doklady AN SSSR*, 293(**5**), 1102–1105.
2. Zhadkevich, M.L., Tyurin, Yu.N., Kolisnichenko, O.V. et al. (2006) Effect of parameters of plasma detonation unit discharge circuit on gas-dynamic characteristics of pulsed plasma flows. *The Paton Welding J.*, **8**, 37–39.

EFFECT OF GRAPHITE ON KINETICS OF TRANSFER OF CARBON TO WELD POOL IN FLUX-CORED WIRE CLADDING

A.P. ZHUDRA, S.Yu. KRIVCHIKOV and **V.V. PETROV**
E.O. Paton Electric Welding Institute, NASU, Kiev, Ukraine

Given are the results of investigations into the effect of grain size composition of graphite powder in the core of a self-shielding flux-cored wire on absorption of carbon by the weld pool and arc stability in electric arc cladding. It has been established that the maximal value of the coefficient of transfer of carbon to deposited metal and high arc stability can be achieved by using the electrode graphite with a grain size of 200–250 μm in the flux-cored wire core.

Keywords: arc cladding, flux-cored wire, deposited metal, graphite, grain size composition, transfer of carbon, arc stability, metal transfer

Graphite is the main carbon-containing material which is added to the core of flux-cored wires used for cladding of high-carbon alloys. Unlike other core components (metal powders, ferroalloys, minerals, salts, oxides, fluorides, etc.), graphite is the most heat-resistant non-consumable material with a crystalline lattice destruction temperature of about 4000 °C [1]. In this connection, the presence of graphite in flux-cored wire is likely to affect both character of its melting and kinetics of transfer of carbon to deposited metal.

The purpose of this study was to investigate the effect of graphite and its grain size composition on the kinetics of transfer of carbon to the weld pool, as well as on melting of flux-cored wire, parameters of the electrode metal transfer process and arc stability in cladding using self-shielding flux-cored wire.

Graphite of the GL-2 grade (GOST 5279–74), milled and separated into four fractions, i.e. with grain size of 100–160, 200–250, 250–315 and 400–500 μm, was used for the investigations. The graphite content of each fraction in experimental flux-cored wires with diameter $d_{\mathrm{wire}} = 2.4$ mm was varied discretely from 0 to 7 wt.%. In addition to graphite, the flux-cored wires also contained the constant amounts of ferromanganese, ferrosilicium, ferrotitanium, aluminium powder, marble, sodium fluorsilicate and iron powder. The constant value of the fill factor (21 %) with increase in the weight content of graphite was maintained by reducing the content of iron powder.

The beads were deposited at a direct current of reverse polarity under the following conditions: welding current $I_{\mathrm{w}} = 220$–240 A, arc voltage $U_{\mathrm{a}} = 24$–25 V, flux-cored wire feed speed $v_{\mathrm{f}} = 97.2$ m / h, and deposition speed $\nu_{\mathrm{d}} = 7.2$ m / h. The carbon content of the third layer of deposited metal was determined by chemical analysis. Operational characteristics of the process of melting of flux-cored wires (arc stability expressed in terms of the value of the coefficient of

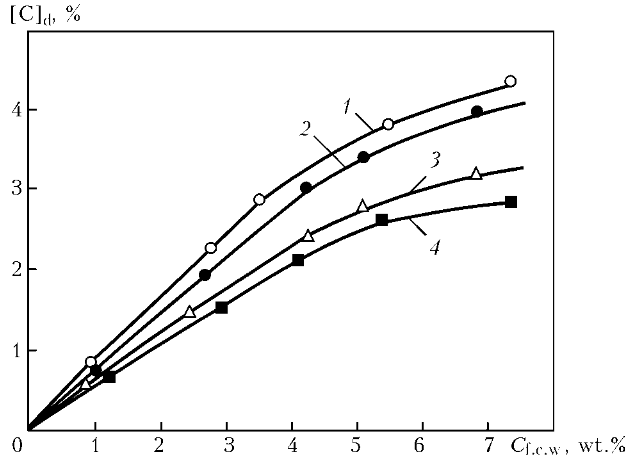

Figure 1. Effect of graphite content of flux-cored wire, $C_{f.c.w}$, on concentration of carbon in deposited metal, $[C]_d$ (I_w = 230 A, U_a = = 24--25 V, d_{wire} = 2.4 mm): *1* — 200–250; *2* — 250--315; *3* — 100--160; *4* — 400--500 μm

variation in arc voltage, K_V^U, quantity $N_{s.c}$ and time $\tau_{s.c}$ of short circuits of the arc gap with electrode droplets transferring to the weld pool) were measured using non-stationary process analyser ANP-2 [2].

It can be seen from the investigation results shown in Figure 1 that at a differing graphite content of flux-cored wires the highest concentration of carbon $[C]_d$ in deposited metal takes place where the graphite grain size is 200--250 μm. Decrease or increase in the graphite grain size leads to decrease in $[C]_d$.

As seen from Figure 2, variations in coefficient η_C of transfer of carbon to deposited metal depend upon the value of *d* of graphite particles (grains). The effect of size of the graphite grains on the kinetics of transfer of carbon to deposited metal can be explained on the basis of mechanisms of solid-state interaction of graphite with liquid and solid phases in melting of self-shielding flux-cored wires.

Fine graphite grains (100–160 μm) are characterised by a relatively developed specific surface, which leads to intensification of chemical interaction between the surfaces of the graphite grains and air oxygen. In this case, the major part of these grains is oxidised and transforms into the gas phase, while the rest of the grains dissolve in a liquid electrode droplet and weld pool. Substantial losses of carbon as a result of oxidation of fine graphite grains result in a relatively low value of η_C.

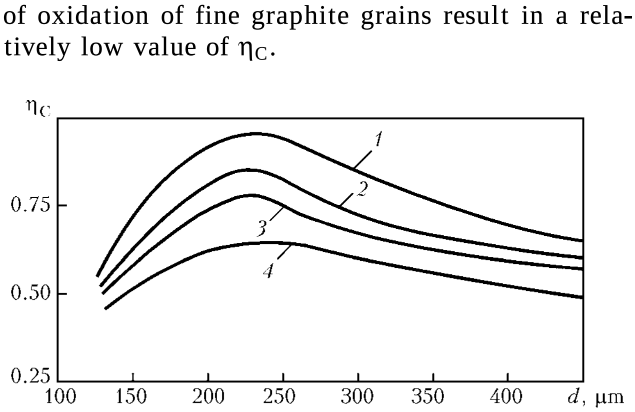

Figure 2. Effect of size *d* of graphite grains on coefficient η_C of transfer of carbon to deposited metal: *1* — $C_{f.c.w}$ = 1; *2* — 2; *3* — 5; *4* — 4 wt.%

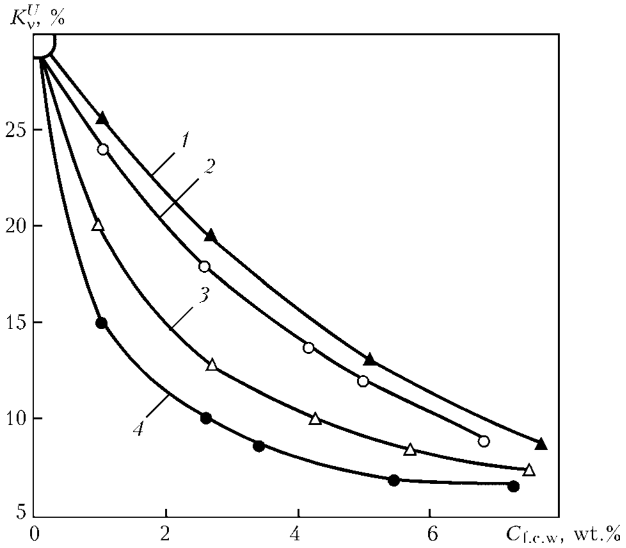

Figure 3. Effect of graphite content and grain size on arc stability in melting of flux-cored wire: *1* — 400–500; *2* — 250–315; *3* — 100–160; *4* — 200–250 μm

As the graphite grains increase in size, their specific surface decreases, the oxidation process transforms from the kinetic to diffusive state, and its rate becomes comparable with the rate of diffusive dissolution of particles in an alloy [3, 4]. The process of dissolution of graphite, which begins in a droplet, continues in the weld pool. As a result, the values of η_C grow

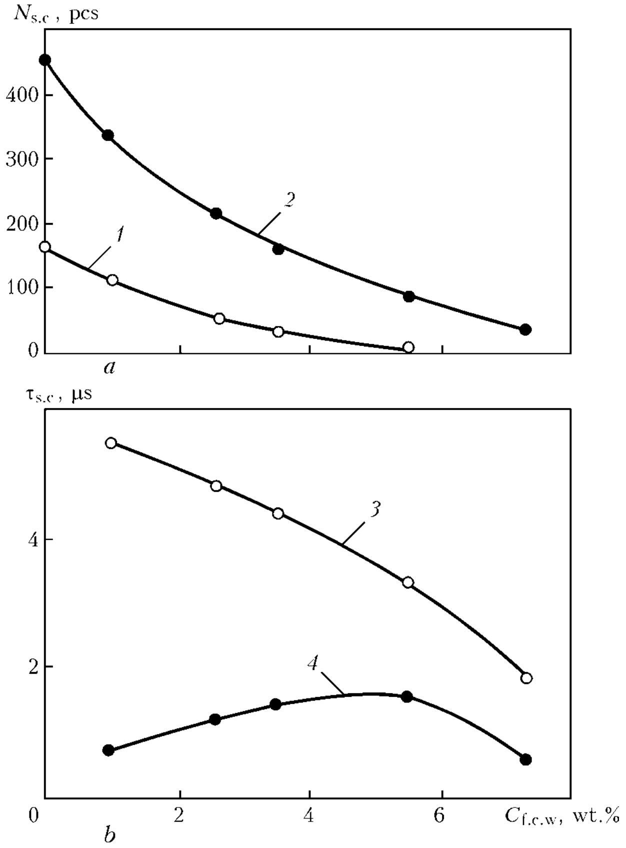

Figure 4. Effect of graphite with grain size of 200–250 μm on quantity $N_{s.c}$ (*a*) and time $\tau_{s.c}$ (*b*) of short circuits of arc gap with electrode droplets in melting of flux-cored wire: *1, 3* — quantity and time of effective short circuits, respectively, in transfer of electrode droplet to weld pool; *2, 4* — same of random short circuits without transfer of electrode droplet to weld pool

because of reduction of carbon losses due to oxidation of graphite and growth of the role of the process of diffusive dissolution of the latter in a liquid melt. The coefficient of transfer of carbon to deposited metal has a maximal value at a 200–250 μm size of the graphite grains.

In the case of using graphite with coarse grains (400–500 μm), the dominating mechanism of carbon losses is that caused by the graphite grains which had no time to fully react at the droplet and weld pool stage. While floating to the surface of molten metal because of their low specific weight, they contact it only partially, which reduces the significance of the process of diffusive dissolution of graphite and, at the same time, decreases the value of the coefficient of transfer of carbon to deposited metal. In this case, the losses of carbon caused by oxidation of coarse graphite grains are insignificant.

Along with the grain size composition, the value of η_C is affected also by the graphite content of the flux-cored wire core. As proved by high-speed filming, at $C_{\rm f.c.w} < 2.0$–2.2 wt.% the values of the rate of melting of the flux-cored wire sheath and core are almost identical. The uniformity of melting is disturbed at a substantial graphite content. «Protrusion» of the core, formed in this case, fractures upon reaching a critical length, and gets onto the surface of the weld pool in the form of more or less coarse conglomerates. Then it is pressed out to the tail part of the weld pool by convective and gas-dynamic flows, having no time to dissolve in a molten alloy. As seen from Figure 2, the higher the graphite content of the wire core, the more frequent are the cases of destruction of the non-melted core, and the higher are the losses of carbon that did not transfer to deposited metal.

In addition to the kinetics of transfer of carbon to deposited metal, the graphite content affects also the arc stability and parameters of electrode metal transfer in melting of self-shielding flux-cored wires. Figure 3 shows that the arc stability grows (values of $K_{\rm v}^U$ decrease) with increase in $C_{\rm f.c.w}$. This is related to the fact that at constant welding parameters the graphite content of the flux-cored wire core affects the arc length. As follows from the results of high-speed filming, the higher the graphite content, the longer the arc in melting of flux-cored wire. Increase in the arc length leads to a change in main parameters of electrode metal transfer, which influence the arc stability, i.e. frequency and time of short circuits (i.e. a droplet flows to the weld pool). As shown in Figure 4, the time of effective short circuits reduces, and the arc stability increases (see Figure 3) with growth of the $C_{\rm f.c.w}$ values.

1. Ostrovsky, V.S., Virgiliev, Yu.S., Kotikov, V.I. et al. (1986) *Artificial graphite*. Moscow: Metallurgiya.
2. Krivchikov, S.Yu., Zhudra, A.P., Petrov, V.V. (1994) Effect of carbonates on welding-technological properties of self-shielding flux-cored wire for surfacing of white iron. *Avtomatich. Svarka*, **7/8**, 18–20.
3. Khitrin, L.N., Golovina, E.S. (1967) High-temperature interaction of graphite with different reactive gases. In: *High-temperature investigations*. Moscow: Nauka.
4. Aleksandrov, V.V., Korchagin, M.A. (1987) About mechanism and macrokinetics of reactions in burning of SHS-systems. *Fizika Goreniya i Vzryva*, **5**, 55–63.

IN MEMORY OF Dr. SOSSENHEIMER

On July 8, 2006 Dr. Sossenheimer passed away, who for many years had occupied the position of General Manager of the German Society of Welding and Allied Technologies.

Dr. Sossenheimer had been active at the International Institute of Welding, was the Treasurer of this international organization and Chairman of IIW Working Group on publications. Dr. Sossenheimer made a tremendous contribution to development of such areas of welding science and technology as simulation, quality and safety in the production processes of joining, cutting and coating.

His contribution to development of international cooperation is great. He was the honorary member of many foreign welding associations and received the awards and prizes of many countries.

In 1991 Dr. Sossenheimer, an outstanding scientist and science coordinator, received the highest award of the German Society of Welding and Allied Technologies — DVS Honorary Medal.

July 2003, IIW established Dr. Sossenheimer Award for innovation in the software field.

E.O. Paton Electric Welding Institute
Editorial Board of «The Paton Welding Journal»

THESIS FOR SCIENTIFIC DEGREE

E.O. Paton Electric Welding Institute of the NAS of Ukraine

V.R. Burnashev (PWI) defended on the 27th of September, 2006, the Candidate of Technical Sciences degree thesis on subject «Upgrading of Plasma-Arc Skull Melting of Special Steels, Alloys and Pure Metals».

The thesis is dedicated to optimisation of the technology for making metals and alloys by plasma-arc skull melting (PASM).

The thesis considers the state-of-the-art in special electrometallurgy methods intended for making critical-application steels and alloys, pure metals and master alloys, and substantiates the demand for the work.

It is shown that PASM in furnaces with a ceramic hearth is indicated for making special steels and alloys with additions of rare-earth and alkali-earth metals used as alloying elements, and that in a copper water-cooled mould is indicated for making pure metals and master alloys.

Optimal additions of aluminium to be used in the previous period of deoxidation were calculated. For chromium steels 05Kh12N2M and 07Kh12NMFBR the optimal addition of aluminium was 2.0–2.6 kg / t, for steel 05Kh14N15NMFBR it was 2–3 kg / t, and for alloy KhN55MBTs — 2.84 kg / t.

Optimal parameters of deoxidation and micro alloying were selected on the basis of the investigation data for the materials studied.

As established as a result of experimental and commercial melting operations, steel castings produced by PASM have a low content of non-metallic inclusions (total content is 0.0035–0.0080 wt.%) and interstitial impurities ([C] = 0.01–0.02 %, [O] = 0.002–0.003 %, [N] = 0.016–0.018 %, and [H] = 0.00150–0.00017 wt.%).

Utilisation of multi-component master alloys for micro alloying of nickel alloys was found to lead to increase in assimilation of alloying elements to 70–80 %. Micro alloying of nickel alloys with hafnium and cerium leads to improvement of strength properties.

The content of non-metallic inclusions was determined to be 2 times as low in the materials melted under optimal deoxidation and micro alloying conditions, mechanical properties of these materials increasing by 30–40 %.

The effect of PASM in a copper water-cooled crucible on its operational indicators was experimentally studied. This made it possible to recommend rational conditions for remelting of refractory metals and their alloys. PASM of refractory metals in a copper water-cooled crucible allows the content of non-metallic inclusions to be decreased several times.

It is shown that the application of PASM in a copper water-cooled crucible is indicated for production of castings of refractory and reactive metals and their alloys, and for making master alloys containing rare-earth and alkali-earth metals.

THESIS FOR SCIENTIFIC DEGREE

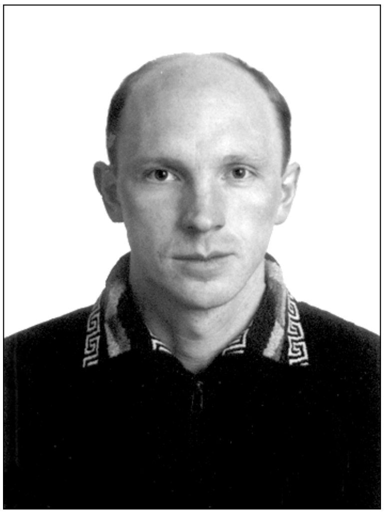

E.O. Paton Electric Welding Institute of the NAS of Ukraine

I.V. Protokovilov (PWI) defended on the 27th of September, 2006, the Candidate of Technical Sciences degree thesis on subject «Magnetically Controlled Electroslag Melting (MCEM) of Multi-Component Titanium Alloys».

The thesis is dedicated to development of scientific and technological principles of the technology for MCEM of titanium alloys.

Flows of the metallurgical melt in electroslag melting under the effect of the external magnetic fields of different spatial orientation were investigated by the physical modelling method. It is shown that hydrodynamics of the metallurgical melt is determined by volume electromagnetic forces formed in interaction of the melting current with the self- or external magnetic fields. Electric vortex flows or reciprocal oscillations (vibration) of the melt can be induced in the metallurgical pool depending upon the characteristics of the external magnetic field.

It is shown through mathematical modelling that the paths of the solid particles and electrode drops in liquid slag flows alter under the effect of the external, longitudinal-radial magnetic field, which allows the time of their dwelling in the slag pool to be increased by 40--50 %. The possibility is shown of removing the solid particles to the periphery of the slag pool at the mould walls.

The flow diagrams of control of hydrodynamics of the metallurgical melts using the longitudinal, longitudinal-radial and transverse magnetic fields were developed on the basis of the investigations conducted.

Metallurgical and technological peculiarities of MCEM of titanium alloys in the transverse magnetic field were experimentally studied. It was established that vibration of the melt caused by introducing the transverse magnetic field to the melting zone leads to decrease in the melting current, increase in the frequency of detachment of electrode drops (accordingly, decrease in their mean mass), decrease in depth of the metal pool, and smoothing of the solidification front. The possibility is shown of controlling structure of titanium alloys using the vibration induced by the transverse magnetic field. Characteristics of the magnetic field, which provide melting of ingots free from solidification defects and having a uniform fine-grained structure, were determined.

The process of pressing of consumable electrodes and the metallurgical flux for MCEM were developed.

Properties of titanium alloys produced by the MCEM method were studied. The new technological process was proved to provide ingots of titanium alloys with high chemical and physical homogeneity, fine-grained structure and absence of defects of the type of slag inclusions, microporosity and cracks. The chemical composition of metal meets requirements of the corresponding standards. It is shown that strength characteristics and impact toughness of the MCEM metal are higher than those of similar samples produced by the VAR method, the level of strength being the same. The possibility was established of using the MCEM method for production of ingots of titanium alloys with an intermetallic reinforcement. The ingots of heat-resistant titanium alloys with a level of long-time strength equal to 320 MPa at 750 °C were produced.